POLITECNICO DI TORINO

Collegio di Ingegneria Chimica e dei Materiali

Master of Science Course
in Materials Engineering

Master of Science Thesis

Development of polymeric materials as gas sensors

Relator:
Prof. Marco SANGERMANO
Dr. Andrea FASOLI

Candidate:
Lorenzo VIGNA

March 2018

Politecnico di Torino

Abstract

Collegio di Ingegneria Chimica e dei Materiali
DISAT

Master of Science Course in Materials Engineering

Development of polymeric materials as gas sensors

by Lorenzo VIGNA

The development of miniature and portable gas sensors able to detect gas analytes in real time with good sensing performances will significantly change our daily life. Polymer-based sensors are widely used because of their versatility, flexibility, low energy consumption and operational temperature and low cost. These materials act as chemiresistive gas sensors, so that they transform the concentrations of analytes to detectable physical signals, such as currents variables. After the exposure to the vapor to detect, the active sensing material of the sensor interacts with the analyte, which causes its physical properties to change. The interactions between the analytes and the sensing materials are multiform, according to different analytes and different active materials.

The aim of the thesis is the fabrication of simple and more efficient polymeric responsive vapor sensors with the goal of optimizing the three main requirements that are set for any kind of sensors: sensitivity, selectivity and stability. This study was a joint project between Politecnico di Torino, where the samples were fabricated, and IBM Research Center in Almaden, where the sensors were electrically tested by means of a chamber connected to a gas delivery system.

We followed different strategies for sensors preparation. In the first one, we performed a simultaneous UV-curing of an acrylic insulating network and a conductive polymer, Polypyrrole (PPy), starting form their precursors. Conductive polymeric sensors were also prepared by dispersion of a conductive filler (MWCNTs). The last strategy was the use of block copolymers (PS – co – PDMAEMA), prepared by

ATRP, mixed with a carbon black suspension (filler load from 5 wt% up to 60 wt%) and then flow coated on a silicon wafer.

The detection mechanism involves proton transfer on the PPy chains, for the films containing the conductive polymer, and this effect can be macroscopically observed by electrical impedance variations. In the films with the conductive fillers, the resistance is determined by the number of percolation paths accessible between the two electrodes, through which the carriers are transported. When the polymer matrix is exposed to the target gas, it starts to swell with a consequent reduction of the number of accessible conductive paths.

The electrical measurements were performed with a flow of saturated vapor pressure of five different analytes (Acetone, ethanol, isopropanol, toluene and water) diluted with dry air. The concentrations reached were between tens of ppm up to thousands ppm. Different systematics were studied, changing multiple parameters: the carbon black concentrations, the polymer matrix, the film thickness, the deposition technique and the electrodes distance. The Nyquist plots and the I vs time graphs show that sensitivity increases with higher concentrations of the analyte and when the filler concentration approaches the percolation threshold.

The polymeric sensors are very promising because they can be tuned and tailored; changes in the films structure can influence and control the reactions between gases and the material. In fact morphology, composition, solubility and other physical properties are strictly linked to the sensing performances. In the future, it will be possible to create an array of polymeric sensors in order to build an electronic nose, which is able to detect particular gases at low concentrations, giving a fingerprint response that can be identified by a pattern recognition engine.

Acknowledgements

Firstly, I would like to express my sincere gratitude to my advisor Prof. Marco Sangermano for the continuous support and motivation. His door office was always open whenever I ran into a trouble or had a question about my research or writing. He made this fantastic experience possible.

I would also like to thank Dr. Andrea Fasoli who has been my mentor for the five months I spent at IBM Research Center in Almaden for his unfailing support and assistance. Without his precious help and availability it would not be possible to conduct this research.

I'm grateful to Dr. Luisa Bozano who provided me the opportunity to work on a such interesting project in her team.

I also thank all the Nanofabrication Group for the stimulating collaboration. In particular I am grateful to Bo Yuan for the synthesis of the carbon black-polymer composites, Campbell Scott for helping me with the Impedance Analyzer and Linda Sundberg for all the advices.

I also thank Nicolò Razza who explain me how to work in a chemistry laboratory.

A special thank goes to Esther Quement and her enlarged "Ohana". They welcome me in their beautiful house and treat me like their son. They are so much fun.

I thank my friend Matteo Caprioli for the interesting discussions and for all the fun we have had in the last six months.

Last but not the least, I would like to thank my mother for listening to my explications for hours and hours keen to know what I was doing although it is likely that she has never grasped what it was all about.

And finally I thank Kona and Stordi for make me relaxed walking on my keyboard while I was writing or sleeping on my knees when I didn't know what to write on my thesis.

Contents

List of Figures

List of Tables

I dedicate this master thesis to my dad and my grandfather Sandro

Riassunto

L'olfatto è il più misterioso e complesso dei sensi umani. Un odore è in grado di riportare indietro la memoria ai ricordi del passato, eliminando la barriera del tempo. Le abilità di questo senso sono state utilizzate in diversi campi nell'ambito del controllo qualità. Tuttavia l'uso del naso umano presenta molte limitazioni collegate alle condizioni soggettive della persona.

La realizzazione di sensori di ridotte dimensioni in grado di rilevare in modo accurato tracce di gas in tempo reale può cambiare in modo significativo la vita quotidiana. L'idea della realizzazione di un naso elettronico ha preso forma a metà degli anni cinquanta ma solo nel 1988 ne è stata data una definizione come strumento che comprende una matrice di sensori dotati di una specificità parziale collegata ad un sistema di riconoscimento capace di identificare odori semplici o complessi. Infatti, il singolo sensore non è sensibile ad un unico analita, ma risponde in modo differente ad una vasta gamma di gas. Per questo motivo, preso singolarmente, non è in grado di fornire allo stesso tempo informazioni sia sulla concentrazione del gas che sulla sua classe di appartenenza. Solo quando tutti i singoli sensori rispondono in concerto, combinando i diversi segnali, si genera un'impronta digitale di quel gas o mix di gas. Si tratta di un'identificazione univoca che può essere riconosciuta tramite diversi algoritmi come l'analisi delle componenti principali (PCA) o l'analisi di discriminazione lineare (LDA).

Questo dispositivo elettronico può trovare ampio utilizzo in diversi settori che spaziano dal controllo della qualità nell'industria alimentare alla diagnosi di varie patologie nel campo medico; dal controllo della qualità dell'aria in ambienti chiusi al rilevamento di gas tossici e pericolosi nelle industrie chimiche. Possono essere impiegati inoltre in ambito aerospaziale come rilevatori di gas incediabili e per monitorare le emissioni, fino agli scopi militari come il rilevamento di mine anti-uomo.

L'obiettivo è quello di creare un dispositivo miniaturizzato che possa essere integrato in un oggetto di uso quotidiano come ad esempio il cellulare.

Attualmente, in commercio esistono diversi tipi di nasi elettronici che si differenziano in base al materiale e alle caratteristiche dei sensori impiegati per comporre le matrici.

Il principio di funzionamento è unico e di per sé è molto semplice: quando il sensore viene esposto al vapore da analizzare, le molecole di gas vengono adsorbite sulla superficie del dispositivo e da queste interazioni deriva un cambiamento delle proprietà fisico-chimiche del materiale attivo. In base alla modificazione delle proprietà fisiche intervenuta, si possono individuare i seguenti dispositivi: sensori chemiresistivi, sensori piezoelettrici, MOSFET e sensori ottici.

Mentre i primi misurano una variazione delle proprietà elettriche, i secondi, rilevando una differenza di massa, sono in grado di analizzare lo spostmento della frequenza di risonanza. I MOSFET, invece, misurano un cambiamento della funzione lavoro mentre i sensori ottici presentano una variazione delle proprietà ottiche in seguito all'esposizione all'odorante.

Le migliori prestazioni si possono ottenere ottimizzando le "tre esse" che rappresentano i tre principali requisiti che ogni sensore possiede: sensitività, selettività e stabilità. La sensitività è un numero puro che descrive la risposta di un sensore verso un determinato gas o ambiente. Rappresenta la bontà della risposta associata al cambiamento del segnale di output rispetto ad una variazione del segnale in input. Migliore è la sensitività, più facile è rilevare una bassa concentrazione di gas. La selettività è, invece, la capacità di un sensore di discriminare tra diversi analiti. Infine, la stabilità indica il grado di deterioramento funzionale in rapporto all'uso e al tempo. Nessuno di questi parametri prevale sull'altro, dipendendo tutto dal tipo di impiego che verrà fatto dal sensore. Si deve arrivare ad un compromesso basato sull'applicazione che può richiedere ora una buona risposta a basse concentrazioni oppure come priorità la possibilità di riconoscere diversi tipi di odoranti o ancora la presenza di un'ottima stabilità in quanto la manutenzione e la sostituzione risultano essere molto complesse, difficili e costose.

I dispositivi elettronici basati sui polimeri presi in considerazione in questo studio rientrano nella categoria dei sensori di gas chemiresistivi, poiché il cambiamento della proprietà fisica è associato ad una variazione della resistenza elettrica. In pratica, questi materiali convertono le interazioni dovute al rilevamento dei gas in un segnale elettrico che può essere monitorato, come una corrente o la relativa resistenza elettrica. In questo ambito, i sensori polimerici rappresentano una valida opzione per la loro versatilità, flessibilità, economicità e capacità di operare a temperatura ambiente con un basso consumo energetico.

Questi dispostivi possono essere fabbricati usando sia i polimeri intrinsecamente conduttivi (ICP) che i polimeri caricati (LP).
Normalmente, i polimeri sono considerati materiali isolanti poiché presentano un energy gap tra la banda di valenza e quella di conduzione abbastanza ampia da non permettere il passaggio degli elettroni agli stati di eccitazione più elevati. Per questo motivo la loro resistenza è molto alta ($\approx$ MΩ-GΩ). Tuttavia nel 2000 Heeger, MacDiarmid and Shirakawa vinsero il Premio Nobel per aver sviluppato materiali plastici elettricamente conduttivi. I più utilizzati sono il polipirrolo (PPy), la polianilina (Pani), il politiofene (PTh), il poliacetilene (PA) e i loro derivati. Questi ICP sono stati utilizzati come materiale attivo nei sensori di gas fino dagli inizi degli anni ottanta. Si è dimostrato che la struttura di questi polimeri deve contenere l'alternanza di legami singoli e doppi lungo la catena principale in modo da permettere la formazione di stati elettronici delocalizzati. Interazioni di carica, fattori conformazionali e sterici possono controllare il livello di delocalizzazione, portando alla formazione di energy gap simili a quelli dei semiconduttori. Grazie alla struttura insatura di questi polimeri coniugati è possibile avere elettroni π disaccoppiati che possono muoversi lungo le catene, permettendo il passaggio di una corrente. Questa conduttività nasce da un doping primario del polimero che consiste in reazioni di ossido-riduzione, generando polaroni e bipolaroni. Le reazioni chimiche che intercorrono tra gli agenti dopanti e le catene portano ad un eccesso o una deficienza di elettroni π lungo le catene del polimero. Questi difetti che vanno ad occupare la zona proibita permettono di ridurre l'energy gap, avvicinando il LUMO all'HOMO e favorendo nuove transizioni percorribili.
Una volta che il polimero risulta conduttivo dopo essere stato dopato, l'interazione tra il materiale attivo e il gas porta ad una variazione della conducibilità e questo effetto è chiamato doping secondario. La donazione o il prelievo di cariche da parte del gas produce un cambiamento delle proprietà elettriche del film polimerico. Considerando un polimero di tipo p come il polipirrolo, i trasportatori di carica principali sono le buche. Quando il sensore viene esposto ad un gas riducente, il polimero cede elettroni. Quindi, la resistenza si abbassa poiché ci sono più hole in grado di contribuire alla conduttività. Invece, quando esposto ad un gas ossidante, che si riduce, il materiale acquista elettroni. In questo caso la resistenza aumenta. Al contrario, per un polimero di tipo n dove gli elettroni sono i principali trasportatori

di carica, le relazioni citate sono invertite. Quando il gas viene rimosso, il film polimerico perde l'effetto del doping secondario e la resistenza torna al valore originale. Questi cicli possono essere ripetuti molte volte poiché si tratta di processi fisici di natura reversibile. Queste variazioni di resistenza elettrica sono associate dunque alla natura del gas e alle sue abilità di ridurre o ossidare il film polimerico, aumentando o diminuendo i trasportatori di carica e influenzando la conduttività grazie al meccanismo di trasferimento di cariche.

Gli LP invece sono a tutti gli effetti dei materiali compositi polimerici. Essi sono costituti da un polimero isolante che agisce da matrice dentro il quale vengono dispersi in modo omogeneo dei filler conduttivi come particelle di carbon black (CB), nanotubi di carbonio (MWCNT) o altri polimeri intrinsecamente conduttivi come il polipirrolo (PPy). Per questa classe di sensori il meccanismo di rilevamento è lo *swelling* della matrice ed è ben spiegato dalla teoria di percolazione. In questi polimeri caricati, la resistenza elettrica è determinata dal numero di cammini conduttivi accessibili tra i due elettrodi tramite i quali le cariche sono trasportate. Quando la matrice polimerica è esposta al gas, incomincia a rigonfiare con una conseguente riduzione del numero di cammini conduttivi accessibili; questo porta ad una riduzione della conduttività in quanto le particelle si allontanano fra di loro impedendo l'*hopping* degli elettroni.

Lo scopo della tesi è lo sviluppo, la fabbricazione e la caratterizzazione elettrica di sensori di vapore polimerici. La maggior parte dell'attività si è concentrata sull'investigazione dei principi di funzionamento di questi dispositivi e delle interazioni che intercorrono tra i gas e il materiale attivo per stabilire le relazioni esistenti tra le proprietà fisico-chimiche e la risposta elettrica. L'obiettivo è quello di giungere alla fabbricazione di semplici chemiresistori polimerici che ottimizzino le tre caratteristiche che sono richieste per ogni tipo di sensore: sensitività, selettività e stabilità.
Questo studio è stato realizzato nell'ambito di un progetto congiunto fra il Politecnico di Torino, dove i campioni sono stati fabbricati, e il centro di ricerca dell'IBM di Almaden, dove i sensori sono stati caratterizzati elettricamente in AC e DC tramite una camera collegata ad un sistema di erogazione di gas.
Gli studi principali sono stati condotti su due importanti classi di chemiresistori: i compositi polimerici con il carbon black e i compositi fotopolimerizzati in situ.

Per quanto riguarda la prima categoria, la realizzazione del sensore finale può essere divisa in cinque fasi principali. La prima consiste nella preparazione del wafer che viene utilizzato come substrato. Si tratta di un passaggio molto delicato e complesso tramite il quale gli elettrodi vengono depositati sul wafer di silicio grazie ad un processo di litografia a fascio elettronico. Il secondo step consiste nella sintesi del polimero dielettrico. In questo lavoro sono stati sintetizzati diversi omopolimeri, copolimeri random o a blocchi e blend (PS, PS-co-PDMAEMA, PS-co-PMAA, PS-co-PMMA) tramite FRP e ATRP. Allo stesso tempo è stata preprarata una sospensione di carbon black e PGMEA. Infine, le diverse soluzioni polimeriche sono state mescolate con la sospensione di carbon black in diverse concentrazioni dal 5 wt% fino al 60 wt%. La fabbricazione dei sensori è avvenuta tramite *flow coating* della soluzione ottenuta sopra il wafer di silicio precedentemente preparato depositando più strati dello spessore di circa $150\,\mathrm{nm}$.

Per quanto concerne la seconda categoria, quella dei polimeri fotopolimerizzati in situ, lo studio si è focalizzato sulla comprensione del complesso meccanismo di *sensing* di questi sensori basato gran parte sul trasferimento di cariche e residualmente sul rigonfiamento della matrice. La strategia innovativa di questi chemiresistori riguarda la loro realizzazione. Questa avviene eseguendo un UV-curing simultaneo di una resina acrilica isolante con, in alternativa, un polimero conduttivo, il polipirrolo (PPy), o un filler conduttivo, i nanotubi di carbonio (MWCNT), partendo dai loro precursori. Grazie a questo processo costituito da un'unica fase di fotopolimerizzazione UV è possibile creare dei reticoli interpenetrati partendo da una formulazione liquida foto-curabile. Le resine utilizzate sono state il PEGDA 200, il PEGDA 575, il PEGDA 700, il BPA e un blend di PEGDA 200 e PEGMEMA. Per permettere la fotopolimerizzazione, sono stati aggiunti alle formulazioni liquide due fotoiniziatori, uno radicalico, Darocure 1173 fissato al 2 wt% per la polimerizzazione della matrice; e l'Irgacure 250 in concentrazione variabile, un fotoiniziatore cationico responsabile della polimerizzazione e del doping primario del polipirrolo. Il sensore risultante è nella forma di film polimerico con uno spessore di circa $200\,\mu\mathrm{m}$ sopra al quale vengono depositati gli elettrodi costituiti da $5\,\mathrm{nm}$ di cromo e $50\,\mathrm{nm}$ di oro tramite un processo di sputtering. Si tratta quindi di campioni *self-standing* flessibili che non necessitano il supporto di un substrato, a differenza della prima categoria. La flessibilità è raggiunta grazie alle proprietà fisico-chimiche della matrice. Infatti queste resine presentano delle temperature di transizione vetrosa molto base al di sotto degli $0\,^{\circ}\mathrm{C}$. In questo modo i polimeri sono nel loro stato gommoso a temperatura ambiente e la mobilità delle catene permette una buona flessibilità.

Una volta terminata la fabbricazione di questi dispositivi elettronici, i sensori sono stati testati elettricamente nel laboratorio del centro di ricerca dell'IBM con un sistema realizzato in casa per produrre e fornire al campione determinate concentrazioni di gas in modo controllato ed affidabile. Nel sistema, composto da diversi tubi che formano una linea per la distribuzione del gas quasi perfettamente stagna, un flusso di aria secca è utilizzata sia come gas carrier che come gas di diluizione e proviene dalla fonte generale di aria compressa del laboratorio. Il flusso principale è diviso in due getti regolati dalla presenza di due Mass Flow Controller forniti dalla MKS e chiamati MFC Solvente e MFC Carrier. Il fluso di aria secca, controllato dal MFC Solvente, scorre dentro un tubo di PE collegato ad una camera termostatica composta da un gorgoliatore situato dentro un contenitore Dewar, usato per mantenere la temperatura costante. Il gas carrier fluisce dentro il gorgoliatore, riempito con il composto organico volatile da testare, generando un flusso di vapore saturo. Due micro-valvole permettono la ricombinazione del flusso di vapore saturo con il flusso di aria secca pura, che arriva dal secondo tubo controllato dal MFC Carrier. In questo modo vi è un processo di diluizione e, all'intersezione dei due tubi, si forma un flusso omogeneo della concentrazione voluta. Grazie ad una terza valvola meccanica, il flusso generato è immesso nella camera di rilevamento, dove è situato il sensore. Una volta entrato nella camera, il gas interagisce con il campione e, infine, viene coinvogliato nella linea dei gas esausti.

Tutti gli esperimenti sono stati eseguiti testando cinque analiti diversi: acetone, etanolo, isopropanolo, toluene e vapor acqueo. Naturalmente questi solventi presentano pressioni parziali diverse calcolate tramite la legge di Antoine. Inoltre, per ampliare le concentrazioni (in ppm) utilizzabili per testare i campioni, sono stati utilizzati diversi bagni di raffreddamento. I test sono stati performati a temperatura ambiente ($19\,^{\circ}\mathrm{C}$), a $0\,^{\circ}\mathrm{C}$ mediante un bagno di ghiaccio e a $-45\,^{\circ}\mathrm{C}$ ottenuti con una soluzione di acetonitrile e ghiaccio secco. In questo modo, abbasando la pressione parziale dei solventi, è stato possibile mirare a concentrazioni di gas più basse nell'ordine di qualche ppm.

In questo sistema di caratterizzazione, un componente fondamentale è rappresentato dalla *Polymer Chamber*. Grazie a questo assemblato realizzato in acciaio inox prodotto da IBM, è possibile monitorare il cambiamento della resistenza elettrica in funzione del tempo. Per quanto riguarda i campioni fotopolimerizzati in situ, il contatto è stabilito per mezzo di due molle metalliche toccanti gli elettrodi del campione. Viceversa, i dispositivi situati sul substrato vengono collegati alla camera per mezzo di pogo-pins. In entrambi i casi viene eseguita una misura a due punte, dove una è utilizzata per applicare il voltaggio e l'altra è usata come ground. Un Keithley model 6430 Source Meter® viene utilizzato per applicare una tensione di $100\,\mathrm{mV}$ e allo stesso tempo per misurare la corrente che attraversa il campione. Durante l'esperimento, i dati acquisiti dal Keithley vengono automaticamente salvati su di un personal computer e processati da un programma scritto con Python che plotta in tempo reale l'andamento della corrente, la quale è strettamente legata alla resistenza elettrica tramite la prima legge di Ohm.

Ogni volta che un sensore entra nel *Sensor Lab*, vi è un ben preciso protocollo da utilizzare per la caratterizzazione elettrica, in modo da riprodurre i test nello stesso modo rendendo i risultati confrontabili. Dopo essere stato prontamente registrato in modo da poter seguire tutti gli step successivi, la resistenza elettrica viene misurata tramite un Fluke 177 Digital Multimeter. Questo strumento presenta un limite superiore di $50\,\mathrm{M\Omega}$. Successivamente, i dispositivi a base di carbon black disposti sul campione vengono incisi in modo da isolare i singoli sensori all'interno dello stesso campione. In questo modo è stato possibile eliminare una o più resistenze parassite in parallelo con i sensori. La reisitenza viene dunque misurata una seconda volta e generalmente risulta aumentata. A questo punto il campione è inserito nella camera di rilevamento e le rispettive resistenze vengono misurate una terza volta per controllare il contatto elettrico all'interno della camera. Successivamente, il campione è stabilizzato introducendo un flusso di aria secca. La durata di questo passaggio può variare da trenta minuti a più di un ora in base alla natura del campione. Infatti, i campioni polimerici in generale sono molto influenzti dall'umidità e presentano un drift considerevole della resistenza elettrica anche senza la presenza di alcun analita. È abbastanza evidente che maggiore è il drift e più instabile è il film. Una volta raggiunta una baseline della corrente e della rispettiva resistenza elettrica, la misurazione può iniziare. $100\,\mathrm{mV}$ sono applicati fra gli elettrodi del campione e la corrente viene monitorata come output. Per ciascun test il campione viene esposto a 100 secondi di aria secca per raccogliere i dati della baseline; successivamente il sensore è travolto dal flusso di gas da analizzare nella concentrazione desiderata per 600 secondi, seguiti da altrettanti secondi fissati come tempo di recupero in cui il gas viene rimosso e aria secca viene introdotta nuovamente per permettere al film di ricoverare. In questa fase la corrente approcia nuovamento il valore della baseline iniziale in poche decine di secondi.

Invece l'impedance analyzer è stato utilizzato per caratterizzare elettricamente i sensori in AC. In questo modo è stato possibile acquisire maggiori informazioni dalle singole misure poichè questo strumento permette di misurare la parte reale ed immaginaria dell'impedenza insieme al suo modulo e alla sua fase. Effettuando diverse sostituzioni e usando ben note relazioni è possibile correlare tutti questi parametri alla resistenza e alla capacità del film. Infatti, nel regime di corrente alternata, questi sensori possono essere ben rappresentati da un circuito elettrico equivalente costituito da una resistenza in parallelo con una capacità. Le misure effettuate possono essere di tipo statico o di tipo dinamico. Le ultime permettono di seguire il comportamento della resistenza e della capacità del campione in tempo reale per un range di frequenze limitato in un range da $40\,\mathrm{Hz}$ fino a $10\,\mathrm{MHz}$. Tuttavia questo tipo di analisi non è risultato molto soddisfacente per via di alcune limitazioni imposte dal sistema. L'altro tipo di analisi consiste invece nella misurazione di tutti i paramentri rilevanti per l'intero spettro delle frequenze che va da $40\,\mathrm{Hz}$ a $110\,\mathrm{MHz}$ nelle tre configurazioni di equilibrio ragiunte dal sensore: ambiente con aria secca, ambiente con il gas da testare e ambiente in aria secca successivo all'esposizione del gas. In questo modo i risultati vengono mostrati attraverso il grafico di Nyquist, dove sull'asse delle ascisse viene collocata la parte reale dell'impedenza e su quella delle ordinate la parte immaginaria per tutte le diverse frequenze. Il tipico grafico che si ottiene per il circuito RC è una semi-circonferenza in cui la resistenza del film può essere ricavata dalla parte reale dell'impedenza a basse frequenze e la frequenza del picco della curva rappresenta la frequenza di risonanza.

Per quanto riguarda la prima categoria di sensori studiati, l'analisi ha dovuto tenere conto della molteplicità dei parametri variabili e quindi si sono studiate le performance dei sensori mutando una variabile e mantenendo costante le altre. Per ottenere la miglior risposta elettrica i sensori devono contenere la giusta quantità di filler conduttivo. La conduttività in funzione della concentrazione di carbon black è ben descritta dalla curva di percolazione. L'andamento di questa curva è di tipo sigmiodale a soglia. A basse quantità di filler, i compositi sono isolanti perchè non esistono cammini conduttivi formati dalle diverse particelle tra gli elettrodi. Man mano che la concentrazione aumenta, avviene una transizione molto netta dove la resistività del composito può diminuire di diversi ordini di grandezza per piccole variazioni della quantità di carbon black. A questo punto di transizione, designato come soglia di percolazione, le particelle conduttive si trovano alla giusta distanza per formare dei cammini in cui gli eletronni possono muoversi, producendo una corrente. In questa regione il rigonfiamento della matrice risulta essere massimizzato e questo significante cambiamento di resistenza porta ad avere le miglior risposte in termini di sensitività.

Per entrambi i carbon black testati (Vulcan XC72 e Black Pearl 2000) la soglia di percolazione si colloca tra il 15 wt% e il 25 wt%. Il Black Pearl 2000 è più conduttivo e la caduta della curva di percolazione è più ripida; il Vulcan XC72 presenta invece una miglior facilità di lavorazione sia durante la preparazione della sospensione del carbon black che nel flow coating. Inoltre, rispetto al primo, quest'ultimo ha una miglior sensitività verso l'etanolo in qualsiasi concentrazione del filler. I risultati ottenuti confermano quanto prospettato in teoria: la sensitività risulta maggiore quanto più la concentrazione di carbon black si avvicina alla regione di percolazione. In aggiunta, la risposta di questi dispositivi migliora all'aumentare della concentrazione dell'analita testato. Infatti, meno molecole sono presenti nella camera di rilevamento, minore sarà l'adsorbimento e minore sarà il contributo del rigonfiamento della matrice. La miglior efficienza si ottiene quando i sensori hanno una resistenza elettrica nell'ordine del $\mathrm{k}\Omega$.

Per quanto riguarda la geometria degli elettrodi, si è dimostrato che questa variabile influisce sulla conducibilità e non sulla sensitività. Infatti, la resistenza aumenta linearmente al crescere della distanza fra gli elettrodi, mentre la risposta elettrica rimane costante.

Questo studio ha anche permesso di individuare un risultato interessante: il limite inferiore di rilevamento è molto basso e ciò consente di utilizzare questi sensori per applicazioni dove è necessario rilevare decine di ppm di un determinato gas. Si è potuti giunger a questa conclusione testando un sensore formato da un copolimero a blocchi PS/PDMAEMA con una concentrazione di carbon black del 35 wt%. Questo sensore è stato caratterizzato molteplici volte con diverse temperature e diversi flussi di gas di vapor saturo.

È stato inoltre dimostrato il ruolo del polistirene (PS) come stabilizzatore universale poiché, in diversi rapporti con un'altra unità ripetitiva, aiuta la dispersione del carbon black dentro la soluzione polimerica.

In fine, una criticità di questi sensori è rappresentata da una selettività solo parziale. Tuttavia, sintetizzando polimeri con gruppi funzionali diversi, è possibile osservare risposte differenti al contatto con vari gas, specialmente discriminando tra vapori di solventi polari e non polari. Si è osservato che i campioni costituiti da PS e da PS/PMAA hanno una sensitivtà maggiore verso l'acetone, mentre i copolimeri PS/PDMAEMA presentano una miglior risposta verso l'etanolo. Questi risultati possono essere spiegati dal fatto che i primi due polimeri interagiscono meglio con l'acetone in quanto sono entrambi non polari. Inversamente, l'etanolo con il suo gruppo OH polare forma legami ad idrogeno con l'ossigeno e i gruppi amminici del PDMAEMA, presentando cosi un'affinità maggiore ed interazioni pi'Íforti. In generale si vale la regola: "*Similia similibus solvuntur*".

Apparentemente, i risultati ottenuti dai sensori a base polipirrolo non sembrano soddisfacenti, anche se non devono essere considerati come definitivi. Nel presente studio si sono incontrate numerose difficoltà sia riguardo il funzionamento dei campioni che sul modo di caratterizzazione elettrica in AC effettuato tramite lutilizzo di un impedance analyzer e dei suoi relativi cavi che contribuiscono in maniera significativa sui risultati. Questi dispositivi hanno mostrato una difficile riproducibilità nella loro fabbricazione e risposte elettriche differenti a medesimi test. Sono risultati inoltre scarsamente stabili, mostrando un drift della resistenza elettrica anche senza la presenza di alcun analita e altamente influenzati dallumidità. La ragione per cui questi film polimerici non rispondono in modo adeguato potrebbe essere legata al fatto che la loro resistenza è superiore ai $50\,\mathrm{M\Omega}$. Sarebbe molto interessante aumentare la concentrazione di polipirrolo che era fissata al 5 wt% in modo da abbassare la resistenza e migliorare la conducibilità e la stabilità.
Riguardo i campioni con i MWCNT, è stato effettuato uno studio approfondito sulla selettività, testando cinque diversi analiti (acetone, etanolo, isopropanolo, toluene e vapor acqueo) in concentrazioni diverse tramite analisi in DC e in AC. Da questi dati è stato possibile osservare risposte diverse verso i vari gas. I risultati ottenuti sono consistenti per entrambi i tipi di analisi e si può affermare che la selettività ottenuta è dovuta ad entrambe le interazioni del gas analita con la matrice e con la superficie dei nanotubi di carbonio.

In conclusione, i sensori polimerici sono molto promettenti poiché possono essere facilmente modificati e personalizzati per tutte le esigenze. Cambiamenti nella struttura dei film possono influenzare e controllare le interazioni che avvengono tra le molecole di gas e il materiale attivo. La morfologia, la composizione, la solubilità ed altre proprietà sono fortemente legate alle performance di questi sensori. L'obiettivo finale futuro è quello di creare una matrice di sensori polimerici per lo sviluppo di un naso elettronico in grado di rilevare determinati gas a concentrazioni molto basse, dando unimpronta digitale che può essere univocamente identificata da un algoritmo di riconoscimento del pattern ottenuto.

Chapter 1

Introduction

Smelling is the most mysterious and complex sense and its experience is so potent that it is anchored by a long buried memory that is gradually brought to the surface of consciousness. A well-known idea, called the "Proustian phenomenon", proposes that distinctive smells have more power than any other sense to help us recall distant memories. The theory is named after the French writer Marcel Proust, who described a vividly recalling long forgotten memory from his childhood after smelling a tea-soaked madeleine biscuit. In his novel "*À la recherche du temps perdu*" he wrote: "*When from the distant past nothing remains, after the beings have died, after the things are destroyed and scattered, still, alone, more fragile, yet more vital, more insubstantial, more persistent, more faithful, the smell and taste of things remain poised a long time, like souls, ready to remind us, waiting and hoping for their moment, amid the ruins of everything else; and bear unfaltering, in the tiny and almost impalpable drop of their essence, the immense architecture of memory.*" A soft and delicate fragrance is enough for the nose to find a way in the memory and the past becomes present. Human beings do not recognize the odor of things, but the brain recalls the pattern related to the memory of that particular smell.

The above introduces the topic of this thesis, which aims to illustrate the results of the development, fabrication and electrical characterization of polymeric vapor sensors. This study was a joint program between Politecnico di Torino and IBM Research Center in Almaden, in the frame of the Gas Sensors Project.

1.1 Gas Sensor Project

The human nose has been exploited as an analytical tool in many fields. It is commonly used for assessing quality through odor and this is carried out using sensory panels, where a group of people fills out questionaries on the smell associated with the substance being analyzed.
In order to achieve better consistent results and accuracy, human panels are often complemented with gas chromatography and mass spectrometry analysis (GC/MS). However, they present many limitations. Panelists may be subjected to individual variability, fatigue with the process of testing and influenced by physical and mental health. Furthermore, they can't be exposed to hazardous or toxic compounds. Analytical traditional techniques, on the other hand, are very expensive, high power and high vacuum, time-consuming, require extensive personnel training and are seldom used on the field for real time monitoring because of their considerable dimensions (Arshak et al., 2004).
The solution to the shortcomings of sensory panels and the associated analytical techniques is the electronic nose. Thanks to today's new technologies, this electronic device is able to perform real time measurements at a specific site in the field over hours, days and weeks. It is inexpensive, low power, reliable, fast, lightweight and, above all, portable and simple in concept (Nagle, Schiffman, and Gutierrez-Osuna, 1998).

The idea of an electronic system that can measure odors was first published by Hartman (1954) and Wilkens and Hartman (1964). Only in 1982, Persaud and Dodd introduced the concept of a "smart device" able to detect and identify different analytes through a chemical sensors array system. Later, in 1988, the term "electronic nose" was coined by Gardner, who defined it as *"an instrument which comprises an array of electronic chemical sensors with partial specificity and an appropriate pattern recognition system, capable of recognizing simple or complex odors"* (Gardner, 1988; Gardner et al., 1990; Gardner and Bartlett, 1999).
Unlike conventional chemical sensors, which use a single sensing element for the detection of a single analyte, an electronic nose is composed of a sensors array of overlapping sensitivity and selectivity. The strict "lock-and-key" design of traditional sensing mechanism is abandoned. The reason of utilize multiple sensors instead of a single one is inspired by the superb performance of the biological olfactory

systems in odor detection, identification, tracking and location tasks (Albert et al., 2000).

There are different steps that characterize how the human nose works. The perception of odors begins with sniffing, which brings air samples that contain odorant molecules into the turbinates. These last create turbulent airflow patterns that allow the mixture of volatile organic compounds (VOCs) to reach a thin mucus layer coating the olfactory epithelium. Inside the epithelium there are specialized neurons responsible to detect odor gases through the binding of the molecule of the odorant with the receptor proteins. There are more then 100 million protein receptors of about 1000 different types (Nagle, Schiffman, and Gutierrez-Osuna, 1998). The cells respond by transmitting signals first to the olfactory bulb and then higher up in the brain, that represent the central odor information processing center. These receptors are not highly selective toward one analyte only; in fact, one receptor is sensitive to many analytes. Therefore, it is the pattern of responses that the brain interprets and recognizes from past training (Gardner et al., 1990).

Likewise, the cross-reactive sensors array respond in concert to a given odor and the combinations of all the single outputs generate a pattern, called fingerprint, that is unique for that specific analyte or mixture of gases (Fig. 1.1). This univocal correspondence allows to identify and categorize odorants by processing a pattern recognition engine (Fig. 1.2). This system utilizes different algorithms and analysis like principal components analysis (PCA) and linear discriminant analysis (LDA).

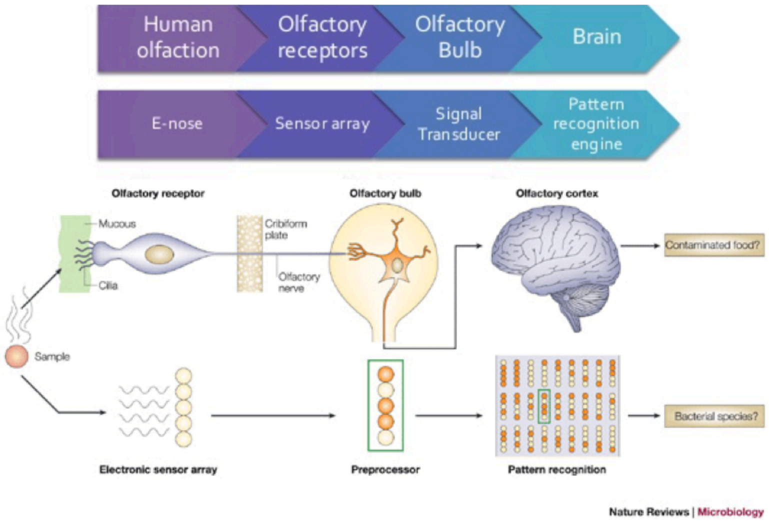

FIGURE 1.1: Comparison between the human olfactory system and the electronic nose. *Adapted from: Nature Reviewes-Microbiology.*

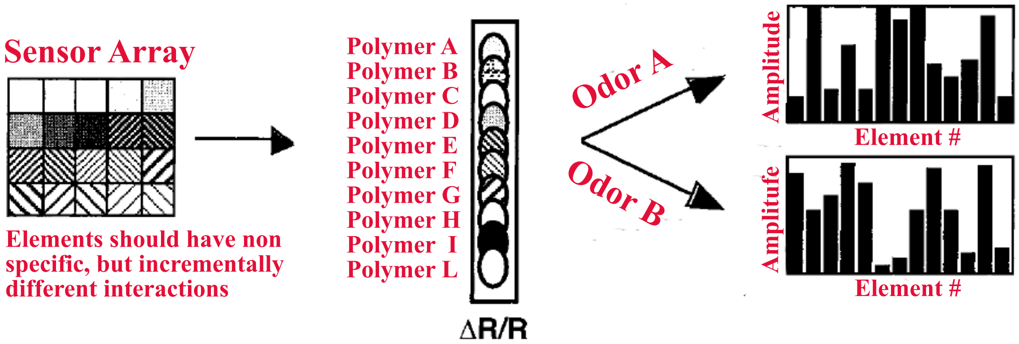

FIGURE 1.2: The response of a sensors array generates different fingerprints of different odors. *Adapted from: Albert et al., 2000.*

There are many present and potentially exciting applications in a variety of different fields where the e-nose can have an important impact due to its portability, fast response, selectivity towards different gases and sensitivity to low concentrations. It has been tested in all the fields where odors and gases can play a key role (Potyrailo, 2016). In particular, it can be helpful in the food and beverage industries, where quality control is needed to avoid contaminations and infections; it is useful for test freshness and monitoring the variations occurring in fresh fruits and vegetables after harvest (Di Natale et al., 2001; Concina, Falasconi, and Sberveglieri, 2012). It can be useful to scan an indoor environment to check the air quality (Zhang et al., 2012; Leidinger et al., 2014), or it could detect hazardous or toxic gases (Wilson, 2012).

Many researches pointed out the effectiveness of the electronic nose in the healthcare as a novel diagnostic tool based on the chemical information contained in the exhaled volatile (Di Natale et al., 2003).

Different companies are trying to miniaturize these sensors in order to integrate them into smartphones. In this way wireless gas detection with a smartphone via rf comunication will be possible (Azzarelli et al., 2014).

There are also applications for military scopes: the sensors array may be a promising alternative to sniffer dogs for detecting buried landmines and explosive traces (Goschnick and Harms, 2002).

Not less important are aeronautic and space applications in the areas of interest that include vehicle safety monitoring, emission monitoring and fire detection (Hunter et al., 1998).

The interest in electronic nose technology has increased exponentially and today many devices are available. However, there are some limitations and the price is still very high, ranging from 20.000 $ up to 100.000 $. In order to be more competitive, high-tech companies are trying to exploit the latest technology advances to improve electronic noses, making them smaller, faster and cheaper (Chiu and Tang, 2013).

One of the main high-tech companies that is working on this project is IBM, well-known all over around the world. In the facility of IBM Research Center in Almaden (California), the Nanofabrication group is pursuing the aim of implementing a working smart device composed of in-house made chemical sensors, able to detect different analytes.

As mentioned before, the realization of such a sensors array is very complex and it requires scientists with different backgrounds. Therefore, in order to achieve the common goal, the Sensor Group is made of people with different expertise. Chemists and materials engineers are trying to develop new synthesis techniques and novel materials that can have the best sensing performances. Their focus is on two main categories: organic sensors based on polymeric composites and inorganic ones, based on metal oxide semiconductors (MOS). The attention is put on the understanding of the working principles and the interactions between the gas and the material. Various systematics have been studied in order to find relationships between physical, chemical, and electrical properties that are key in the context of sensing performance.

Electronic engineers work on the electric circuits and digital apparatus needed for the acquisition of the raw data from the sensors (Chiu and Tang, 2013).

Finally, once the output data are pre-processed, data analysts and computer science engineers compile algorithms in order to identify univocally the fingerprint of an unknown mixture of gases. Only the union and harmony amid these different competences can lead to successful results.

1.2 Fundamental Parameters: the 3 "S"

As we mentioned before, the development of miniature and portable gas sensors able to detect gas analytes in real time with good sensing performances will significantly change our daily life. The materials used act as chemiresistive gas sensors, so that transform the concentrations of analytes to detectable physical signals. Having the best performances can be translated with the optimization of the three main requirements that are set for any kind of sensors: the three “S’s”, which are sensitivity, selectivity and stability.

Sensitivity is an absolute number describing the response of a sensor to a given analyte or environment. Fundamentally, it represents the goodness of the response associated with the output change for a change in the input. It shows the degree to which the response rises as the concentration of the analyte increases. The higher is the sensitivity, the better is the response with a low signal-to-noise ratio and the easier will be the detection of a small fraction of the gas. This parameter is of an essential importance because it is related the lowest detectable limit.

Secondly, selectivity plays a crucial role in sensors. It is the ability of discriminate between different gases or odors. In order to build an electronic nose, it’s indispensable to fabricate sensors which give different responses toward a specific gas. Even if some overlapping on the sensing is required, the goal is to have a sensor that respond to various gases in different ways. For this reason when it comes to a sensors array, each single device is chosen carefully to widen the range of detectable gases. Selectivity can be improved by modifying the functional groups present at the surface, working on the affinity between the gas and the substrate during the interactions (Pearce et al., 2004).

Last but surely not the least, stability shows how rapidly the device will deteriorate in the environment, reducing its sensing properties. Basically, it tells the number of cycles, and so the lifetime, a sensor can undergo. If the stability is poor, maintenance and recalibration are required more often and costs become relevant due to the high replacement frequency.

Not less important are the response and recovery times. The first one refers to the time the sensor needs to be exposed to the odorant in order to show the change of its physical properties. The latter is the time it takes the sensor to return to its original baseline before it was exposed to the analyte (Arshak et al., 2004).
On the above mention requirements, there is none that prevails on the others. As a function of the ultimate application, the manufacturer have to find a trade-off between them, deciding whether it is better to be able to detect very low concentrations or increasing the lifetime as well as having a specific response towards various

chemical compounds. All these details have to be taken carefully into account when considering the choice of a gas sensor.

1.3 Overview on Gas Sensors

On the market, there are many different e-noses based on the type of gas sensors utilized. Despite their differences, the main working principle is the same for all of them. After the exposure to the vapor to detect, the active sensing material of the sensor interacts with the analyte, either by chemisorption or physisorption, which causes its physical properties to change. The interactions between the analytes and the sensing materials are multiform, according to different analytes and different active materials. According to the typology of the physical change, it is possible to categorize these smart devices in: conductivity sensors, piezoelectric sensors, MOSFET sensors and optical sensors as it is shown in the Table 1.1 (Arshak et al., 2004).

TABLE 1.1: Physical changes in the active film and the sensor devices used to transduce them into electrical signals.
Adapted from: Arshak et al., 2004.

Physical Changes	**Sensor Devices**
Conductivity	Conductivity Sensors
Mass	Piezoelectric Sensors
Work Function	MOSFET
Optical	Optical Sensors

1.3.1 Conductivity Sensors

At IBM Research Center the main focus of the Sensor Group is to implement an electronic nose based on conductivity sensors. Metal oxide semiconductors, conducting polymer composites and intrinsically conducting polymers (ICP) are three of the materials most commonly utilized of this class. Even if the sensing mechanism is different for the three cited materials, the working principle behind them is the same. Indeed, they are also called chemiresistors because, after the adsorption of the gas on the sensor′s surface, they base their detection on an electric resistance variation, which is usually seen as a change in the output current.

Of the two types, MOS sensors represent the most mature class and they are normally made of oxides of tin, zinc, iridium and titanium (n-type) or tungsten and cobalt (p-type). These kinds of sensors are often doped with a noble metal catalyst (Pt or Pd) in order to improve their stability. The change in resistance is due to reactions that occur between the analyte and the oxygen present in the atmosphere that has been adsorbed on the MOS surface as O^-, O_2^-, O^{--}. The oxygen adsorption generates a space-charge layer on the surface of each SnO_2 grain, leading to a potential barrier to conduction at the grain boundary. In this case, the resistance of the material increases because the electrons are trapped by the oxygen species and they can't give their contribution to the conductivity. When the device is exposed to vapor, it reacts with the oxygen species and it can free or trap electrons from the MOS surface, depending on the nature of the gas to detect. In the case of n-type materials, reducing gases will increase the conductivity by releasing electrons, while oxidizing gases will lower the conductivity by trapping more of them. Usually, n-type semiconductors are used for the detection of reducing gases, while the p-type metal oxides are exploited for the sensing of oxidizing species (Albert et al., 2000).
Normally, the active material is deposited between interdigitated electrodes, which permit the electrical connection in order to measure the change in resistance, as shown in Figure 1.3. In order to be very efficient, MOS sensors need to work at high temperatures (200 °C up to 400 °C) so that a heater is required during the measurements.

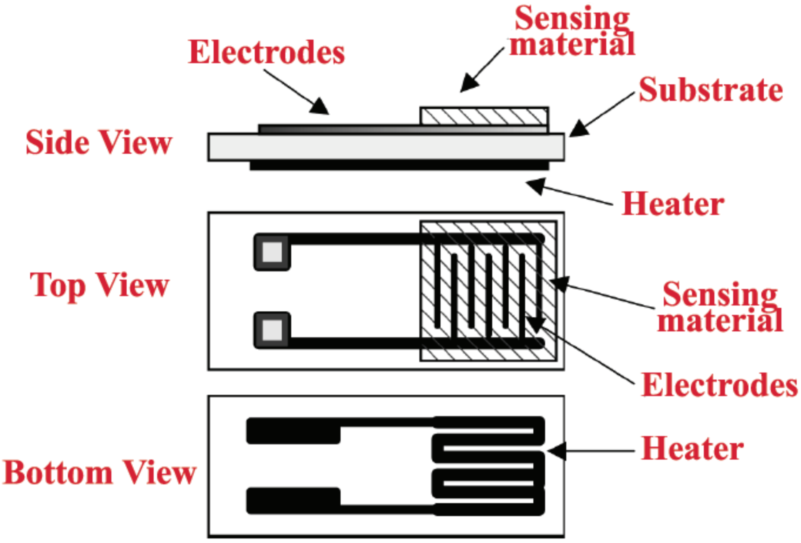

FIGURE 1.3: Typical structure of MOS sensors.
Adapted from: Arshak et al., 2004.

In this section the other categories of conductivity sensors are briefly discussed because more emphasis and more details will be given in Chapter 2, where all the polymer sensors are presented. The ICP, that are normally insulator, are made electrically conductive by a doping effect on the linear backbones, composed of the alternation of single and double bonds. The structure is obtained by repeating conjugated organic monomers. The conducting polymers can be n-type or p-type, depending on the kind of doping that increases either the mobility of the holes or of the electrons (Muñoz, Steinthal, and Sunshine, 1999). The operation of these devices is based on a charge transfer process where conductivity is affected by the reactions that occur between the VOCs and the active material. Donation or withdrawal by the analyte vapors of the charged carriers leads to conductivity changes in the sensor films, in addition to the polymer doping by counter ions before gas exposure. Different changes in resistance are related to the nature of the gas or vapor and its ability to reduce or oxide the film.

In conducting polymer composites, the sensor element is built from a film developed using either polypyrrole (PPy) or carbon black (CB) as a conductive filler homogeneously dispersed in a non-conductive organic polymer matrix. The film is deposited across two metal electrodes placed on a silicon substrate (Fig. 1.4).

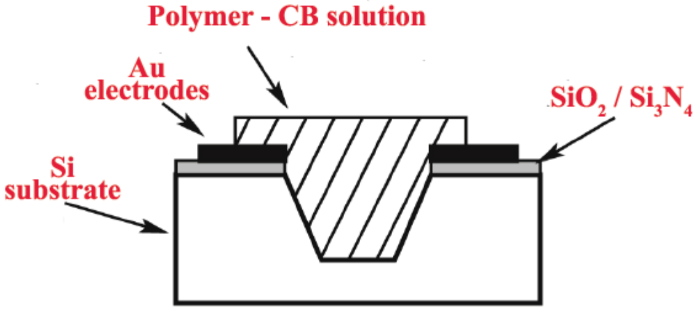

FIGURE 1.4: Typical structure of polymeric sensors.
Adapted from: Arshak et al., 2004.

The main sensing mechanism for this type of sensors is the swelling of the matrix and it is well-described on the basis of percolation theory. Conducting paths are formed inside the composite due to quantum mechanical tunneling effect, where the distance between the filler is such that electrons hopping can occur. The swelling of the polymer due to absorption of organic vapors may also increase the volume and thus increase the distance between particles, decreasing the conductivity of the films. It is a reversible process, where the solubility of the polymer in the solvent and the affinity between the matrix and the variety of analytes through different functional groups play an important role. The transduction mechanism of the PPy composites, on the contrary, is more complex because the swelling of the matrix is in convenient or disadvantageous competition with the aforementioned charge transfer process, related to the intrinsic conductivity of the polypyrrole. Both the insulating matrix and the conductive filler interact with the vapor that needs to be analyzed (Albert et al., 2000; Muñoz, Steinthal, and Sunshine, 1999).

Each typology of this class of sensors has different advantages and drawbacks. One is preferred respect to the other depending on the final application. Conducting polymers possess several potential advantages because they are inexpensive and easy to process. In fact, in many applications ceramic-based sensors can't be exploited because of their high cost multi-step fabrication process and high temperature treatments. In addition, because of the wide range of polymers available, they can be tailored with adjustable properties such as flexibility as opposed to the MOS. Another important feature that affects the power consumption is the operating temperature. While metal oxides sensors require a heater to reach temperatures in the range of $200\,^{\circ}\mathrm{C}$ up to $400\,^{\circ}\mathrm{C}$ to work properly (Fine et al., 2010), polymeric sensors operate at room temperature (Röck, Barsan, and Weimar, 2008). A direct consequence is the reduction of the possible applications of the MOS due to the fact that not all environments can withstand such temperatures. Additionally, polymer composites do not suffer from sulfur poisoning like metal oxide semiconductors (Nagle, Schiffman, and Gutierrez-Osuna, 1998). However, MOS have a higher sensitivity and faster response and recovery times compared to the polymer composites. They are able to detect much lower concentrations of analytes. The main drawback of conducting polymer sensors is their higher sensitivity towards water vapor. This feature makes them susceptible to humidity and it might mask the response to some volatile organic compounds. Today it's very difficult to control humidity and almost everywhere water vapor is in the air in different percentage, reducing the possible applications (Chiu and Tang, 2013). Both polymeric and metal oxide sensors exhibit a undesirable instability. In fact, they drift over time even without the presence of any vapors.

1.3.2 Piezoelectric Sensors

Another class of smart devices that can be used to engineer an electronic nose takes advantage of the piezoelectric effect: materials produce a voltage when mechanical stress is applied, and conversely will deform if a voltage is applied across them. In gas sensing there are two different types of devices that work on this principle, where a change on the mass of the piezoelectric sensor coating due to the gas adsorption results in a change in the resonant frequency (Albert et al., 2000). The surface acoustic wave (SAW) and quartz crystal microbalance (QCM) sensors are the most commonly employed.

As you can see from the Figure 1.5, in the SAW devices there are an input and an output transducers deposited on top of a piezoelectric substrate, normally made of ZnO, $LiNbO_3$ or quartz. The active layer that lies between the transducers is generally a polymer or a liquid crystal. When an AC signal is applied to the input, the electrical signal is traduced in an acoustic wave that surfs over the piezoelectric substrate with a frequency in the range between 100 MHz and 400 MHz (Pearce et al., 2004; Khlebarov, Stoyanova, and Topalova, 1992). Because of the adsorption of the gas in the membrane, the frequency is shifted. The change in frequency, as already said, is directly related to the change in mass.

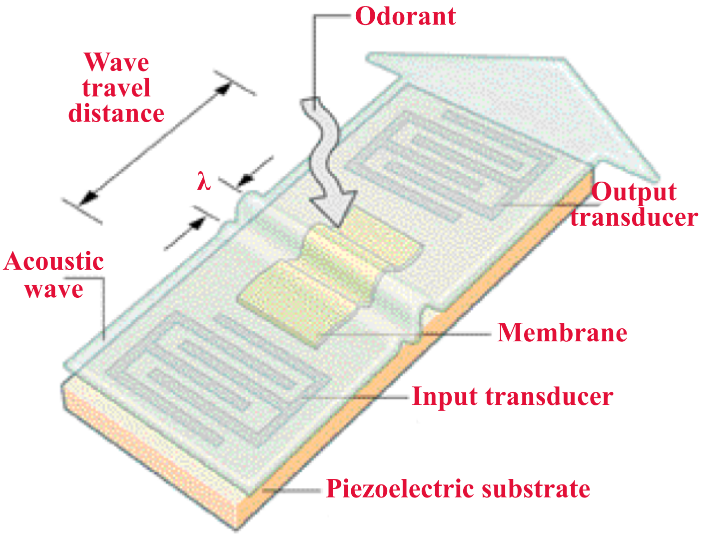

FIGURE 1.5: Typical structure of SAW sensors.
Adapted from: Nagle, Schiffman, and Gutierrez-Osuna, 1998.

The working principle of the QCM and SAW is the same but, while in the SAW the acoustic wave propagates along the surface of the sensors, the QCM produces a wave that travels through the bulk of the sensors. The QCM is made of a quartz resonating disk covered with a polymer that represents the sensing material and connected to two electrodes, one on each side. When the sensor is exposed to the gas, the specific resonant frequency of the quartz, set between 10 MHz to 30 MHz (Schaller et al., 2000) is altered and the increase of mass corresponds to a shift in the resonant frequency, which is directly correlated to the amount of gas collected on the surface by Sauerbrey equation (Fig. 1.6).

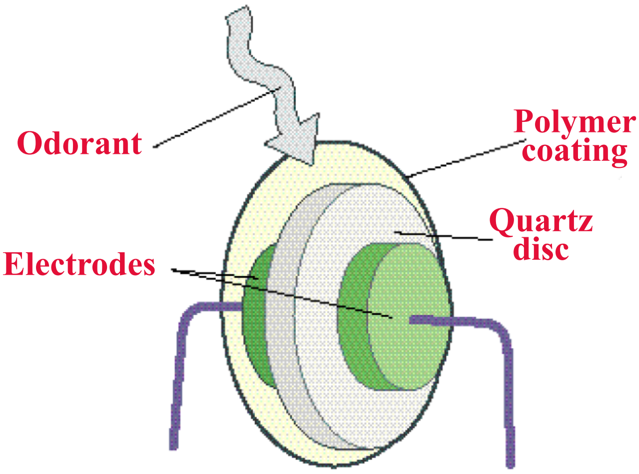

FIGURE 1.6: Typical structure of QCM sensors.
Adapted from: Nagle, Schiffman, and Gutierrez-Osuna, 1998.

Both of them share the same advantages and drawbacks. They can detect low concentrations because they have quite high sensitivities and the response time is very fast as well as the availability of multiple polymer coatings. At the same time, they aren't so commonly used in e-nose due to the expensive and complex interface circuitry, lack of batch to batch reproducibility and very poor signal-to-noise ratio due to the high frequencies of the signal.

1.3.3 MOSFET Sensors

The metal oxide semiconductor field effect transistors (MOSFET) structure consists of a catalytic metal gate on top of an insulator layer and a p-type substrate with two n-doped regions called source and drain (Fig. 1.7). The catalyst-coated gate must be porous because it allows the diffusion of the gas at the metal-insulator interface. The physical property that is measured is the change in the work function. In fact, in order to maintain a constant surface potential, the applied gate voltage must be tuned in relation to the change in the work function due to the interaction and chemical reactions that occur between the volatile compounds and the catalyst-coated gate. The reaction products alters the gate charge, modifying the conducting channel and, therefore, the drain-source current (Albert et al., 2000).

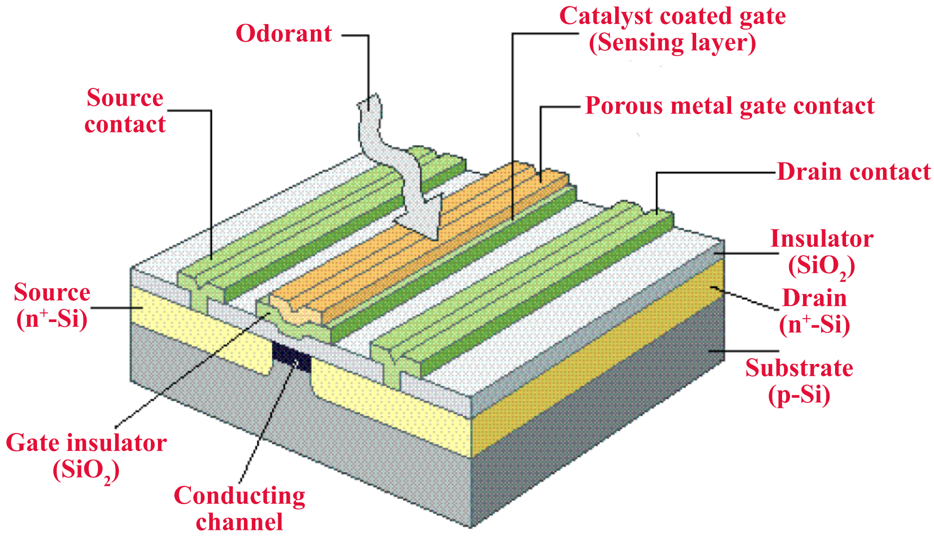

FIGURE 1.7: Typical structure of MOSFET sensors.
Adapted from: Nagle, Schiffman, and Gutierrez-Osuna, 1998.

The main advantages of MOSFET are the low cost, reproducibility from batch to batch and the possibility of being integrated directly on the circuit. However, as the conductivity sensors, they suffer of baseline drift and they need a controlled environment.

1.3.4 Optical Sensors

Considering a change in optical properties, another category for e-nose devices is the one of optical sensors. To exploit this technology, the typical device consists of an optical glass fiber coated on its sides with an active fluorescent dye dispersed in an organic polymer matrix (Fig. 1.8). A pulse of light with a specific wavelength and energy is forced to pass inside the fiber and propagates along it, interrogating the active layer, which is in contact with the different gases. Due to the interaction between the fluorescent material and the volatile compounds, there is an alteration in the polarity of the dye that leads to a shift in the fluorescent emission spectrum and a change in color. It's a powerful technique because it has the ability to obtain multiple information simultaneously, including fluorescence lifetime, the spectral shape, the wavelength and changes in intensity with a high accuracy and fast response. On the contrary, even if the different coatings are available with many different dyes, the fabrication process is expensive and the interface circuitry is quite complex. The stability is another drawback because the lifetime of these devices is reduced due to the photobleaching effect (Nagle et al., 1998).

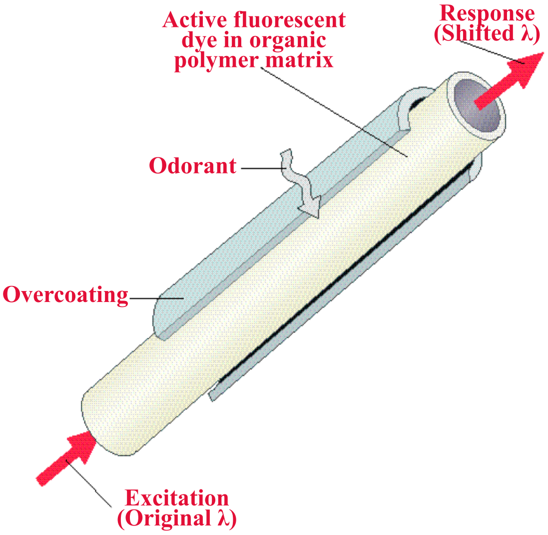

FIGURE 1.8: Typical structure of optical sensors.
Adapted from: Nagle, Schiffman, and Gutierrez-Osuna, 1998.

1.3.5 Spectrometry-based sensing methods

There are also other approaches to develop sensor arrays resulting in what may be called spectrometric pseudo-sensor arrays (Nagle, Schiffman, and Gutierrez-Osuna, 1998). Gas chromatography and mass spectrometry are part of this class. They provide very accurate measurements but the analysis are very slow and the size and complexity of the electronics for instrument control is very high. Not less important is the non-portability of these devices because they are used as laboratory analysis.

In conclusion, the following Figure 1.9 summarizes clearly all the properties of each sensors type reviewed for the implementation of a sensors array: from their working principles to the materials used and the points of strength and weaknesses.

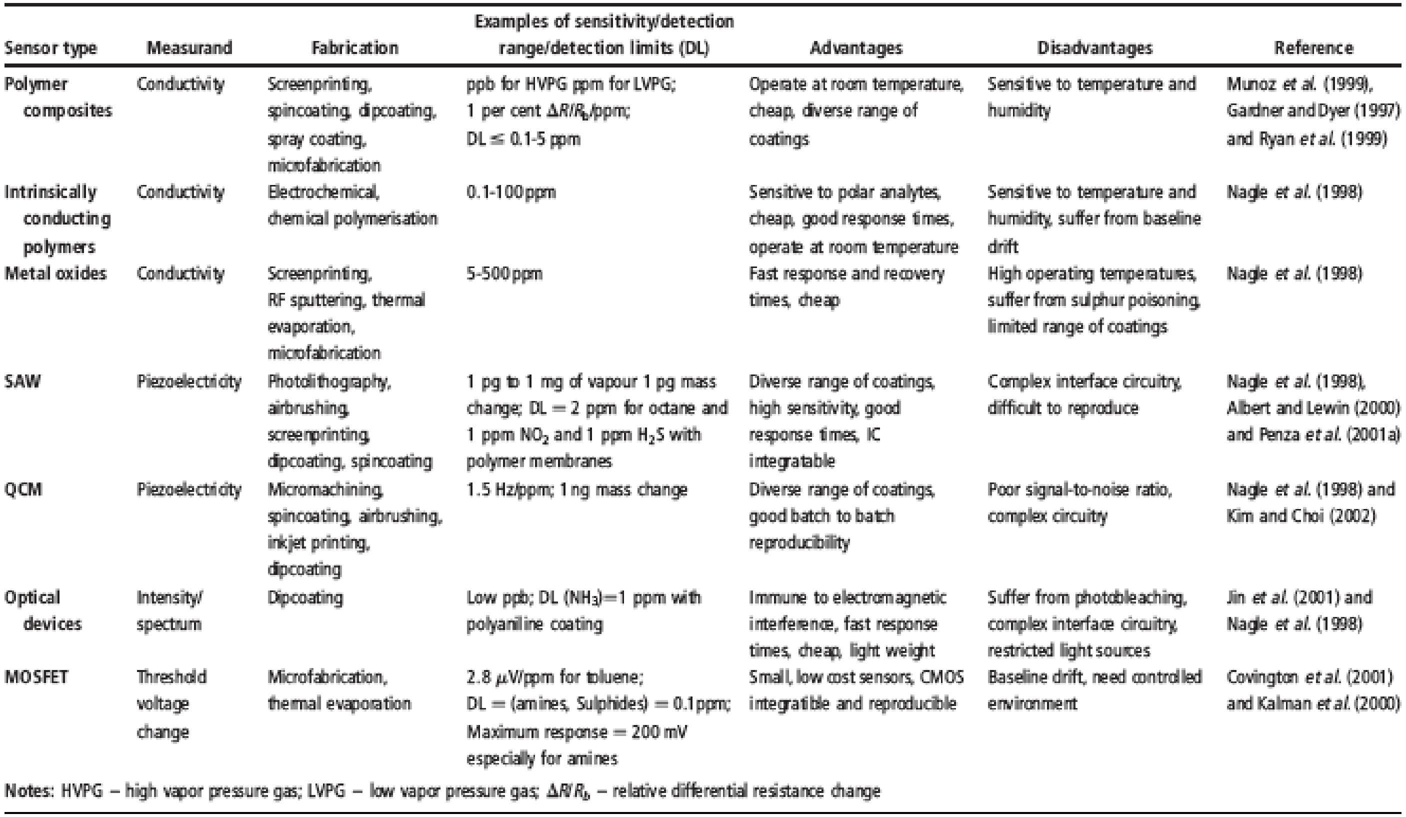

Sensor type	Measurand	Fabrication	Examples of sensitivity/detection range/detection limits (DL)	Advantages	Disadvantages	Reference
Polymer composites	Conductivity	Screenprinting, spincoating, dipcoating, spray coating, microfabrication	ppb for HVPG ppm for LVPG; 1 per cent $\Delta R/R_b$/ppm; DL ≤ 0.1-5 ppm	Operate at room temperature, cheap, diverse range of coatings	Sensitive to temperature and humidity	Munoz *et al.* (1999), Gardner and Dyer (1997) and Ryan *et al.* (1999)
Intrinsically conducting polymers	Conductivity	Electrochemical, chemical polymerisation	0.1-100 ppm	Sensitive to polar analytes, cheap, good response times, operate at room temperature	Sensitive to temperature and humidity, suffer from baseline drift	Nagle *et al.* (1998)
Metal oxides	Conductivity	Screenprinting, RF sputtering, thermal evaporation, microfabrication	5-500 ppm	Fast response and recovery times, cheap	High operating temperatures, suffer from sulphur poisoning, limited range of coatings	Nagle *et al.* (1998)
SAW	Piezoelectricity	Photolithography, airbrushing, screenprinting, dipcoating, spincoating	1 pg to 1 mg of vapour 1 pg mass change; DL = 2 ppm for octane and 1 ppm NO_2 and 1 ppm H_2S with polymer membranes	Diverse range of coatings, high sensitivity, good response times, IC integratable	Complex interface circuitry, difficult to reproduce	Nagle *et al.* (1998), Albert and Lewin (2000) and Penza *et al.* (2001a)
QCM	Piezoelectricity	Micromachining, spincoating, airbrushing, inkjet printing, dipcoating	1.5 Hz/ppm; 1 ng mass change	Diverse range of coatings, good batch to batch reproducibility	Poor signal-to-noise ratio, complex circuitry	Nagle *et al.* (1998) and Kim and Choi (2002)
Optical devices	Intensity/ spectrum	Dipcoating	Low ppb; DL (NH_3)=1 ppm with polyaniline coating	Immune to electromagnetic interference, fast response times, cheap, light weight	Suffer from photobleaching, complex interface circuitry, restricted light sources	Jin *et al.* (2001) and Nagle *et al.* (1998)
MOSFET	Threshold voltage change	Microfabrication, thermal evaporation	2.8 μV/ppm for toluene; DL = (amines, Sulphides) = 0.1 ppm; Maximum response = 200 mV especially for amines	Small, low cost sensors, CMOS integratible and reproducible	Baseline drift, need controlled environment	Covington *et al.* (2001) and Kalman *et al.* (2000)

Notes: HVPG – high vapor pressure gas; LVPG – low vapor pressure gas; $\Delta R/R_b$ – relative differential resistance change

FIGURE 1.9: Summary of the properties of each sensor type. textitAdapted from: Arshak et al., 2004.

1.4 Thesis Content

After the review of all the different classes of sensors for the implementation of an e-nose, the main focus of this thesis it is on the conductivity sensors, in particular the polymeric ones. The goal is to gain a better understanding on the sensing mechanisms that affect this class of materials, establishing relationships amid chemical and physical properties compared to the electrical response and performances.

In order to give a general overview of this work, in this section it is described how the final project is structured. The thesis has been divided into six main chapters. After this short introduction where the purpose of the thesis is stated and the background of the Gas Sensor Project is explained, Chapter 2 will review the state of the art of the polymeric sensors. The fundamental sensing parameters will be defined, the different sensing mechanisms will be described with a particular focus on two classes of polymers: conductive polymers based on carbon black composites and the in situ photopolymerized composites, either fabricated from intrinsically conductive polymers or loaded polymers incorporating a conductive filler. This part will be fundamental for the understanding of the experiments discussed later in this work.

In Chapter 3 there will be reported all the details about the experimental part, starting from the synthesis of the materials up to the fabrication of the sensors. Furthermore, the experimental setup used to carry out the electrical characterizations will be described in detail and all the protocols followed in order to complete the experiments.

Subsequently, Chapter 4 and Chapter 5 will illustrate the set of systematics analyzed for the two categories of interest. For both the classes, the relevance of the measurements will be pointed out, showing and discussing the results.

Ultimately, Chapter 6 will present the conclusions that we came with at the end of this experimental thesis during six months of internship, developing new polymeric materials as gas sensors and there will be given hints for possible future works.

Chapter 2

Polymeric Gas Sensors

After the overview on all the different types of gas sensors, this chapter will focus on polymeric devices, in particular on the ones employed in the development of chemiresistors. The main advantages and drawbacks will be highlighted and the different sensing mechanisms will be explained in details. These devices can be fabricated either using intrinsically conductive polymers (ICP) or loaded polymers (LP) where a non-conductive polymeric matrix incorporates a conductive filler (Partridge, Jansen, and Arnold, 2000).

Even if the sensing mechanism is different for the cited materials, the working principle behind them is always the same. They all fall under the same category of chemiresistors where on exposure to the gas, they base their detection on an electric resistance variation, which is usually seen as a change in the output current.

2.1 Intrinsically Conductive Polymers

Typically, polymers are considered insulating materials in their neutral state because they present a very high resistance ($\approx$MΩ-GΩ) due to the fact that the charge carriers mobility is very low and the energy gap between the valance band and the conductive band is large enough not to allow electrons excitations from the lower to the upper levels.

However in 2000, Heeger, MacDiarmid and Shirakawa won the Nobel Prize for the development of electrically conductive plastics. These can be employed in many different applications, including gas sensors. They demonstrated that the molecular arrangement of conductive polymers must contain alternating single and double bonds along the polymer backbone in order to allow the formation of delocalized electronic states (Janata and Josowicz, 2003).

Steric, conformational factors and charge interactions can control the level of delocalization, leading to the formation of energy gaps similar to semiconductors like silicon or germanium. Between the two bands, there is the Fermi energy level, corresponding to the electrochemical potential of an electron. Thanks to this unsaturated structure of these conjugated polymers there are some π electrons that are unpaired from the linear chain and can move along it, increasing the conductivity. This electric conductivity arises from a doping process of the polymer, which consists in some redox reactions (Miasik, Hooper, and Tofield, 1986). This process is called primary doping where charge carriers are generated in the polymer chain creating defects in the lattice and it involves charge exchanges between the polymer and the dopant species.

Since every repeating unit is a potential redox site, conjugated polymers can be doped n-type (reduced) or p-type (oxidized) to a relative high density of charge carriers. The chemical reactions occurring between the dopant ions and the polymer induce an excess or deficiency of π electrons in the polymer. Having said that, small distortions occur locally in the lattice so that the conformational changes as well as charge inequalities are induced into the chains. In this way, the highest occupied molecular orbital (HOMO) and the lowest unoccupied molecular orbital (LUMO) become closer, reducing the energy gap (Fig. 2.1). The net effect is that the oxidizing state changes and the equivalent of free radicals can be formed.

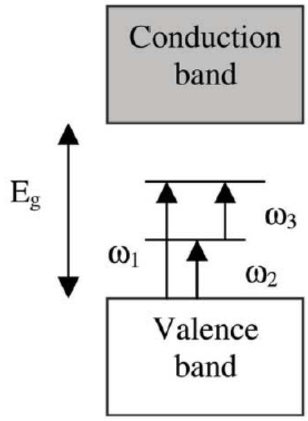

FIGURE 2.1: When the polymer is doped, new transitions are possible, reducing the overall energy gap. *Adapted from: Persaud, 2005.*

A charged site interacting with a free radical forms a polaron. Polarons are highly unstable, but can be stabilized by further oxidations in order to form a bipolaron. Polarons can be cationic or anionic but oxidation removes an electron from the system forming a dication, which is spinless defect of the polymer. These defects lie within the band gap. Introducing dopants and inducing bipolarons has consequences for the mechanism of electrical conduction (Persaud, 2005).

Once the polymer is doped and has acquired some conductive properties ($\sigma \approx 10^0 - 10^5 Scm^{-1}$), the interaction between the active sensing material and the analyte induces the secondary doping. This is the real sensing mechanism. The material can be seen as a polymeric film dotted with redox sites that define an electron transfer pathway. Changes in the electronic properties are related to changes of electronic coupling between redox sites in the matrix that define a physical electron transfer pathway in the conducting polymers, recognized in conductivity and work function. The electron transfer pathway relies on the premise that covalent bonds, hydrogen bonds and van der Waals contacts between atoms all modulate electronic coupling differently.

Donation or withdrawal by the analyte vapors leads to conductivity changes in the sensor films, in addition to polymer doping by counter ions before gas exposure (primary doping). A similar idea has been applied to the more common analytes of VOCs, leading to a model of partial charge transfer between the polymer and the analytes. Partial electron transfer may increase or reduce the concentration of the charge carriers (polarons and bipolarons) in the polymer backbone and, hence, polymer conductivity; as the conductive polymer interacts with gaseous species, it can act either as an electron donor or an electron acceptor. All these changes affect the overall conductivity of the polymer that can be described by three terms as follow:

$$\frac{1}{\sigma} = \frac{1}{\sigma_c} + \frac{1}{\sigma_h} + \frac{1}{\sigma_i} \tag{2.1}$$

where the intrachain conductivity σ_h is related to the alteration of conductivity along the backbone; the intermolecular conductivity σ_c which is due to electron hopping to different chains because of analytes sorption and ionic conductivity σ_i, which is affected by hydrogen bond interaction at the backbone and also by ion migration through the polymer (Albert et al., 2000; Hao, Kulikov, and Mirsky, 2003).

The nature of the gas to be detected is very important. Considering a conductive polymer doped p-type the main carriers are the holes. When the sensor is exposed to a reducing gas, the polymer loses some electrons. Therefore, the resistance will decrease because more holes are able to contribute to the conductivity. Instead, an oxidizing gas, reducing itself, oxides the material that gains some electrons. In this case, the resistance will increase. On the contrary, for a n-type polymeric sensor where the carriers are electrons, the above relations are reversed. The doping of the material is a reversible process. When the gas is gone, the polymeric film will de-dope and the resistance will go back to its original value. This cycle can be repeated multiple times.

The most common intrinsically conductive polymers are polypyrrole (PPy), polyaniline (Pani), polytiophene (PTh), polyacetylene (PA) and their derivatives (Fig. 2.2). These ICP have been used as the active layer of gas sensors since early 1980s (Bai and Shi, 2007).

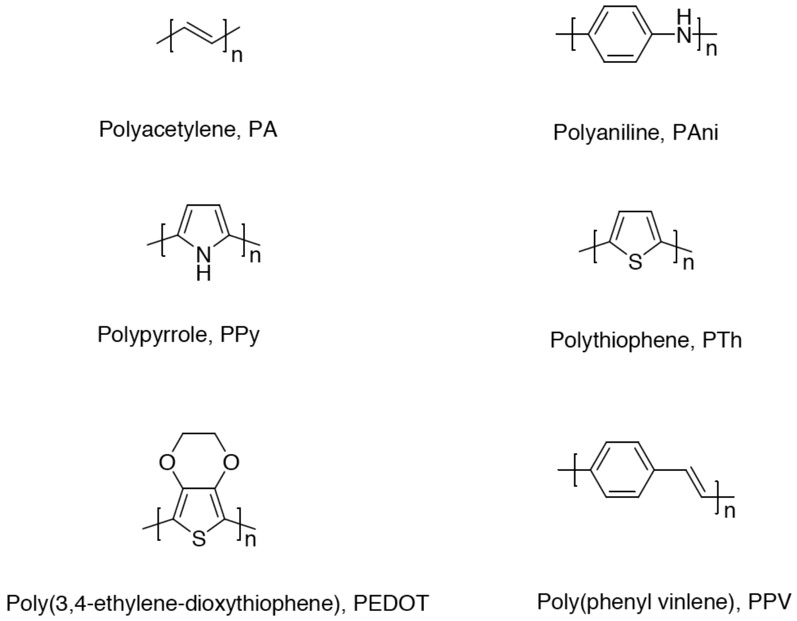
Polyacetylene, PA

Polyaniline, PAni

Polypyrrole, PPy

Polythiophene, PTh

Poly(3,4-ethylene-dioxythiophene), PEDOT

Poly(phenyl vinlene), PPV

FIGURE 2.2: Several typical intrinsically conductive polymers.
Adapted from: Bai and Shi, 2007.

They are usually synthetized by chemical or electrochemical techniques, where the different starting monomer is oxidized. The reactions involve mixing the monomer with an oxidant agent in solution. The most widely used oxidants are ammonium persulfate, iron (III) chloride, hydrogen peroxide, potassium dichromate, cerium

sulfate and so on.
For the electrochemical synthesis different techniques can be used: the galvanostatic, potentiostatic, cyclic voltammetry and other potentiodynamic methods. For all of them, a three electrodes system is used to conduct the electrochemical polymerization. The cell is composed of a working electrode, a counter electrode and a reference one. A voltage is applied between the electrodes and the polymerization begins. The polymer is initially deposited on the electrodes and then it grows between them, producing a complete thin film. Electrodes thickness can range from $1\,\mu\mathrm{m}$ up to $10\,\mu\mathrm{m}$ and the gap between them is generally $10\,\mu\mathrm{m}$-$100\,\mu\mathrm{m}$ (Arshak et al., 2004). The total charge applied during the polymerization process determines the thickness of the film, while the final applied voltage control the primary doping concentration. Partridge et al. described the sensors characteristic of ICP produced by pulsing the potential during polymerization and observed a 1-50% relative differential resistance change for saturated gas (Partridge, Jansen, and Arnold, 2000).

Once the polymer is synthetized, various methods have been developed to fabricate the devices, creating thin polymeric films. In order to deposit the conductive polymers film it is possible to perform an electrochemical deposition, as it was described above, where the substrate has to be conductive. Starting from a polymeric solution, the dip-coating is well-exploited along with the spin coating. A famous method to produce thin films of polymers is also the Langmuir-Blodgett technique. Other methods are the layer by layer self assembly technique, the thermal evaporation, the vapor deposition polymerization, the drop coating and the flow coating (Bai and Shi, 2007).

Dealing with the polypyrrole-based sensors, recently conductive PPy has been synthetized through a single-step process where the cross-linked network is UV photopolymerized starting from the precursor, the pyrrole. In this case, the primary doping is carried out by the counter ion of the photoinitiator (Onium salt), generating polarons inside the polymer.
They reported that the electrical resistance of sensors decreases when exposed to humidity. This is due to a phenomenon called proton transfer (Fig. 2.3). PPy films are p-type semiconductors, where the carriers are holes. Interacting with the proton from the self-ionization of water, a partial positive charge displays on the chain, increasing the positive charges and, therefore, reducing the electrical resistance of the sensors. Different changes in resistances are related to the nature of the gas/vapor

and its ability to reduce or oxide the film, increasing or decreasing the positive charges and affecting the conductivity (Razza et al., 2017).

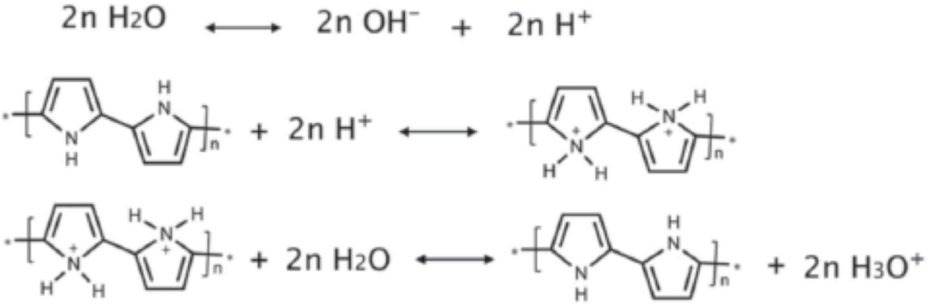

FIGURE 2.3: Proton transfer process involved in the PPy humidity detection mechanism. *Adapted from: Razza et al., 2017.*

Cho et al. investigated the sensing properties of PPy sensors by controlling the range of temperature and relative humidity. The starting resistance was increased according to increase of humidity and decrease of temperature. This could be explained due to the fact that the number of charge carrier holes in the PPy layer were reduced by the absorption of water vapor from the humid atmosphere. The sensitivity of PPy sensors was higher under dry condition than humid condition, and decreased when humidity increased. That is because the water molecules are absorbed faster than the methanol ones. The more water vapor was increased, the less methanol vapor was adsorbed on the surface of PPy sensor. The sum of sensitivity to methanol and water vapor was larger than the mixture gases. As the relative humidity increases from 5% to 20%, the sensitivity of methanol vapor was decreased. The reproducibility of PPy sensor was excellent during 10 on-off cycles by switching between N_2 and 1000 ppm methanol gas, indicating that the sensor could be used cyclically at various humilities. The sensitivity of methanol sensors was increased with lower RH and lower temperature, but the fastest response and recovery time was shown at $25\,^{\circ}\mathrm{C}$ (Cho et al., 2005; Chen and Lu, 2005).

Other researchers discovered that the resistance of the vapor-deposited polypyrrole film increases upon exposure to ethanol, fitting the typical model for polypyrrole response to the class of alcohols. The observed resistance increase of conducting polymers upon exposure to organic vapors such as ethanol is attributed to different mechanisms that are in competition one another. The organic solvent forms hydrogen bonds with the polymer, resulting in swelling of the matrix and distortion of the conductive pathways of the polymer chain. The other sensing method is that the conduction occurs by the movement of the positive charge carriers along the polymer chain. An electron donating gas, such as ethanol, reduces the polymer, decreasing the number of positive charge carriers (Savage, 2009).

In addition, upon an acetone exposure, the conductivity of the electrochemically deposited PPy film is reduced. Studying the different electrical response of the polymeric film where the polypyrrole was doped with different ions, it was possible to state that a PPy film with a larger amount of N^+ (polaron and bipolaron species) and correspondingly a higher specific conductivity value has a higher response towards acetone vapor. The fewer the imine groups, the better the sensitivity towards acetone vapors. This change indicates that acetone destroys the dispersion force between aromatic PPy units and increases the disorder section in PPy which hinders the electron mobility and hence decreases the specific conductivity of the sensor (Ruangchuay, Sirivat, and Schwank, 2004a; Ruangchuay, Sirivat, and Schwank, 2004b).

In general, it is difficult to explain the sensing mechanism in a single physical process. Furthermore, the working principle is very complex and, in some parts, it is still unclear.
A number of different mechanisms might lead to a change in the conductivity of the polypyrrole films. The presence of the organic compound could oxidize or reduce the polymer, changing the number of charge carriers on the polymer chains; interact with the mobile charge carriers on the polymer chain and affect their mobility; modify the potential barrier for the hopping process of charge carriers between the polymer chains; interact with the dopant molecules or provide a morphological change, for example, by producing self-assemblies of conductive polymers clusters. Over time (devices stored at room temperature and in air) the resistivity of the polypyrrole devices increased from about $1,1 \times 10^6 \Omega cm$ to over $2 \times 10^6 \Omega cm$ in a period of 45 days. This may be attributed to a decrease in the doping level of the polymer. However, despite this increase in resistance, the sensitivity of the films to alcohols was unchanged (Mabrook, Pearson, and Petty, 2006; Kopecká et al., 2016).

Lastly, these polypyrrole-based devices seems to have problems when tested with DC measurements. When analyzed in AC, on the contrary, the electrical response is better but the sample must be modeled as a RC circuit where the capacitance component can not be neglected (Amrani, Persaud, and Payne, 1995; Musio and Ferrara, 1997).

2.2 Loaded Conductive Polymers

The sensor element of the other class is a polymeric composite that is made of a thermoplastic insulating polymer that acts as the matrix of the active layer. The conductive properties are achieved by dispersing homogenously a conductive filler, such as carbon black particles and multi-walled carbon nanotubes (MWCNTs), or another intrinsically conductive polymer as the polypyrrole.
The transduction mechanism for the polypyrrole composites is quite complex because the analyte can interact potentially with both the organic insulating matrix and the conductive polymer. Contrarily, the other nanocomposites base all their sensing mechanism on the swelling of the matrix. This transduction process is well-explained by the percolation theory. The conductivity arises from the filler, while the selectivity to different gases results from the polymer (Muñoz, Steinthal, and Sunshine, 1999).
Upon the exposure to an odorant, the polymeric composites reversibly swell to varying degrees according to the polymer-gas interactions. The swell results in a change in conductivity that can easily be monitored. This happens because the conductive particles are close to each other when the film is in the neutral state and, due to the quantum mechanical tunneling effect, electrons can hop between them, generating conductive pathways that contribute to the conductivity of the polymeric film. During the swelling, organic vapor molecules physically adsorb on the surface and penetrate between the different polymeric chains. This effect breaks the entanglements between the chains and the free volume increases along with the distance amid the conductive particles. In this way electrons can not hop and, thus, the resistance increases (Fig. 2.4).
This is a reversible process because the vapor molecules are not chemically bound and so they desorb, allowing the nanoparticles to regenerate the conductive paths.
Very important is the solubility of the polymer in the solvent and the affinity between the matrix and the variety of analytes through different functional groups because they can highly influence the level of swelling and a certain degree of selectivity.

In order to achieve the best electrical response, the film should contain the right amount of conductive filler. The conductivity versus filler concentration in the matrix is well-described by the percolation curve (Fig. 2.5). The behavior of the specific

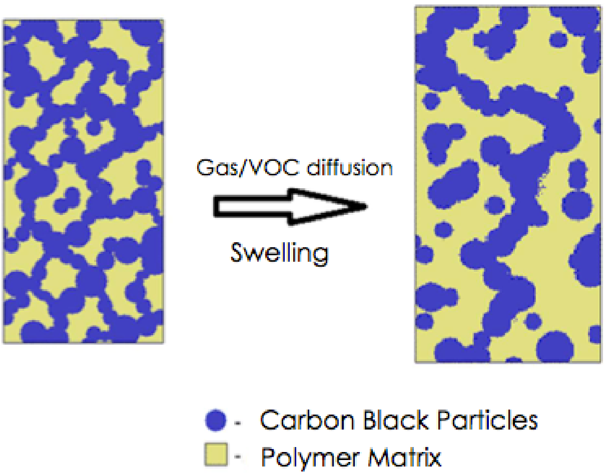

FIGURE 2.4: Swelling mechanism in polymeric nanocomposites.
Adapted from: Potyrailo, 2016.

resistance reflects a sigmoid to threshold curve. At low filler loadings, the composites are insulators, because no connected pathway of conductive particles exists across the material. As the amount of conductive particles increases, a sharp transition occurs in which the resistivity of the composite can decrease dramatically (by up to 10 orders of magnitude) with a small variation in the filler concentration. At the transition point, designated as the percolation threshold, a connected pathway of particles is formed (Lonergan et al., 1996). In this region the swelling is maximized and the extensive variation of resistance produce the best electrical response.

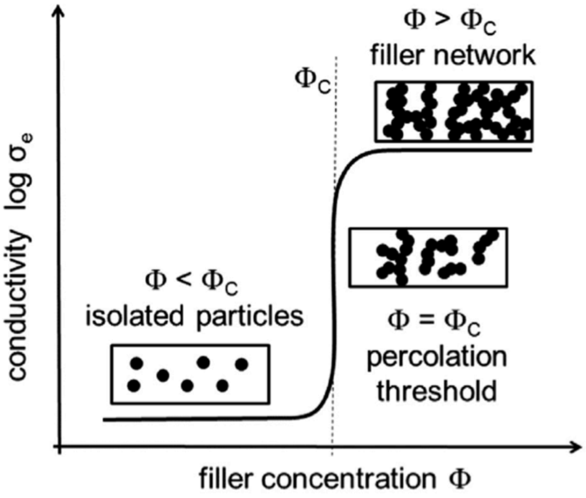

FIGURE 2.5: Percolation curve. *Adapted from: Munstedt and Stary, 2016.*

Also the temperature coefficient of a loaded polymer sensor in an inert environment is very important and it depends on the inherent thermal expansion properties of the host polymer and the filler and how close the composition is to the percolation threshold. These devices are more sensitive at high temperatures and close to the threshold (Partridge, Jansen, and Arnold, 2000).

The partial pressure, hence the concentration, of the penetrant vapor at the gas-polymer interface affects the response of the sensor. The response is inversely related to the vapor pressure of the analyte at the surface. Low vapor pressure compounds can be detected in the low ppm range, while high vapor pressure compounds need to be in the high ppm range to be detected. This is due to the gas partition coefficient where low vapor pressure gas molecules have a higher tendency to inhabit the polymer and thus can be detected at much lower concentrations (Muñoz, Steinthal, and Sunshine, 1999; Albert et al., 2000).

Generally, sensors have operating resistances of approximately $1\,\mathrm{k\Omega}$ to $1000\,\mathrm{k\Omega}$. The sensitivity to hydrophobic analytes were found to be one or two order of magnitude higher respect to the intrinsically conducting polymers. The polymer composites show linear responses to concentration of various gases and also good repeatability after several exposures (Partridge, Jansen, and Arnold, 2000).

In the literature, thermoplastic polymers are chemically synthetized and mixed with a carbon black suspension diluted with a suitable solvent. Different techniques are used to apply the solution on the substrate with the relative interdigitated electrodes, such as spray coating, dip coating or spin coating. The percolation threshold seems to lie between 12 wt% and 25 wt% of carbon black concentration. The low-mass-fraction composites generate larger signals often better resolve analytes and are generally more sensitive above concentrations of $P/P^0 \approx 0,06$. The main drawbacks are though the drift of resistance, the lack of linearity and lesser response reproducibility (Sisk and Lewis, 2006).
Different strategies are used to choose the matrix material, from crystalline polymers to amorphous ones like polystyrene (PS). For the latter a in situ polymerization is exploited to improve the sensitivity and lower the percolation threshold of the carbon black concentration. When the sensors are exposed to organic vapors, the electrical resistance increases up to six orders of magnitude (Gao et al., 2006; Rong et al., 2003).

Another alternative to fabricate polymeric composites for gas sensing is the dispersion of MWCNTs inside the insulating matrix. The sensing mechanism is the same as the carbon black-based sensors, although, if the filler is uniformly dispersed in the matrix, the percolation threshold is much lower and it is between 4 wt% and 10 wt%.

These nanocomposites are synthetized by polymerization filling and they show significant responsivity to organic vapors of good solvents of the matrix within short time of exposure and the resistance can be quickly and completely recovered to its original baseline as soon as the sensor is transferred into air. Compared to the composites made by solution mixing, the ones by in situ polymerization have much higher sensitivity over a wide MWCNTs range and present a lower percolation threshold as it is possible to see in Figure 2.6 (Zhang et al., 2012). It indicates that MWCNTs is less efficient to build up conductive networks in PS during solution mixing.

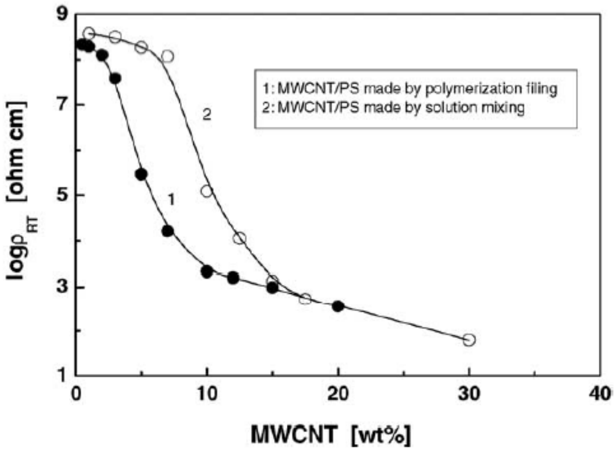

FIGURE 2.6: Percolation curve of MWCNT-based sensors.
Adapted from: Zhang et al., 2012.

Other studies were made substituting PS with thermoplastic polyurethane multifilament (TPU). In this way a thin layer of MWCNTs coats the filament inducing sensing properties and conductive paths only on the surface for the current transport (Fan et al., 2011).

In general, MWCNTs do not have sensing response to all gases but only the ones with high adsorption energy that can interact with them. Therefore, coating or doping of an enhance element on MWCNTs could broaden the application range (Yeow and Wang, 2009). A kind of selectivity could be achieved by functionalizing the MWCNTs with polar groups allowing interaction with a wider range of analytes. Grafting of ε-caprolactone on the CNTs surface through in situ ring opening polymerization was demonstrated to boost sensitivty to many differerent solvents (Castro et al., 2009). This behavior can be attributed to the charge transfer between the molecules and the nanotubes, or the change of the charge carriers lifetime in MWCNTs (Alves et al., 2018). In addition, it was observed that the surface modified MWCNT/PMMA composite shows a higher response respect to the unmodified ones. The resistance change was two orders of magnitude higher, due to surface modification, when exposed to dichloromethane, chloroform and acetone (Philip et al., 2003).

It has been widely proven that the disconnection of conductive paths, induced by the swelling of the matrix due to their adsorption of solvent molecules, is the main reason for the resistance sensitivity in vapors and liquids. It is accepted that organic chemicals can be adsorbed by the MWCNTs based on hydrophobic interactions, π-π bonds, electrostatic actions and hydrogen bonds. It can be said that the resistance variation is attributed to both the adsorption of molecules gas by the matrix and the MWCNTs surface. It still needs to be proven which mechanism is the predominant. MWCNT/PMMA composites shows good response both to polar and non polar solvents. For the former ones the predominant mechanism is the interaction between the molecules and the functional groups on the surface of the nanotubes (Fig. 2.7). For the latter, it is very important the solubility of the solvent in the matrix. Dichloromethane, chloroform and acetone are good solvents in PMMA and the resulting swelling is larger, increasing the sensitivity based on the other mechanism (Philip et al., 2003; Jia and Shi, 2011).

Several challenges still need to be faced like the synthesis of pure and ideal CNT that is difficult and expensive; the grow of defect-free nanotubes of relevant length; the preparation and dispersion of this type of filler inside the polymer solution. This is an hard task because the high aspect ratio and the high surface area allows easily the aggregation of the one-dimension particles (Badhulika, Myung, and Mulchandani, 2014).

In conclusion, intrinsically conductive polymers and polymeric composites are widely used as the sensing active layer in chemiresistors. The main advantages of this class are that they operate at room temperature because of the quite strong interactions between the analyte molecules and the film. Without using any heater,

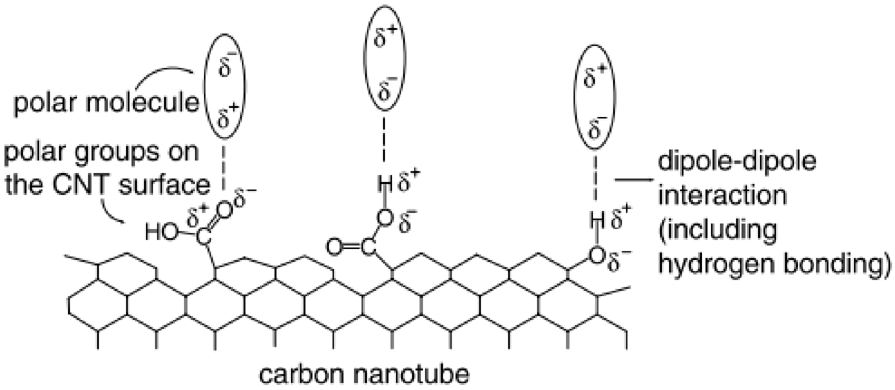

FIGURE 2.7: Interaction of gas molecules with the surface of a CNT.
Adapted from: Philip et al., 2003.

also the power consumption is low and the device configuration is simple. Furthermore, the backbones of common conductive polymers are build up with aromatic rings, which are easy to attach various grafts through electrophilic substitutions. By grafting different functional groups, it is very facile to adjust all the physical and chemical properties that are useful to improve sensitivity and selectivity towards particular gases. Even if the sensitivity is lower than MOS sensors, the response time is very fast in the order of hundreds of seconds and it is related to the thickness of the film. The fabrication in general is very simple and straightforward because polymers are easy to process and many techniques are available, increasing the reproducibility. However, they present long time instability and irreversibility as well as a very high sensitivity towards water vapor. In addition, the selectivity still needs to be improved because one single sensor can not discriminate from a wide range of different analytes (Bai and Shi, 2007).

Chapter 3

Experimental Details

In this chapter it will be reported all the details about the experimental part in order to have a better understanding of the results explained in Chapter 4 and Chapter 5. First, it will be analyzed the synthesis of the materials and the fabrication processes utilized to develop the sensors of the two polymeric classes relevant for this study: the carbon black-polymer composites and the in situ photopolymerized composites. Secondly, all the setup used to electrically characterize the devices will be presented, describing the operating principle of the gas delivery system and the different gas sensing chambers associated and their electronic instruments employed to collect the data.
A particular study will be dedicated at learning how the impedance analyzer works with basic studies.
Furthermore, all the procedures followed for each sensor will be specified, in order to discern, step by step, the electrical experiments carried out at IBM Research Lab.

3.1 Carbon Black-Polymer Composites Synthesis and Sensor's Fabrication

The realization of the final sensor can be divided into five main phases. Firstly, there is the wafer preparation, which is used as the substrate. The second step concerns the dielectric polymer synthesis, while the third one regards the carbon black suspension; the forth stage consists in mixing the carbon black suspension with the polymer solution. Finally, the liquid formulation can be deposited on the previously prepared wafer.

3.1.1 Wafer Preparation with Electron Beam Lithography

During the synthesis, the carbon black-polymer formulation is liquid. Therefore, it is needed a substrate with the electric connections on which the formulation can be deposited.

The wafer preparation is a very delicate, articulated and precise procedure that requires attention, as the desired features are below 100 nm in dimension. In the lithography process, exploited to transfer patterns at the nanoscale on the surface of the substrate, many steps are required and all of them are performed inside a clean room with different classes, where there is a controlled environment. In fact, any kind of contaminations need to be avoided because they can ruin the devices, poison the equipment and pose a health risk to the people who work inside it.

IBM doesn't produce its own wafers, but purchase them as their starting materials. The manufacture companies are involved in the wafer processing from the Czochralski single crystal growth to the finishing and oxidation processes that permit to have a 1 µm SiO_2 layer on both sides over Si.

Usually, the wafer cut on the <100> plane, recognized by the flat, is the predominant due to its anisotropy structure, high electrons mobility and superior SiO_2 formation. The wafers can be divided based on the material: silicon dioxide (SiO_2) or silicon nitride (Si_3N_4). The second ones should provide a better isolation at the interface between the electrodes and the semiconductor, avoiding current leakages.

The first step of the process is a proper cleaning of the wafer glossy surface done by oxygen plasma for around thirty seconds. This action is very important, as I said before, to eliminate completely every trace of organic residues and avoid contaminations from the beginning that would affect all the following steps.

At this point, the second action is a surface modification of the wafer. The surface oxide, normally, forms long-range hydrogen bonds with water adsorbed from the air. When the resist is spun, it adheres on the water molecules rather than the oxide surface. In order to solve this problem, the wafer is placed in a vapor-priming oven at 150 °C for twenty minutes. The time process is quite long because the oven first pumps down to dehydrate the sample, and then it sprays pure hexamethyldisilazane vapor (HMDS). This effective coating is used to promote the adhesion between the wafer and the polymeric resist. In fact, on water-free surfaces, the silicon atoms of HMDS create chemical bonds with the oxygen of the SiO_2, releasing ammonia molecules (NH_3) in the environment (MicroChemicals, 2017).

In this way HMDS exposes its methyl groups, creating a hydrophobic surface that improve resist wetting and adhesion (Fig. 3.1).

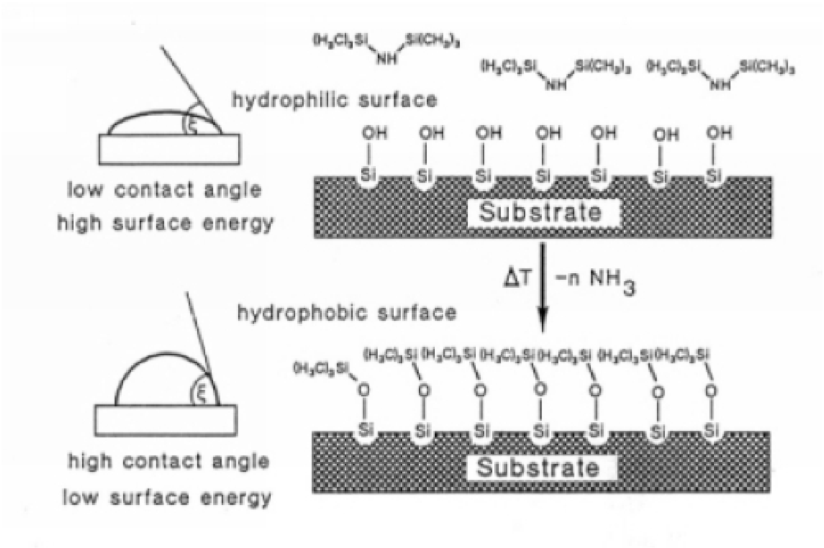

FIGURE 3.1: HMDS surface modification.
Adapted from: MicroChemicals, 2017.

The third step is the spin coating process, used to get the KRS formulation, a specific polymeric thick resist developed by IBM, onto the substrate with the required uniform thickness. The deposition is carried out at 1500 rpm for sixty seconds. Immediately after, it follows a soft bake at 120 °C for one minute in order to dry the solvent from the resist.

At this stage, the wafer is finally ready to be written in ultra high vacuum environment. The lithography technique utilized to write on the wafer is called electron beam lithography (EBL) (Fig. 3.2).

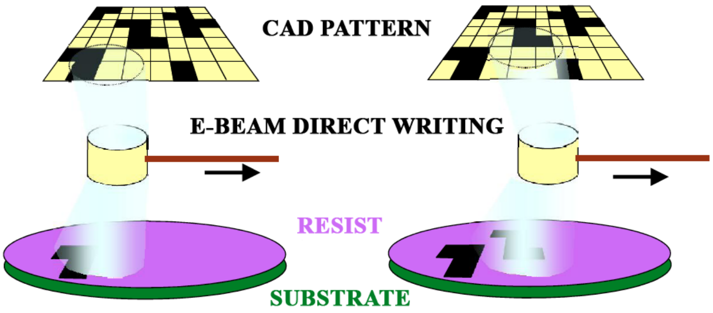

FIGURE 3.2: Electron Beam writing.

Basically, a tightly focused and precisely controlled electron beam is scanned on the surface, transferring the pattern of the electrodes on the wafer only in specific regions. In the areas where the wafer has been exposed, there is a depolymerization process in which the positive resist changes its solubility becoming more soluble and enabling a selective removal of the exposed part. This type of resist has a better sensibility and resolution compared to the negative one. This technique allows patterning of very small features under 10 nm without using any kind of mask because the electron beam writes directly on the resist according to a defined CAD pattern. At the same time, it is a very slow method due to its low writing speed.
The geometry of the electrodes used to fabricate the polymeric sensing device is illustrated in Figure 3.3.

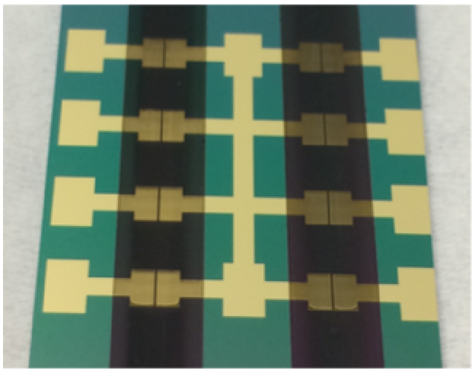

FIGURE 3.3: Electrodes geometry.

The sample contains four devices on the right and four on the left; in the inner part they are all grounded. The gap between the two parallel pads of each device is 100 µm and the width is 2 mm. The separation from device to device is 3 mm, the big pads size are 2 mm x 3 mm.
After the wafer has been written via electron beam, the resist rests for a few moments at room temperature and standard pressure. In this way the material is rehydrated, improving the stabilization of the coated wafer.
The following step takes place under a solvent hood where the wafer is developed in an alkaline solution made of tetramethylammonium hydroxide (TMAH) for sixty seconds. In this stage the resist exposed is dissolved.
The development is then followed by a plasma oxygen cleaning with a duration of five seconds.
The next step is the metal deposition achieved in a custom-made electron beam

evaporation room. In order to improve the adhesion of the metallic electrodes onto the substrate, a 5 nm thin layer is deposited on the developed wafer.
Successively, the e-beam makes possible the sublimation of the electrode's material, either gold or platinum for high temperature applications, present in the crucible in order to form a 50 nm layer.
Finally, the last step involves the process called "lift off", where the magic happens and the pattern is transferred. First, the wafer is placed in a hot bath of N-Methyl-2-pyrrolidone (NMP) at 60 °C for twenty-five minutes; then it is moved in a cleaner bath of NMP at 50 °C and in a cold one at 20 °C. During this procedure, only the metal on top of the sacrificial material is stripped, while the targeted material that is in direct contact with the substrate stays. Once the desired pattern is transferred to the substrate, the wafer is further cleaned through a rinse in IPA at 20 °C for five minutes, followed by an additional rinse in water and finally dried by spinning (Fig. 3.4).
At this moment there is a quality control of the surface by means of an optical microscope. If the quality is good, it is possible to cut the wafer in the smaller devices along the parallel and perpendicular directions respect to the <100> plane.
The author of this thesis performed some steps of the litography process on his own and assisted all the others with IBM researchers.

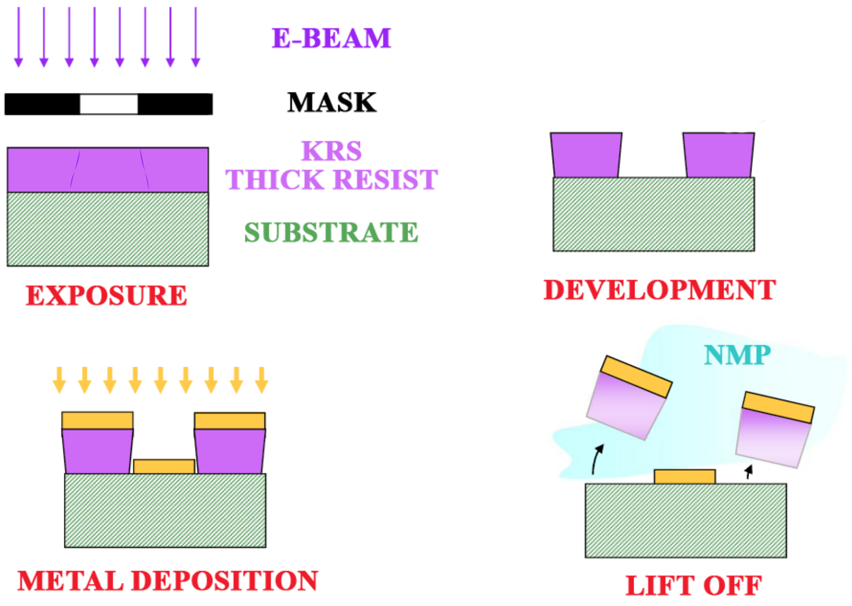

FIGURE 3.4: Lithography main steps.

3.1.2 Dielectric Polymers Synthesis

Once the substrate of the sensor is properly prepared with the electric contacts, the next step is the dielectric polymers synthesis developed by IBM chemists. During the internship, different strategies were used to synthetize the polymer matrix:

- Polystyrene (PS) homo-polymers
- Poly(methacrylic) acid (PMAA)
- Poly(methyl methacrylate) (PMMA)
- Poly(2-dimethylaminoethyl methacrylate) (PDMAEMA)

The last three polymers were prepared in the form of random, block copolymers or blends with PS (Fig. 3.5).

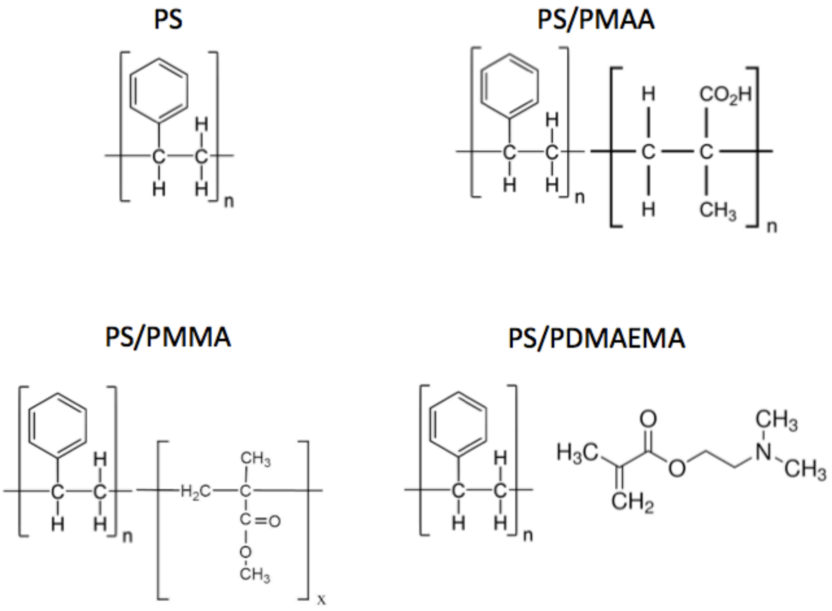

PS

PS/PMAA

PS/PMMA

PS/PDMAEMA

FIGURE 3.5: Polymers used for the insulating matrix.

The role of PS in the copolymers is to help the stabilization and improve the compatibility between the other repeating unit and the carbon black particles.

The synthesis of homo-polymers PS is obtained through a free radical polymerization (FRP) by which the main chain forms by adding free radical building blocks one after the other.

Everything starts with a thermal decomposition where the heat homolytically cleaves the initiator, producing two radicals. In this way free radicals are formed and they present a very high reactivity and poor stability. For this reason they attack the double bond of the styrene, taking the electron from the π bond which is more loose and forming a σ bond with the carbon atom. In this stage a bigger radical called carbocation is formed.

Now the polymerization begins and the main chain propagates adding more repeating units just as it was described. During the synthesis there might be chain transfer and side reactions. All the process stops when the termination occurs (two radicals meet) or the styrene ends.

Concerning the block copolymer PS/PDMAEMA, it is synthetized by Atomic Transfer Radical Polymerization (ATRP), where the main players are the monomer, the initiator, the catalyst, the ligand and the solvent. The whole process can be divided into two stages: PS macro-initiator synthesis and block copolymer synthesis (Fig. 3.6).

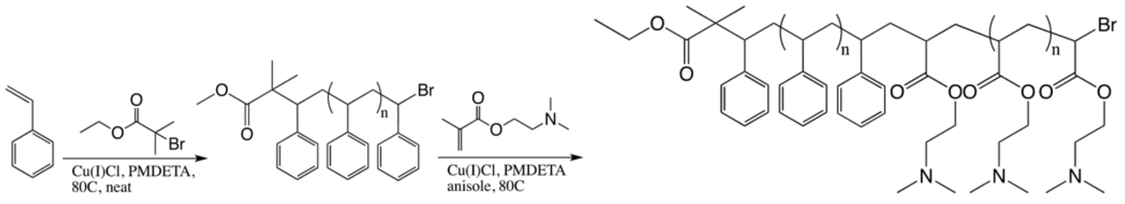

FIGURE 3.6: PS/PDMAEMA synthesis through ATRP.

All chemicals received from the producer are passed through a distilling equipment connected to a vacuum line in order to achieve the highest purity trying to get rid of oxygen and inhibitor. In a Schlenk flask, 0,6336 g of the transition metal complex are added as the catalyst. Cu(I)Cl is used because its good versatility and affinity to halogens.

At the same time 2,2182 g of ligand, N,N,N',N",N"-pentamethyldiethylenetriamine (PMDETA), is poured with 64 g of the monomer, the styrene. The mixture is stirred for five minutes until the catalyst is completely dissolved.

At this point, the initiator is added in the flask in the amount of 1,2483 g and everything is sealed with a rubber septum. The initiator used for this reaction is the ethyl -bromoisobutyrate (EBiB) because of its good reactivity and consistency on the number of growing chains.

Now the reaction can start and the solution is located in an $85\,^{\circ}\mathrm{C}$ oil bath in a protective N_2 atmosphere. The polymerization is carried out for two hours.
When the reaction is completed, the flask is cooled down in a liquid nitrogen bath and the septum stopper is removed in order to restore the equilibrium between the system and the environment. At this point, in order to eliminate the residues of Cu^{2+}, the solution is filtered through a silica gel after being diluted with tetrahydrofuran (THF). The solution is then mixed with some methanol and the PS starts to precipitate on the bottom of the flask. The powder is dried overnight inside a vacuum system.
Thanks to GPC and NMR characterizations carried out by IBM researchers, it is possible to determinate the PS initiator molecular weight (5,5k g/mol) and the polydispersity index (PDI = 1,22). The stoichiometry of this first reaction is:

monomer : initiator : catalyst : ligand = 100 : 1 : 1 : 2 in moles.

At this stage, the dormant species are activated in radicals by the transition metal complex via one electron transfer process. Simultaneously, the transition metal is oxidized to higher oxidation state, $Cu(II)Cl_2$. It is a reversible-deactivation process. Its livingness permits to synthetize polymers by putting together different monomers in a controlled piece-by-piece way.
In fact, in order to reactivate the dormant species to add a block of the second monomer a similar reaction is utilized where, instead of EBiB, PS is added as the initiator.
In particular, in another flask, $20\,\mathrm{g}$ of anisole are poured to dissolve $0{,}018\,\mathrm{g}$ of Cu(I)Cl, $1\,\mathrm{g}$ of PS as initiator, $0{,}063\,\mathrm{g}$ of PMDETA and $1{,}82\,\mathrm{g}$ of the other repeating unit called 2-(dimethylamino)ethyl methacrylate (DMAEMA).
The polymerization ends when all the monomers are used after six hours. Likewise, the solution is filtered and precipitated in hexane.

A similar method is used to synthetize random copolymers where the solutions are prepared by mixing initiators and different ratios of two monomers together. The other copolymers can be derived from this process because the procedure is very similar and only the starting monomers are different.

3.1.3 Carbon Black Suspension

At IBM Research Lab three different kinds of carbon black are used as the conductive filler inside the thermoplastic matrix:

- Vulcan XC72
- Vulcan XC72R
- Black Pearl 2000

All of them are purchased from Cabot Co and they are all designed for application where excellent conductivity and anti-static discharge properties are needed. However, they present different physical properties, percolation thresholds and densities as shown in Figure 3.7.

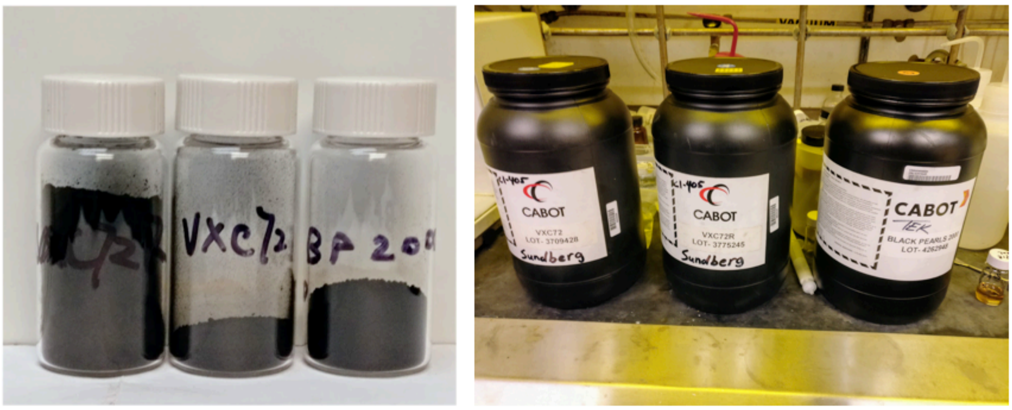

FIGURE 3.7: Different types of Carbon Black from Cabot Co.

In fact, for this reason they are all taken into consideration in order to find the better conductive filler for gas sensors, which gives the best performances in term of processability, sensitivity and selectivity.

In order to improve the compatibility between the polymer and the particles, 1 g of carbon black is suspended in 19 g of propylene glycol monomethyl ether acetate (PGMEA) and everything is put in a vial. The solid content of the solution is 5 wt%. To reach a good and satisfactory dispersion, the solution is sonicated for one hour by means of a probe sonicator. Then the vial, placed in a ice bath to keep the temperature constant and avoiding overheating because of the stress applied to the solution, is shaked and sonicated for another hour. The probe sonicator is set at 30% amplifier power. This step is of essential importance because it's hard to obtain homogeneously dispersed filler and, even after days, it is possible to see that the particles tend to settle down and aggregate. In fact, nanoparticles can be subjected to dipole and/or dispersive forces which promote aggregation very easily.

3.1.4 Carbon Black - Polymer Solution

In the same way, the polymer synthetized is dissolved in PGMEA. The solid content is kept constant at 20 wt%.

Before mixing the polymeric formulation with the carbon black suspension, two important parameters are taken into account: the solution solid content and the carbon black-polymer ratio. The first one is fixed at 4 v% in order to keep the film thickness constant as much as possible around $150\,\mathrm{nm}$. The second parameter reflects the filler load in the mixed solution and affects the percolation threshold. Many formulations have been prepared by IBM scientists with a carbon black content ranging from 5% up to 60% in volume (steps by 5% or lower).

In conclusion, in Table 3.1, all the polymeric formulations are listed, specifying also the carbon black load, the type of polymer and its molecular weight.

TABLE 3.1: List of all the polymeric formulations preprared at IBM.

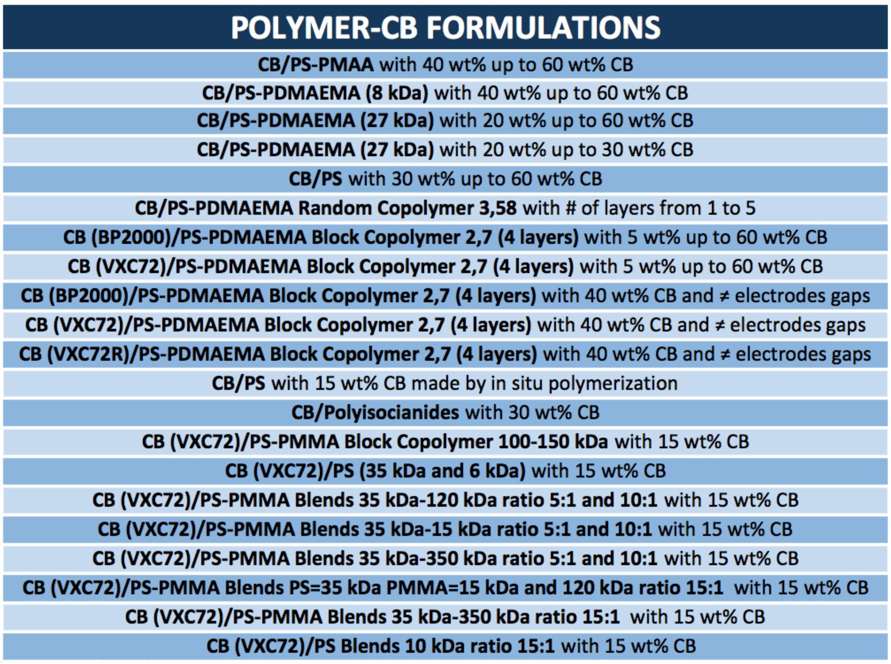

POLYMER-CB FORMULATIONS
CB/PS-PMAA with 40 wt% up to 60 wt% CB
CB/PS-PDMAEMA (8 kDa) with 40 wt% up to 60 wt% CB
CB/PS-PDMAEMA (27 kDa) with 20 wt% up to 60 wt% CB
CB/PS-PDMAEMA (27 kDa) with 20 wt% up to 30 wt% CB
CB/PS with 30 wt% up to 60 wt% CB
CB/PS-PDMAEMA Random Copolymer 3,58 with # of layers from 1 to 5
CB (BP2000)/PS-PDMAEMA Block Copolymer 2,7 (4 layers) with 5 wt% up to 60 wt% CB
CB (VXC72)/PS-PDMAEMA Block Copolymer 2,7 (4 layers) with 5 wt% up to 60 wt% CB
CB (BP2000)/PS-PDMAEMA Block Copolymer 2,7 (4 layers) with 40 wt% CB and ≠ electrodes gaps
CB (VXC72)/PS-PDMAEMA Block Copolymer 2,7 (4 layers) with 40 wt% CB and ≠ electrodes gaps
CB (VXC72R)/PS-PDMAEMA Block Copolymer 2,7 (4 layers) with 40 wt% CB and ≠ electrodes gaps
CB/PS with 15 wt% CB made by in situ polymerization
CB/Polyisocianides with 30 wt% CB
CB (VXC72)/PS-PMMA Block Copolymer 100-150 kDa with 15 wt% CB
CB (VXC72)/PS (35 kDa and 6 kDa) with 15 wt% CB
CB (VXC72)/PS-PMMA Blends 35 kDa-120 kDa ratio 5:1 and 10:1 with 15 wt% CB
CB (VXC72)/PS-PMMA Blends 35 kDa-15 kDa ratio 5:1 and 10:1 with 15 wt% CB
CB (VXC72)/PS-PMMA Blends 35 kDa-350 kDa ratio 5:1 and 10:1 with 15 wt% CB
CB (VXC72)/PS-PMMA Blends PS=35 kDa PMMA=15 kDa and 120 kDa ratio 15:1 with 15 wt% CB
CB (VXC72)/PS-PMMA Blends 35 kDa-350 kDa ratio 15:1 with 15 wt% CB
CB (VXC72)/PS Blends 10 kDa ratio 15:1 with 15 wt% CB

3.1.5 Sensor's Fabrication

This is the last step in order to get the polymeric gas sensor, where the floating system is coated onto the substrate, previously prepared, by flow coating. This is a well-known and exploited technique, invented by Stafford et al., in the realization of polymeric films as gas sensors and in microelectronics in general. It is a very useful and versatile technique for depositing thin, substrate-supported polymer films ($5\,\mathrm{nm}$-$200\,\mathrm{nm}$).

More in detail, a reservoir of coating fluid is held between a nearly horizontal blade placed above the substrate and the horizontal substrate itself. The mount contains multiple screws, each capable of independently adjust the blade: the gap between the blade and the wafer G, the angle between the substrate and the blade in the direction of motion α, the blade tilt and the position of the blade in the transverse direction can all be carefully controlled (Fig. 3.8).

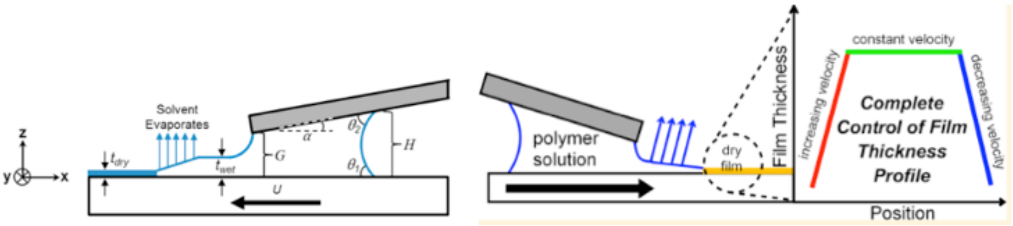

FIGURE 3.8: Flow coating adjustable parameters.
Adapted from: Davis et al., 2014.

During the process, a film of fluid is drawn out of the volume of solution by moving the substrate. Also the velocity and the acceleration can be controlled in order to get perfectly flat films with a controlled thickness all over the strip. It is a fast method that allows to save time, conserve material and minimized unintended sample to sample variation (Stafford et al., 2006; Davis et al., 2014).

Having said that, subsequent layers can be flow-coated on top of the previous layer/s using the same process until the desired film thickness is achieved. After each layer nitrogen is blown on the substrate to accelerate the evaporation of the solvent (Fig. 3.9). The final stack is then baked for two minutes at $120\,^{\circ}\mathrm{C}$.

Thickness and roughness are then measured through the use of a profilometry analysis and the morphology of the film is studied with either optical microscope or a scanning electron microscope (SEM).

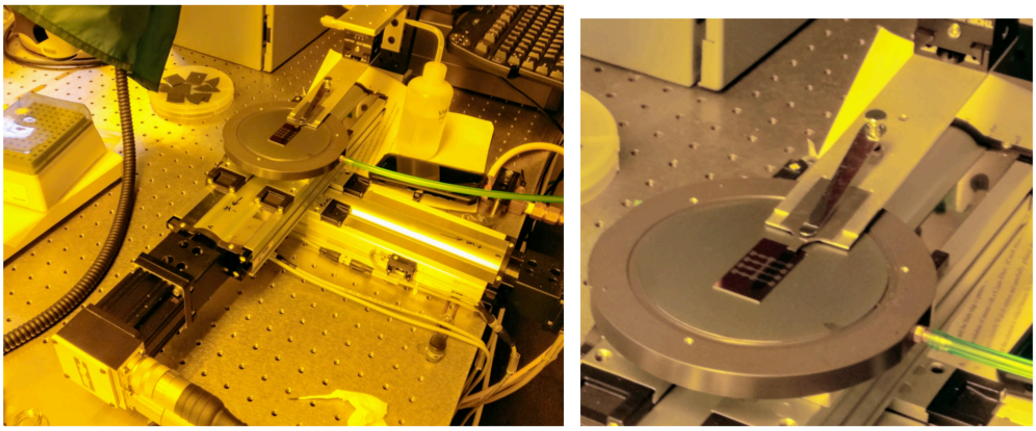

FIGURE 3.9: Flow coating system.

Another technique, less exploited at IBM, is drop casting. This process requires a particular treatment of the substrate (CYTOP) in order to modify the wettability of the wafer. Successively, the carbon black-polymer mix is dropped directly on the wafer by means of an accurate syringe. This method produces thicker films and reproducibility sample to sample is very hard, making almost impossible to compare different films properties.

3.2 In situ Photopolymerized Composites Synthesis and Sensor's Fabrication

The second class of gas sensors is the one of in situ photopolymerized composites. This category can be further divided in:

- intrinsically conductive polymer composites
- multi-walled carbon nanotubes (MWCNTs) composites

The innovation of this work is in the realization of the final sensor that is carried out in a single-step process by means of UV light. After that, in order to apply a voltage and characterize electrically the material, interdigitated metal electrodes (IDEs) are sputtered on the films (Fig. 3.10).

All the photopolymerized self-standing films were fabricated by the author of this thesis in the laboratory of Politecnico di Torino.

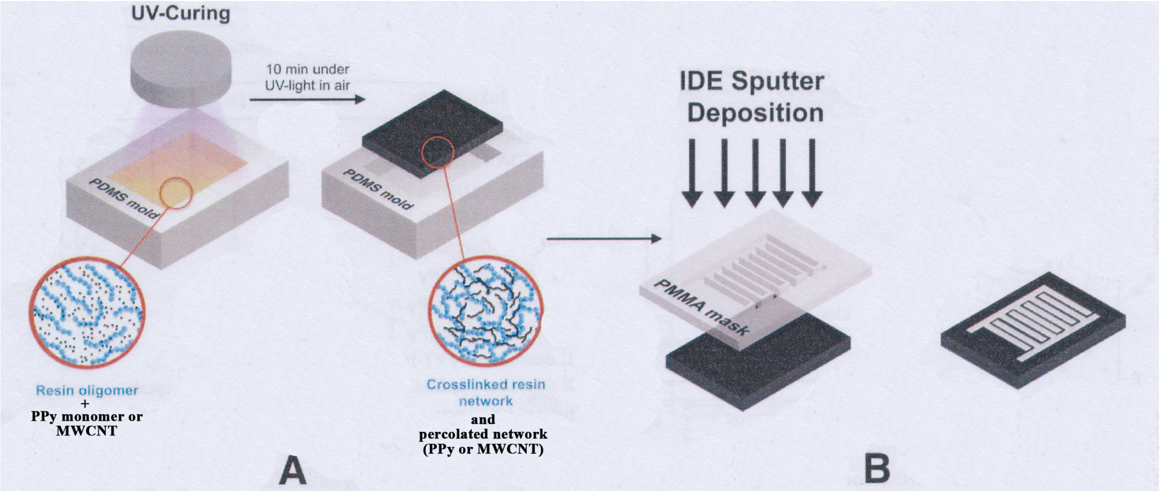

FIGURE 3.10: Schematic rappresentation of sensor fabrication: (A) UV-curing process; (B) Gold interdigitated electrodes deposition. *Adapted from: Razza et al., 2017.*

Generally, the synthesis of PPy is achieved through an oxidative polymerization starting from the pyrrole monomer (Py). The electrons required in this process are obtained either through normal chemical reactions or thanks to the applied voltage in the electrochemical method. However, all this techniques are time consuming because they require several hours of reactions and they are also complex from the procedure point of view. The photopolymerization results in a simple and easy process. Thanks to the UV light, starting from a photocrosslinkable liquid formulation, it is possible to simultaneously cure an insulating thermosetting resin with the in situ photopolymerized polypyrrole. In Figure 3.11, the step-growth photopolymerization of polypirrole is reported (Razza et al., 2017).

On the other hand, it is pursued a top-down approach with the production of nanocomposites containing MWCNTs filler in an acrylic photocurable formulation. It is very well acknowledge the use of MWCNTs as conductive load in order to produce conductive polymeric sensors. Nevertheless becuase of the high aspect ratio, high conductivity and high surface area it is possible to reach the percolation threshold at lower concentrations respect to the carbon black as a filler.
For both the kinds, the most suitable sensitive formulations and curing conditions were investigated in terms of PPy or CNT's load, photoinitiator content, light power and exposition time.

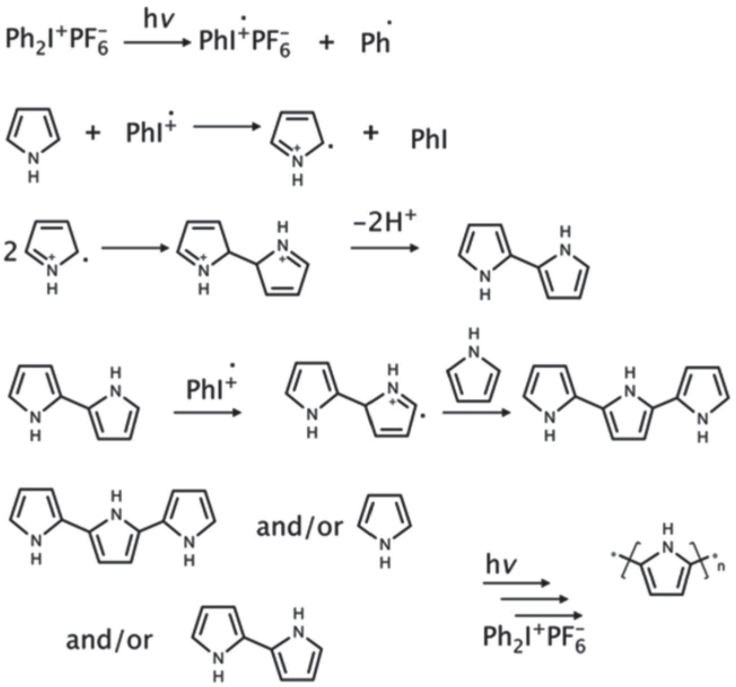

FIGURE 3.11: UV-induced step-growth polymerization of Py initiated by radical cations generated from photodecomposition. *Adapted from: Razza et al., 2017.*

3.2.1 Films Preparation

All chemicals and reagents are purchased from Sigma Aldrich and used as received without any further purification. The oligomers used for the matrix are poly(ethylene glycol) diacrylate (PEGDA, average molecular weight Mn = 200, 575 and 750 g/mol), bisphenol A etoxy dimethacrylate (BPA) and a blend of PEGDA 200 with poly(ethylene glycol) methyl ether methacrylate (PEGMEMA, average Mn = 500 g/mol) in different ratios.

The cationic photoinitiator used is (4-methylphenyl)[4-(2-methylpropyl)phenyl] iodonium; hexafluorophosphate (Irgacure 250, I-250); 75% of the active compound is in propylene carbonate; on the contrary, the radical photoinitiator is 2-hydroxy-2-methyl-1-phenyl-propan-1-one (Darocur 1173, D-1173). Both of them are supplied by BASF.

The liquid pyrrole monomer is reagent grade 98%, while the carbonaceous filler is Multi-Walled Carbon Nanotubes NC7000 purchased from Nanocyl. Figure 3.12 shows the chemical structures of the monomers/oligomers, conductive fillers and photoinitiators used.

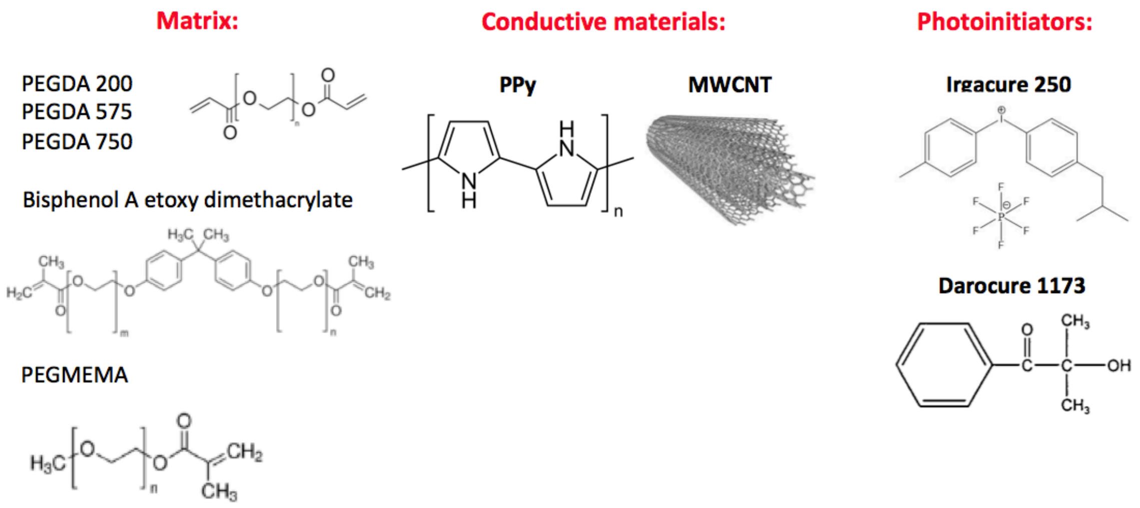

FIGURE 3.12: Chemical structures of the monomers/oligomers, conductive fillers and photoinitiators used.

In order to prepare $1\,\mathrm{g}$ of the PPy formulations, $0{,}1\,\mathrm{g}$ of the pyrrole monomer is added to $0{,}9\,\mathrm{g}$ of the specific resins, either PEGDA 200, PEGDA 750, BPA or the blend of PEGDA 200/PEGMEMA. After that, 2 wt% of Darocure 1173 ($0{,}02\,\mathrm{g}$) is used for the curing of the acrylic matrix and a variable amount of Irgacure 250 (respectively 4%, 6% and 8%) is employed for the pyrrole polymerization. In a plastic vial all the reagents are put together and mechanically mixed for three minutes by means of a Sonifier ultrasonic cell disruptors (Branson 250) in order to achieve a good homogeneity. As references, pyrrole-free solutions are also prepared.

Likewise, 0,3 wt% CNTs are added to a certain amount of PEGMEMA and dispersed using the same Sonifier for thirty minutes at 10% of intensity ($2-3\,\mathrm{W}$). Later, PEGDA 575 and 2 wt% of its photoinitiator Darocure 1173 are added and homogenized for five minutes at 30.000 rpm with the high shear homogenization Ultraturrax IKA T10. The ratio between PEGDA and PEGMEMA is 1:1,5 where the second one is used in order to reduce the viscosity of the photocurable liquid formulations. Because of the strong Van der Waals interactions, bundle of MWCNTs are formed and their usage is a very challenging task due to the poor dispersion into the polymer matrix.

3.2.2 UV Curing

Once all formulations are homogenously processed, they are poured in PDMS molds and UV-cured in air by using a Dymax ECE UV light medium pressure mercury flood lamp with a light intensity on the surface of the sample of about $82{,}6\,\mathrm{mWcm^{-2}}$ measured with EIT photometer. The exposure time is set for ten minutes. After unmolding, self-standing films are obtained with an area of $25\,\mathrm{mm}$ x $25\,\mathrm{mm}$ and a thickness of about $200\,\mathrm{\mu m}$.
For the CNTs composites the presence of the filler causes a decrease of crosslinking density and, for this reason, it is better to increase the intensity light source or place the film closer to the lamp.
Concerning the PPy films, during the irradiation there is an electrochromic effect where the film change its color from yellowish to black. This effect is associated with the primary doping of the polypyrrole by the anion of the onium salt (PF_6^-). The result is a semi-interpenetrated polymeric network characterized by an high flexibility due to the insulating polymeric matrix that is in its rubbery state at room temperature (Fig. 3.13).

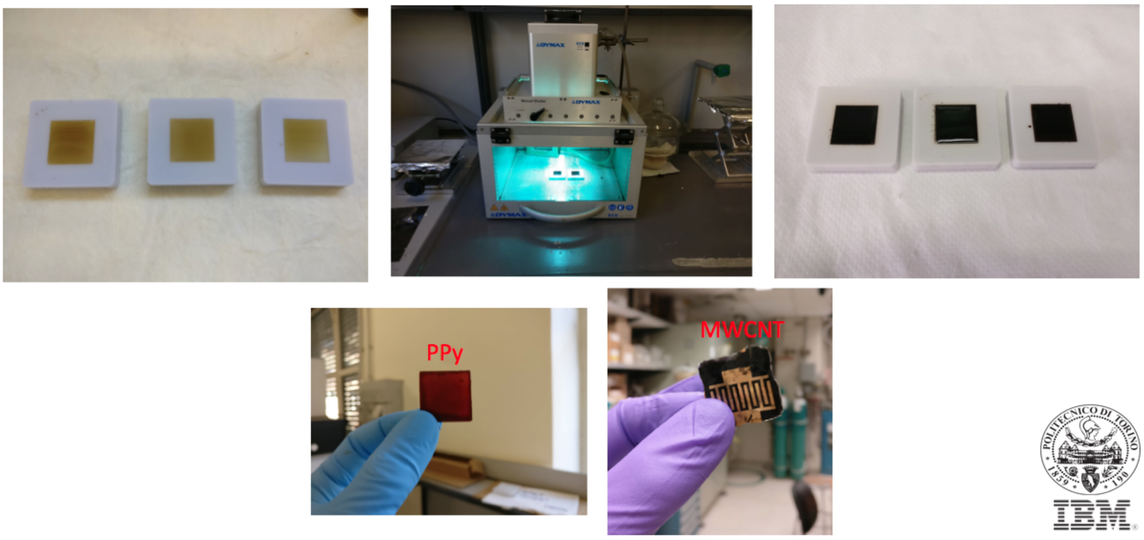

FIGURE 3.13: Photopolymerization process: (a) Liquid formulation inside PDMS molds; (b) UV-curing under flood lamp; (c) Self-standing films; (d) PPy film; (e) MWCNT film.

Thanks to this technique it is possible to develop new conductive materials with tailored properties in order to enhance mechanical strength, flexibility, thermal stability, electrical conduction and dimensional stability of the sensors. Everything just by choosing the polymer with the desired properties, such as glass transition temperature, viscosity, molecular weight (Priola et al., 1993).

3.2.3 Electrodes Deposition

In order to obtain the final sensor, one more step, performed from the author of the thesis, is needed: the deposition of metal interdigitated electrodes on top of the film. IDEs are required to perform the electrical measurements. Usually, it is sputtered a first $5\,\mathrm{nm}$ thin layer of chromium in order to promote the adhesion of the following $50\,\mathrm{nm}$ of either gold or platinum that ensure the contact. Before starting the sputtering, the films are covered with a stainless steel shadow mask of the desired pattern and put inside the main chamber, facing down. In this case, each electrode is composed of six fingers interdigitated one with each other. The length and the width of a single finger are respectively $12\,\mathrm{mm}$ and $1\,\mathrm{mm}$. The distance between the two big main pads is $15\,\mathrm{mm}$ (Fig. 3.14).

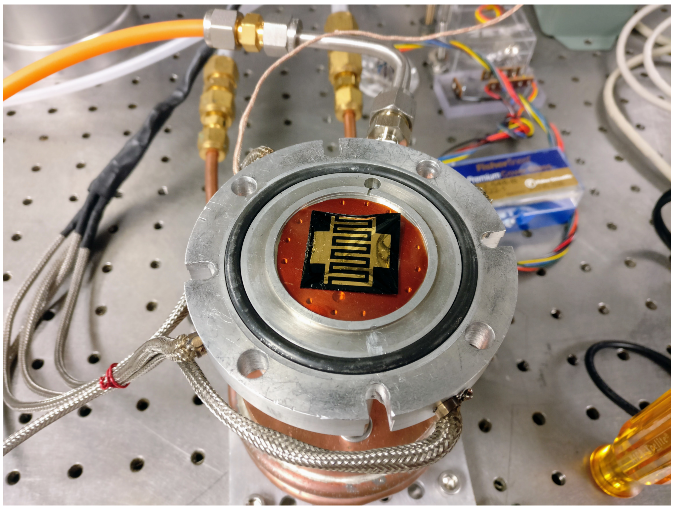

FIGURE 3.14: Electrodes geometry.

The metals that need to be evaporated are placed inside the chamber into two different crucibles made of tungsten because of its high melting point, around $3422\,^{\circ}\mathrm{C}$ (much higher than the gold one, $1064\,^{\circ}\mathrm{C}$ or chromium $1907\,^{\circ}\mathrm{C}$).
At this point the IBM custom-made evaporator is sealed and the vacuum pumps start working. First the rough one that enables the most efficient rotary vane pump. When the pressure inside the chamber reaches around $5\mathrm{x}10^{-6}$ Torr the process can begin.

Typically, a 2 V voltage is applied at the endpoints of the containers and 150 A of current pass through the metal, melting it thanks to the ohmic effect and allowing the deposition on the films (Fig.3.15).

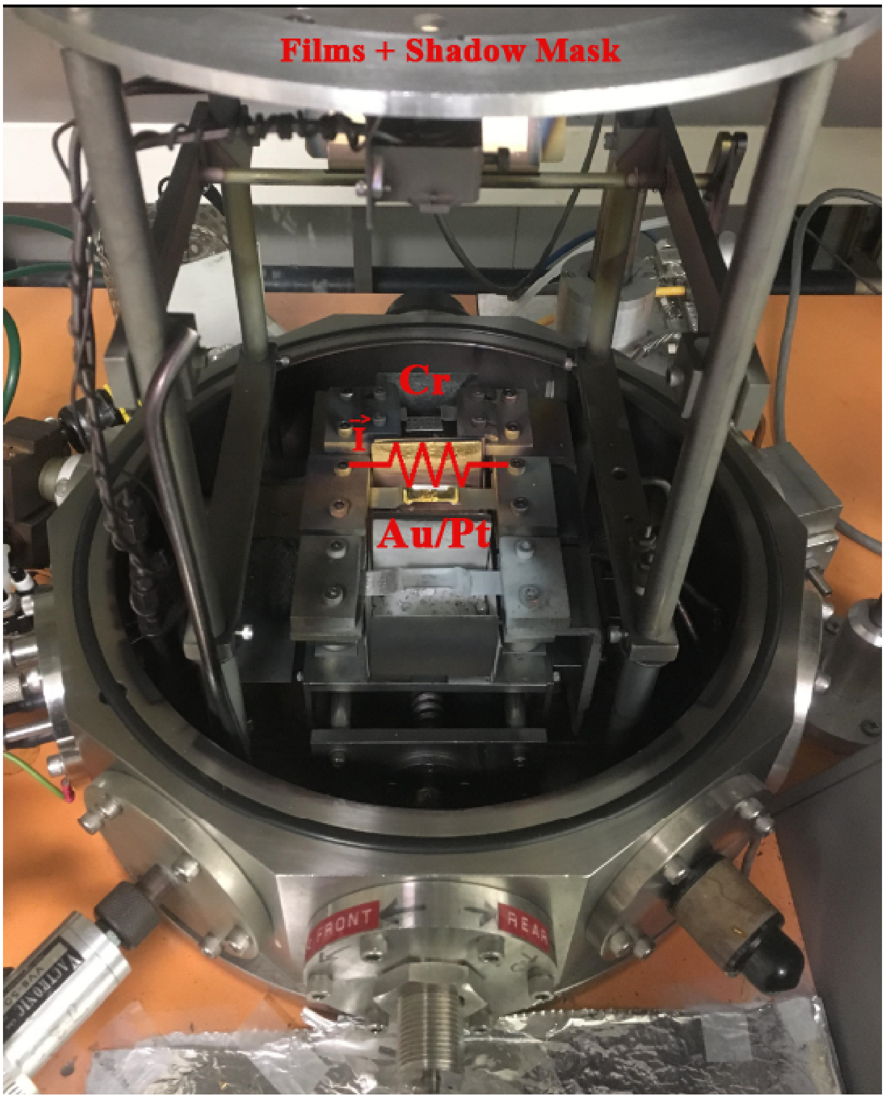

FIGURE 3.15: IBM custom-made public evaporator main chamber.

A sensor inside the chamber is capable of measuring the thickness of the sputtered metal knowing the density and the acoustic impedance of it. When the targeted thickness is reached, the shutter closes, the chamber starts to vent and the system cools down. Sensors are ready to be tested.

3.3 Gas Delivery System

Once the sensors fabrication is terminated, the chemiresistive vapor devices are ready to be tested by sensing measurements. At IBM Research Center in the Sensor Laboratory, a custom-made sensing setup is currently used to produce and deliver selected concentrations of solvent vapors to the samples. It is very important to have a reliable and verified system able to generate the gas, release and deliver it to the sample in a controlled way in order to be sure that the concentrations reached are as close as possible to the theoretical ones, ensuring the goodness of the results.

In the system, composed of multiple pipes forming an almost perfectly sealed line, a stream of oil-free dry air is exploited as carrier and diluting gas and it is obtained from the general compressed air laboratory source. The main stream is divided into two fluxes regulated by the presence of two mass flow controllers supplied by MKS (MFC Solvent and MFC Carrier). The dry air flow, controlled by the MFC Solvent, is connected through a PE pipe to a thermostatic chamber composed of a bubbler system placed inside a Dewar flask, used to maintain the temperature constant. The bubbler is a large glass test tube $30\,\mathrm{cm}$ long with a $3\,\mathrm{cm}$ inside diameter equipped with two exit sidearms (inlet and outlet of the flux). The carrier gas flows through the bubbler, properly filled with the volatile organic compound to be tested, generating a saturated vapor stream. Two precise micro-valves allow the recombination of the saturated flux, exiting from the outlet, with the pure dry air flux, coming out from the second pipe controlled by MFC Carrier.

In this way there is a dilution process and, at the intersection of the two pipes, an homogenous single stream of the desired concentration of the analyte is formed. By means of a third mechanical valve, the mixed controlled flow is allowed to enter in the detection chamber, where the sensor is located (Fig. 3.16).

When the test is performed, all the gases are exhausted from the sensing chamber using an exhaust line connected to the general one of the laboratory. This is a fundamental requirement for a good delivering system in term of safety. In fact, most of the time it is required to work with toxic and dangerous VOCs that can affect the human health.

Another crucial aspect is dealing with the range of concentrations exploitable, going from very low to very high concentrations of the analyte.

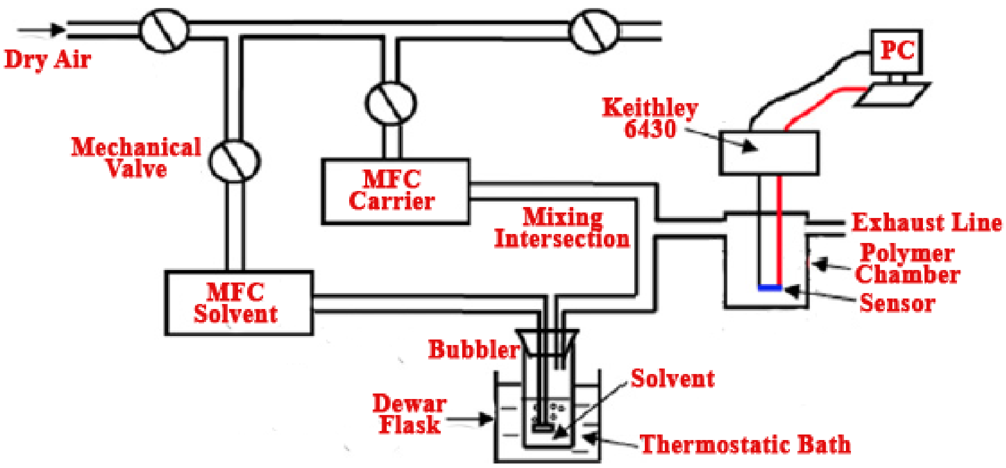

(a) Schematic representation of the system.

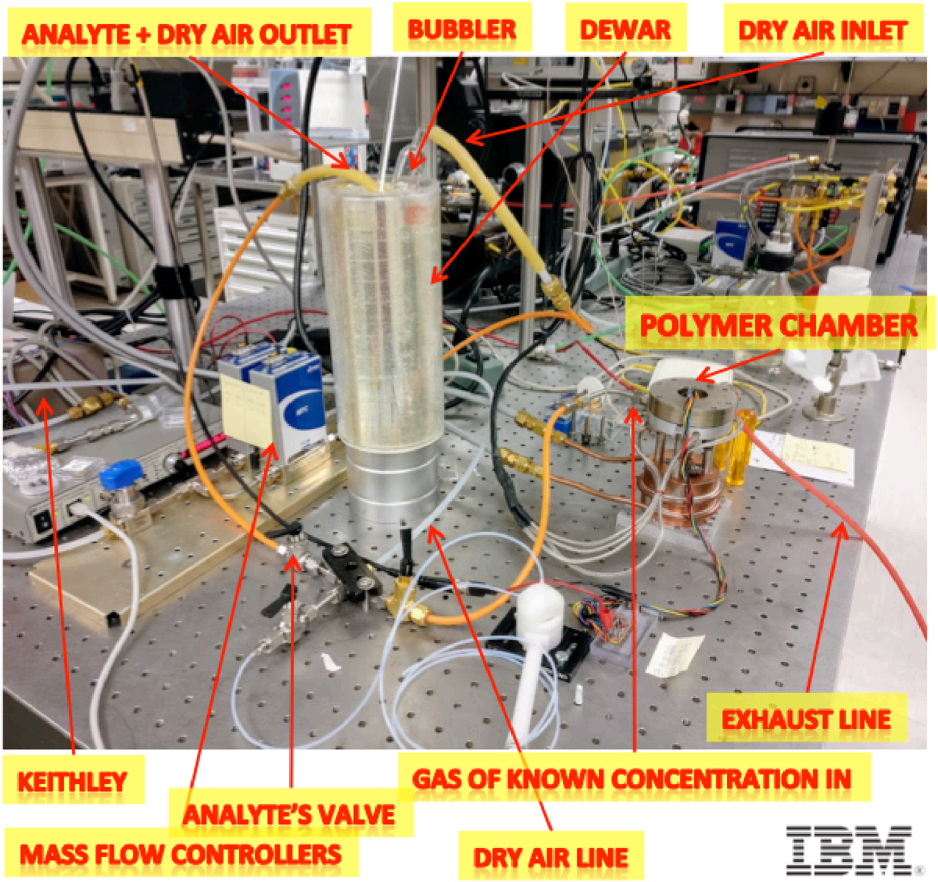

(b) IBM custom-made setup.

FIGURE 3.16: Gas Delivery System.

The two mass flow controllers can select a flow rate ranging from 3 sccm [1] (lower limit) up to 200 sccm (higher limit). During the electrical measurements the total air flow is kept constant at 100 sccm.
The concentration in part per million (ppm) of the volatile vapor is calculated using the following equation 3.1:

$$C(ppm) = \Big(\frac{P^*}{P} \times \frac{f}{f+F}\Big) \times 10^6 \tag{3.1}$$

where P is the input air pressure (which is atmospheric pressure in this case), P^* is the saturated partial pressure of the analyte; f and F are the mass flow rate of MFC Solvent and MFC Carrier respectively. P^* is evaluated by Antoine's equation as a function of the temperature and Antoine's constants A,B and C (Eq. 3.2);

$$P^* = 10^{(A-\frac{B}{C+T})} \tag{3.2}$$

All the experiments carried out in this thesis exploited five different analytes: acetone (Actn), ethanol (EtOH), isopropanol (IPA), toluene (Tol) and water (H_2O). As it is possible to deduct from the previous equations, different analytes have different partial pressures. The following Figure 3.17 shows all the concentrations, expressed in ppm, that it is possible to target at laboratory temperature ($19\,^{\circ}\mathrm{C}$) for the different vapors. Concentrations go from 100% of saturated vapor flow (100 sccm from MFC Solvent only) to 3% of saturated vapor flow (3 sccm from MFC Solvent diluted with 97 sccm from MFC Carrier).

In order to widen the range of exploitable concentrations and explore the lower detection limit, the bath temperature inside the Dewar flask can be changed using different cooling baths. The lower the temperature, the lower the partial pressure. This means fewer molecules in the vapor, bringing very low concentrations to the chamber. In this study, most measurements are performed at laboratory temperature; some experiments are carried out at $0\,^{\circ}\mathrm{C}$, reached with a ice bath; others at $-45\,^{\circ}\mathrm{C}$ by means of a cooling bath realized adding dry ice to acetonitrile (CH_3CN). Once the temperature reaches $-42\,^{\circ}\mathrm{C}$, the acetonitrile will freeze. Therefore, dry ice must be added slowly to avoid freezing the entire mixture (Alan, 1972).

---

[1] sccm: stands for Standard Cubic Centimeters per Minute and it is used as the flow unit. It calculates the amount of gas or volume of gas that passes through a given point in a unit time.

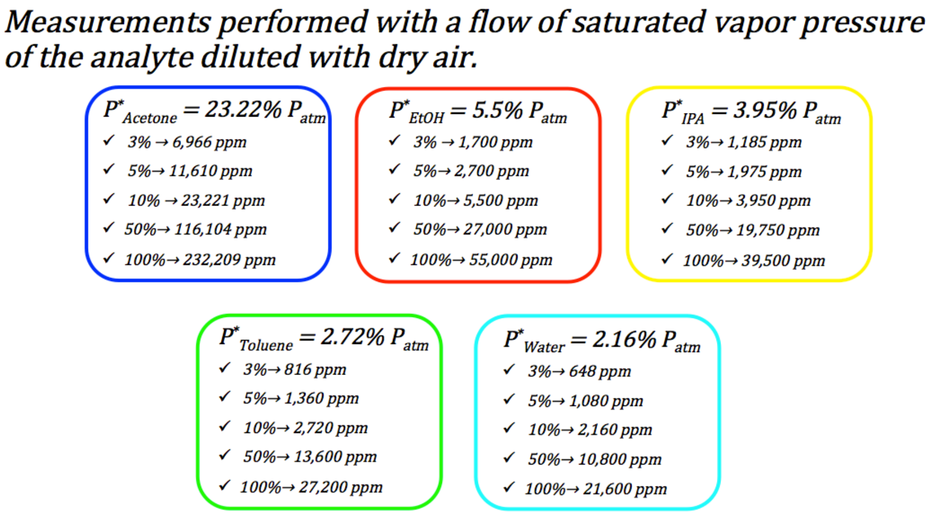

Measurements performed with a flow of saturated vapor pressure of the analyte diluted with dry air.

$P^{*}_{Acetone} = 23.22\%\ P_{atm}$
- ✓ 3% → 6,966 ppm
- ✓ 5%→ 11,610 ppm
- ✓ 10% → 23,221 ppm
- ✓ 50%→ 116,104 ppm
- ✓ 100%→ 232,209 ppm

$P^{*}_{EtOH} = 5.5\%\ P_{atm}$
- ✓ 3% → 1,700 ppm
- ✓ 5%→ 2,700 ppm
- ✓ 10%→ 5,500 ppm
- ✓ 50%→ 27,000 ppm
- ✓ 100%→ 55,000 ppm

$P^{*}_{IPA} = 3.95\%\ P_{atm}$
- ✓ 3%→ 1,185 ppm
- ✓ 5%→ 1,975 ppm
- ✓ 10%→ 3,950 ppm
- ✓ 50%→ 19,750 ppm
- ✓ 100%→ 39,500 ppm

$P^{*}_{Toluene} = 2.72\%\ P_{atm}$
- ✓ 3%→ 816 ppm
- ✓ 5%→ 1,360 ppm
- ✓ 10%→ 2,720 ppm
- ✓ 50%→ 13,600 ppm
- ✓ 100%→ 27,200 ppm

$P^{*}_{Water} = 2.16\%\ P_{atm}$
- ✓ 3%→ 648 ppm
- ✓ 5%→ 1,080 ppm
- ✓ 10%→ 2,160 ppm
- ✓ 50%→ 10,800 ppm
- ✓ 100%→ 21,600 ppm

FIGURE 3.17: Analytes used for the experiments with their relative concentrations at 19 °C.

3.4 Polymer Chamber

The other fundamental component for the electrical characterization is the sensing cell called "Polymer Chamber". Thanks to this IBM self-made equipment, it is possible to follow the resistance change of the sensor over time. Once the mixed flow is generated at the intersection, when the last mechanical valve is open, the gas can be delivered to the sample that is housed in the stainless steel assembly with a 39 mm inner diameter. The cup is then placed on top in order to create a closed chamber sealed with a rubber O-ring and tightened with four screws. The mixed flow comes out from the small hole situated on the bottom part of the chamber and diffuse over the sample, coming out with an 180° angle, where the exhaust line is placed. In addition, thanks to the metal wire connections, it is possible to heat the bottom part of the chamber and control the temperature by a thermocouple placed inside the cell. Normally, this is not necessary because the polymeric chemiresistors operate at room temperature (Fig. 3.18).

In order to characterize the self-standing samples (Fig. 3.18(a)), the contact is achieved by two metal springs touching the electrodes; on the contrary, in the devices fabricated on the substrate (Fig. 3.18(b)), electric contacts are realized by using pogo-pins of 2 mm in diameter. For both of the typologies, the sensing characterization is performed by exploiting two-tips measurements, in which one tip is bringing

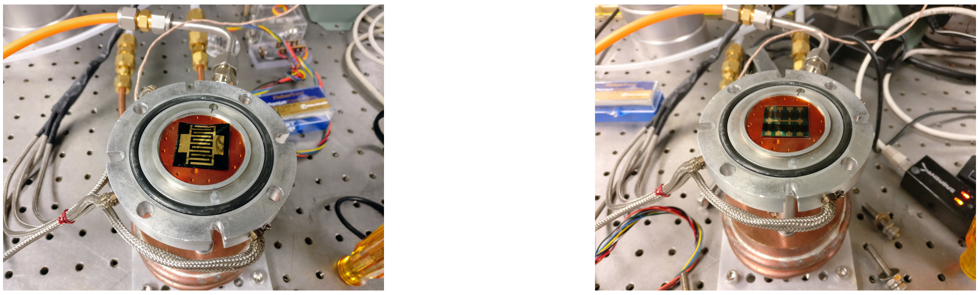

(a) In situ photopolymerized composite inside the chamber.

(b) Carbon black-polymer composite inside the chamber.

FIGURE 3.18: IBM Polymer Chamber.

the actual voltage while the other is used as ground. No ground loops effects are present because all the instrumentations have the same one. As it can be seen in Figure 3.19, the carbon black-polymer composites sample contains eight devices in which the ground is shared. For this reason, outside the chamber two crocodile clips are connected to a board. The black clip is associated with the ground and the red one can be moved in order to select one of the eight devices that needs to be tested. A Keithley model 6430 SourceMeter® is used to apply a fixed voltage of $100\,\mathrm{mV}$ to the pin in contact with the device and reading the current through the other one connected to the ground with the same source meter unit (SMU). When the experiment is run, the response data acquired from the Keithley are automatically saved on a personal computer and processed with a Python-based interface able to plot in real time the behavior of the current, strictly related to the resistance by Ohm's first law.

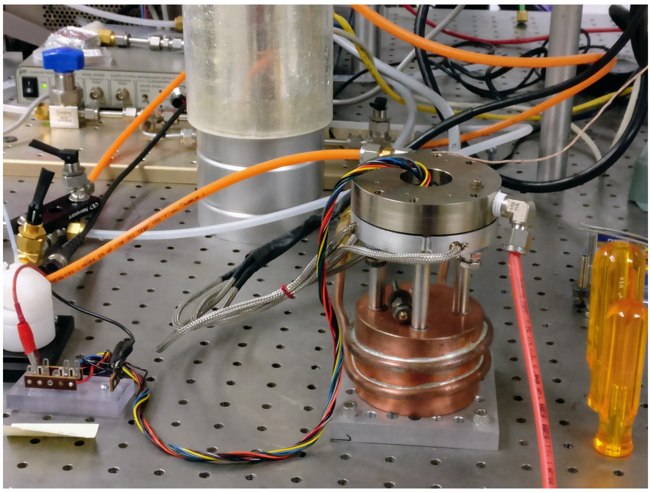

FIGURE 3.19: IBM closed Polymer Chamber.

3.5 Sensing Measurements Protocol

Whenever a new sample enters the Sensor Lab at IBM Research Center there is a precise protocol for the electrical characterization that must be followed in order to ensure a reliable comparison between all the tests performed.
Immediately, all the devices are labeled and registered in order to keep track of all the measurements performed for each device. The labeling allows to remember the type of polymer used and the filler concentration respect to the matrix. After this step, the initial resistance of each device is collected in the laboratory environment by a handheld Fluke 177 Digital Multimeter. This instrument presents an absolute maximum resistance measurement of $50\,\mathrm{M\Omega}$. Secondly, the sample containing the carbon black-polymer composites is scratched multiple times in order to isolate each of the eight devices that lay on the same substrate. In this way the electrical resistance increases because we are eliminating one or more parallel parasitic resistances of the nearest devices. Resistance measurements are performed again a second time. At this point the sample is placed inside the polymer chamber and all the resistances are checked a third time, in order to be sure the contacts are well made. It follows the stabilization of the sensors flushing dry air in the chamber. The duration may vary from thirty minutes to more than an hour depending on the nature of the device and if the baseline is stable. In fact, as we mentioned before, polymeric sensors are affected by a drift in resistance, even without any analytes. This means that the current keeps increasing over time. In this particular case, what is changing is the value of relative humidity. It is straightforward that the greater the drift, the less stable is the sample.
Once the stabilization is completed, the real sensing measurement can be run. $100\,\mathrm{mV}$ voltage is applied between the electrodes and the current is readout. For each test, dry air is introduced for 100 seconds in order to get the current baseline. Successively, the sensor is exposed at the analyte in the desired concentration for 600 seconds, followed by other 600 seconds that is set as recovery time, where the initial condition is restored. In this phase, the current recovers almost all of its change, approaching the initial baseline.

From the beginning of the test resistance, current and time are recorded in a *.txt* file and all the data are post-processed by means of Matlab scripts. This cycle is repeated for *n* number of times based on the range of concentrations being sensed, the different analytes investigated and the devices tested.

From the data analysis the most relevant parameter extracted is the sensitivity. In the frame of polymeric sensors, as it is described in Chapter 2, the resistance can increase or decrease according to the nature of the vapor in the films containing the polypyrrole. For p-type sensors, where the carriers are holes, a reducing gas, oxidizing itself, reduces the material that loses some electrons. Therefore, the resistance will decrease. Instead, an oxidizing gas, reducing itself, oxides the material that gains some electrons. In this case, the resistance will increase. On the contrary, for a n-type sensor where the carriers are electrons, the relations are reversed.
For the other films, where the main sensing mechanism is the swelling of the matrix, the resistance always increases after the exposure to the analyte.

A standard sensing curve is reported in Figure 3.20, where the resistance R is plotted as a function of time t.

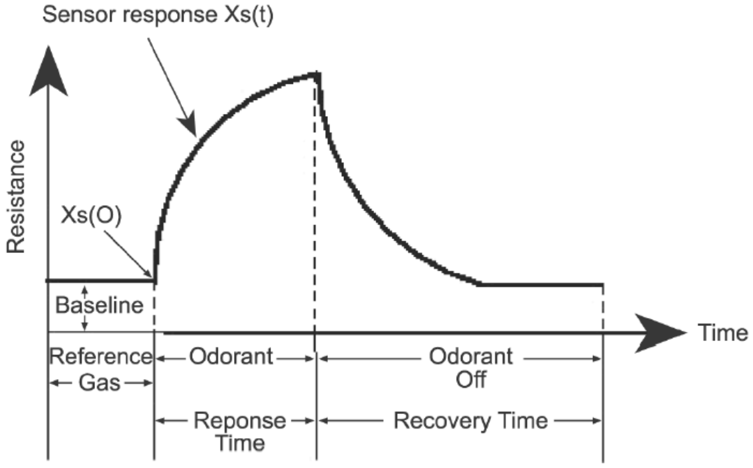

FIGURE 3.20: Typical sensor response towards an analyte. A detailed notation of all the steps for sensing is reported. *Adapted from: Arshak et al., 2004.*

Sensitivity can be defined in different ways. The typical response of the sensor to a particular gas (S) is calculated as the ratio between the steady-state resistance variation ΔR and the baseline resistance of the device:

$$S = \frac{\Delta R}{R_{Baseline}} \tag{3.3}$$

The value of ΔR is always a positive quantity. In order to do that, based on the nature of the analyte, ΔR can be defined into two different ways as shown in equations 3.4 and 3.5:

$$\Delta R_{Red} = R_{Baseline} - R_{Gas} \tag{3.4}$$

$$\Delta R_{Ox} = R_{Gas} - R_{Baseline} \tag{3.5}$$

The value of $R_{Baseline}$ is obtained by averaging the resistance values in the first 80 seconds of the test, while R_{Gas} by averaging the resistance points between 400 and 650 seconds. The response is therefore normalized to the baseline and S is a number between 0 and 1. If two sensors show the same resistance variation ΔR, but the starting baseline is different, the sensitivity will differ. In fact, thanks to the normalization, the change is correlated to the starting baseline.

However, in this thesis, the sensing response is expressed using another slightly different physical parameter called S^*.

For p-type sensors, such as polypyrrole-based, S^* is defined by the following equations (3.6 and 3.7):

$$S^*_{Red} = \frac{I_{Gas}}{I_{Air}} = \frac{R_{Baseline}}{R_{Gas}} = S_{Red} + \frac{1}{S^*} \tag{3.6}$$

(Used for oxidizing gas, which are electrons donators)

$$S^*_{Ox} = \frac{I_{Air}}{I_{Gas}} = \frac{R_Gas}{R_Baseline} = S_{Ox} + 1 \tag{3.7}$$

(Used for reducing gas, which are electrons acceptors)

For composites, where the swelling of the matrix is the main mechanism, S^* is defined in equation 3.8 as:

$$S^* = \frac{I_{Air}}{I_{Gas}} = \frac{R_{Gas}}{R_{Baselin}} = S + 1 \tag{3.8}$$

S^* is a pure dimensionless number that can be greater than 1. This allows an easy and fair comparison between different samples, widening the scale.

It is easy to notice that the two definitions of the sensitivity are linked each other and there is not a preference in using one kind of equation with respect to the other one. However, always remember the typology of the gas and the typology of the sensor (p-type or n-type).

3.6 Impedance Analyzer

All the tests described above are performed in direct current (DC). Sometimes, it is necessary to run some experiments in alternated current (AC) because it might be more efficient and more parameters and information on the films can be extracted. The best way to apply a periodic voltage is through a very powerful tool: the impedance analyzer 4294A supplied by Agilent (Fig. 3.21).

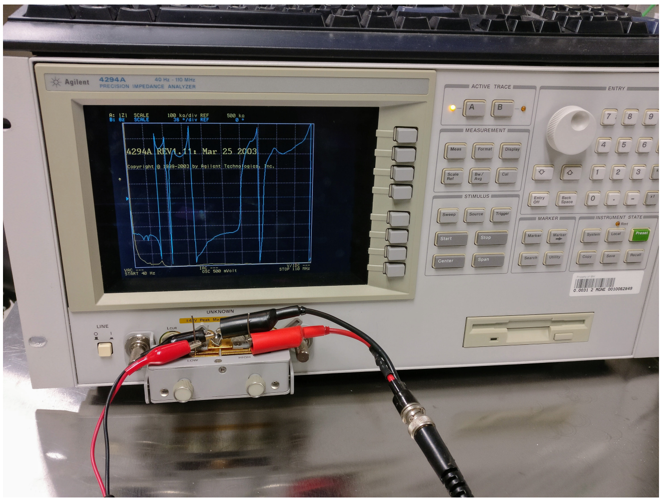

FIGURE 3.21: Impedance Analyzer 4294A.

Thanks to this instrument, it is possible to measure the electrical impedance, which is defined as the opposition that a circuit or electronic component displays to the alternating current when a voltage is applied. Usually, the impedance is a complex number and it extends the concept of resistance in AC analysis. It is characterized by a magnitude $|Z|$ and a phase θ. The unit of impedance, like the resistance, is the Ohm (Ω). In DC measurements, there is no difference between impedance and resistance. The latter one is the impedance with zero phase angle. In other words, the impedance links in a linear way the voltage and the current ($Z = V/I$) for a single complex exponential at a particular frequency ω. It can be written in a polar form as:

$$Z = |Z| \cdot e^{i\theta} \tag{3.9}$$

where the magnitude represents the ratio of the voltage amplitude to the current amplitude, while θ gives the phase difference between voltage and current. The impedance can be also written in a Cartesian form, as shown in 3.10:

$$Z = R + iX \tag{3.10}$$

where the real part is associated to the resistance of the circuit, while the imaginary part, called reactance, is related to the inductance and capacitance of the circuit. The resistance component arises from collisions of the charged carriers, most likely electrons, with the internal lattice of the conductor. The reactance component, instead, is an additional opposition to the movement of electric charges that arises from the changing magnetic and electric fields in circuits carrying alternating current. In other words, it describes how the circuit stores and releases energy as the current fluctuate with each AC cycle.

In this work, sensors made with in situ photopolymerized composites have been also tested in AC by means of this tool. For this type of sensors, it is possible to model an equivalent electric circuit, as shown in Figure 3.22.

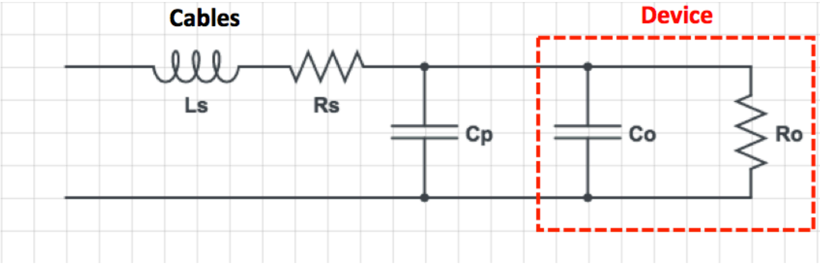

FIGURE 3.22: Equivalent electric circuit.

The sensor can be oversimplified as a RC circuit where the device is a parallel between a resistance R_0 and a capacitance C_0. Moreover, there are some parasitic contributions due to cables connections between the Polymer Chamber and the

impedance analyzer. Respectively, there are a series resistance R_s, a series inductance L_s and a parallel capacitance C_p.
In the frame of gas sensing, it is very useful to be able to monitor the behavior of these two parameters, R_0 and C_0, as the device is exposed to different environments. However, R_0 and C_0 can't be evaluated immediately because from the measurements it is possible to estimate magnitude and phase of the impedance as a function of the frequency. Knowing $|Z|$ and θ, it is simple to notice that they are strictly linked with the real and imaginary part of the impedance Z, as shown in 3.11 and 3.12:

$$|Z| = \sqrt{R^2 + X^2} \tag{3.11}$$

$$\theta = tan^{-1}\Big(\frac{X}{R}\Big) \tag{3.12}$$

Once $Re(Z)$ and $Im(Z)$ are calculated, they can be written as:

$$Re(Z) = \frac{R_0}{1 + [\omega(C_p + C_0) \cdot R_0]^2} + R_s \tag{3.13}$$

$$Im(Z) = -\frac{\omega R_0^2 \cdot (C_p + C_0)R_0}{1 + [\omega(C_p + C_0) \cdot R_0]^2)} + \omega L_s \tag{3.14}$$

Rearranging the equations 3.13, 3.14 and using some sostitutions, R_0 and C_0 can be represented by equations 3.15 and 3.16:

$$R_0 = -\beta \cdot \frac{1 + \gamma^2}{\gamma} \tag{3.15}$$

$$C_0 = \frac{\gamma^2}{\omega\beta \cdot (1 + \gamma^2)} \tag{3.16}$$

where:

$$\alpha = Re(Z) - R_s \tag{3.17}$$

$$\beta = Im(Z) - \omega L_s \tag{3.18}$$

$$\gamma = \frac{\beta}{\alpha} \tag{3.19}$$

The first step to measure the polymer impedance is the evaluation of the parasitic components because without them it will be impossible. Given that different setup geometries may affect the measurements, various configurations to connect the sample to the impedance analyzer were tested and compared using:

- One Coaxial cable
- One Coaxial cable connected to the "Polymer Chamber"
- Regular wires
- Regular wires connected to the "Polymer Chamber"
- No cables, samples sandwiched between glass slides directly connected to the tool with short (few mm) leads

For each configuration, different test were run:

- Short circuit
- Open circuit
- Connected to a resistor of known R
- Connected to a capacitor of known C
- Connected to a polymeric film

Series parasitic contributions R_s and L_s were then subtracted from the measurements and they represented a very minor effect. On the contrary, parallel capacitance C_p was significant but the value obtained was unphysical, likely due to the use of an oversimplified model. It was decided not to remove this contribution from the calculations and thus the capacitance C_{Tot} herein obtained was strongly affected by parasitic effects. Actual sample capacitance C_0 is estimated to be $\approx 2\,\mathrm{pF}$, while R_0 was not affected by C_p. Therefore, it was possible to observe the relative change of C but the real value was unknown. Unable to solve this issue, other three configurations were tested and parasitic contributions were evaluated as follow (Fig. 3.23, 3.24 and 3.25):

- The series resistance R_s was extracted from $|Z|$ when θ approached 0° in short circuit.
- The series inductance L_s was calculated from the slope of $|Z|$ when θ approached 90° in short circuit.

- The parallel capacitance C_p was equal to the slope of $|Z|$ when θ approached -90° in open circuit.

Using one single coaxial cable, R_s and L_s were very small compared to the entire system, while C_p still resulted greater than C_{Tot}.

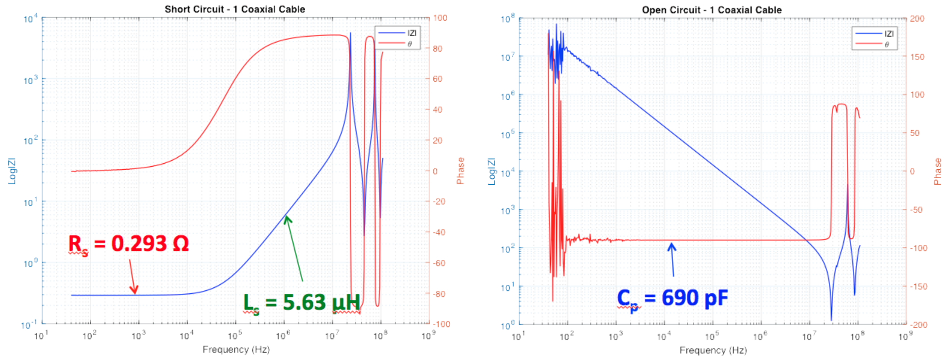

(a) Bode plot in short circuit and open circuit.

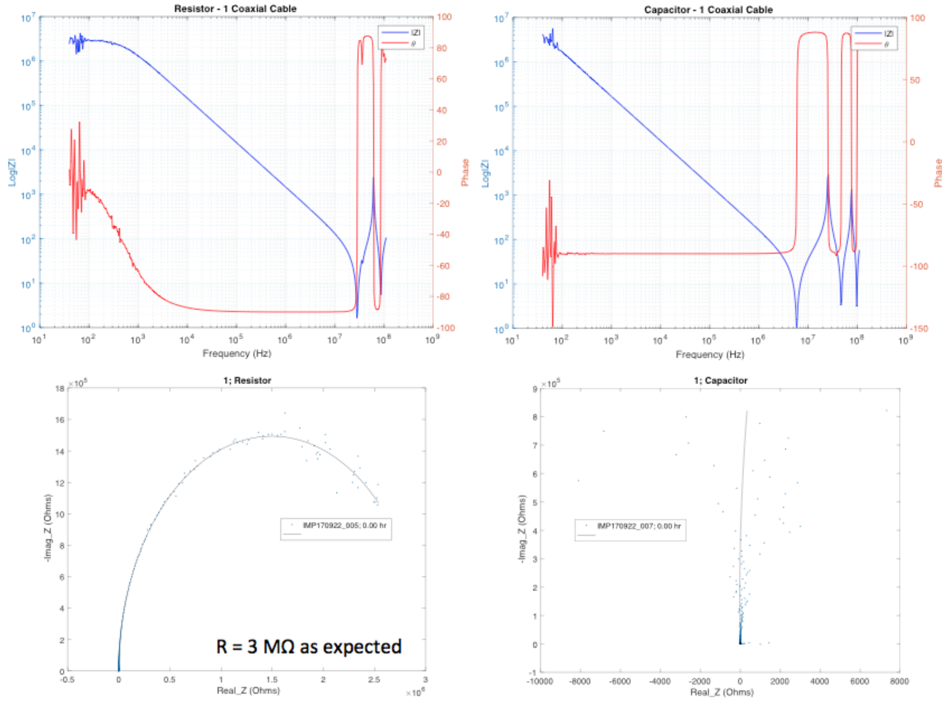

(b) Setup tested with a $3\,\mathrm{M\Omega}$ resistor and a $6\,\mathrm{pF}$ capacitor.

FIGURE 3.23: One single coaxial cable configuration.

Connecting the impedance analyzer with two coaxial cables to the Polymer Chamber, as it is possible to see from the Bode plot in Figure 3.24, the parallel capacitance was two orders of magnitude lower.

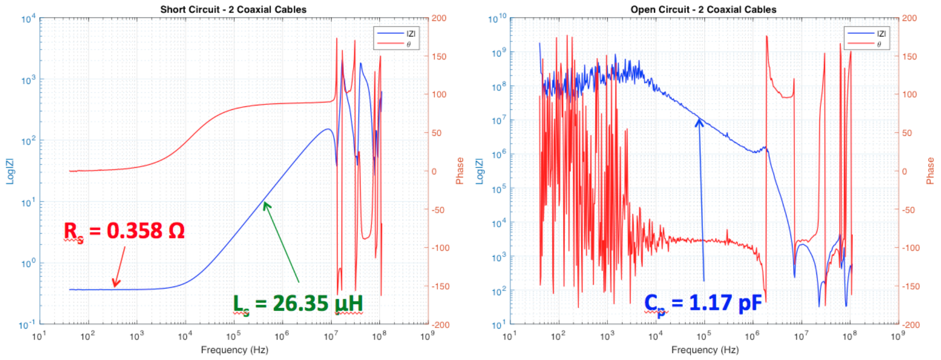

(a) Bode plot in short circuit and open circuit.

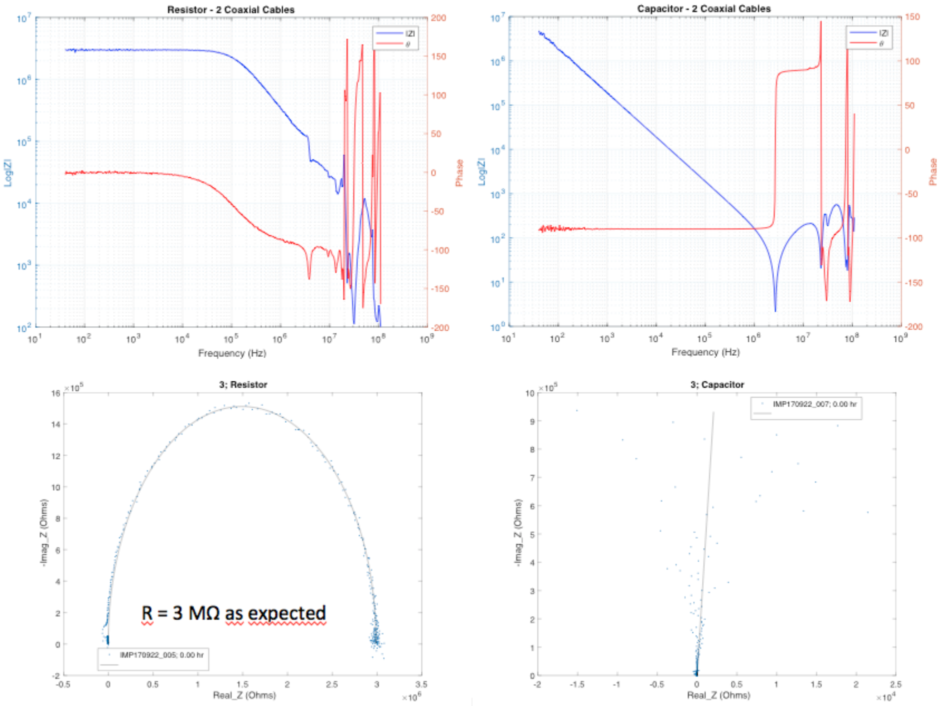

(b) Setup tested with a $3\,\mathrm{M\Omega}$ resistor and a $6\,\mathrm{pF}$ capacitor.

FIGURE 3.24: Two coaxial cables configuration.

Similar results were obtained using four coaxial cables, where C_p was even lower.

In these new configurations, the sample capacitance C_0 was estimated to be $\approx 4\,\mathrm{pF}$; this result has a physical meaning and it is more reasonable with the value obtained connecting directly the sample to the tool without cables (around $\approx 2\,\mathrm{pF}$). However, because of this lack of reliability and reproducibility with the different cables geometries, it was unclear if the errors presented were due to the system setup, the way parasitic contributions were evaluated and subtracted or linked to the sample.

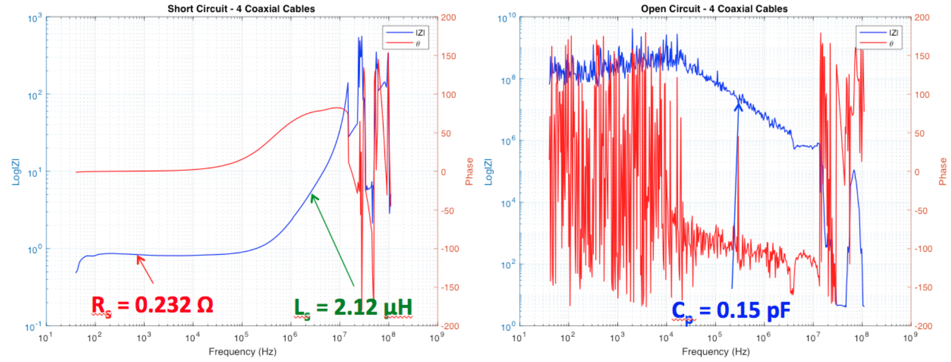

(a) Bode plot in short circuit and open circuit.

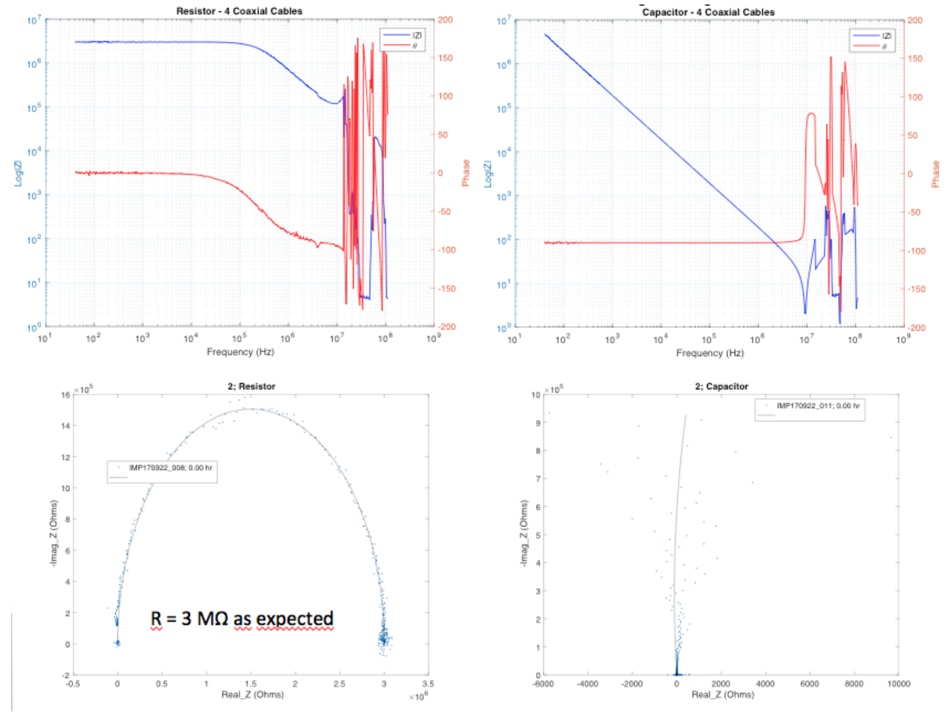

(b) Setup tested with a 3 MΩ resistor and a 6 pF capacitor.

FIGURE 3.25: Four coaxial cables configuration.

It looks like the model used was oversimplified and there was a phase shift as a function of the frequency that delayed the signal from the impedance analyzer to the chamber and back. Some studies were made trying to estimate the shift, testing a series of different resistors and plotting them as a function of the frequency, as shown in Figure 3.26. Based on the various resistances, it is easy to notice the shift is different.

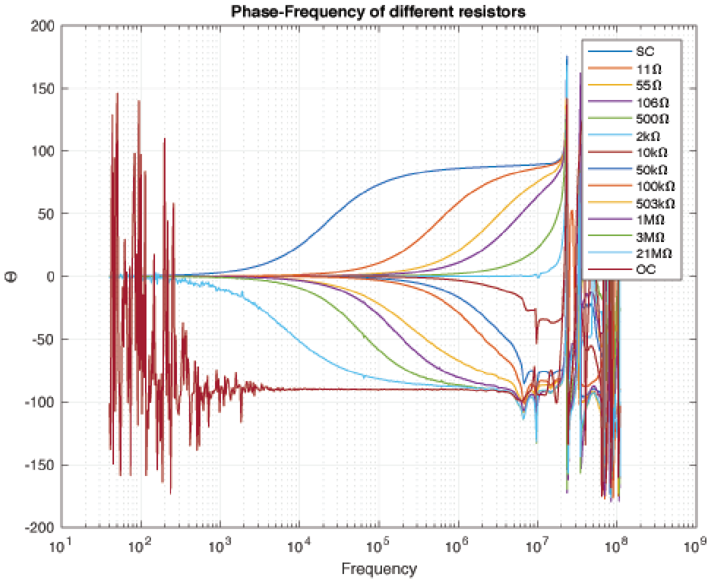

FIGURE 3.26: Phase shift as a function of ω for different resistors.

For all these reasons, in order to eliminate all the parasitic contributions of the cables and improve the contacts between the electrodes and the tool, a new simple portable sensing chamber, called AC Polymer Chamber, was engineered and produced at IBM Research Lab. In this new configuration shown in Figure 3.27, the sample is sandwiched between a microscope glass on the bottom (positioned over a metal support) and a Teflon component on the top. The latter part is empty in the middle, creating a cavity that works as the detecting chamber. In addition, two small holes are placed on the top of the cap in order to connect the mixed flux inside the chamber and letting the exhaust gas out. The AC Polymer Chamber is not completely sealed as the other one. Having said that, a metal structure with an insulating pin is used to maintain the contact well firm, avoiding major leakages. In this way, no cables are needed and no springs are used to make the contacts, avoiding friction and peeling off the gold layer. The parasitic contributions are reduced a lot respect to previous configurations and the value of R_0 and C_0 are more reasonable.

Using the impedance analyzer, two different sensing analyses can be performed: a static and a dynamic test.
In the static analysis, the device is exposed at three different environments: in laboratory humid air, in dry air and in analytes vapor. Measurements of R_0 and C_0 with the system close to steady-state conditions are collected over a large frequency

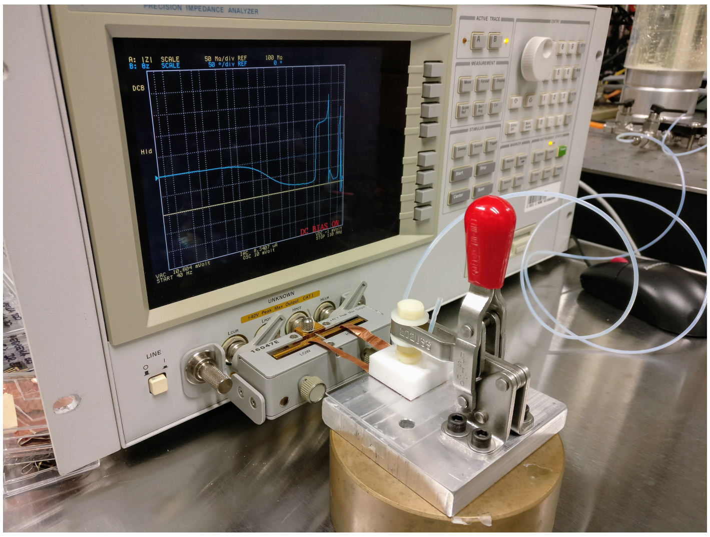

FIGURE 3.27: IBM AC Polymer Chamber.

range from 40 Hz up to 110 MHz. The protocol followed consists in placing the sample inside the chamber with no air flow and the first data are collected in humid air condition. The second run is launched after having switched on the dry air flow and waited 1200 seconds. This measurement allows to see if any drift is present, changing from a humid to dry environment and helps stabilizing the sample. At this point, the vapor to be tested is flushed inside the chamber at the wanted concentration for 600 seconds and data are saved after the exposure. Finally, in order to recover the film from the analytes exposure, dry air is flushed again for 300 seconds and a last measurement is taken.

This type of analysis doesn't allow to follow in real time the behavior of the resistance and capacitance but permits to evaluate the change amid conditions only. $Re(Z)$, $Im(Z)$, $|Z|$ and the phase θ are saved in a *.txt* file as a function of the frequency. The data coming out from the impedance analyzer are then analyzed with a Matlab script that graphs the Nyquist plot for each condition.

The Nyquist plot describes the equivalent electric circuit, plotting the real (x-axis) and the imaginary part (y-axis) for the different frequencies. In a RC circuit, the Nyquist plot is described by a semi-circle, where the frequency of the maximum represents the resonance frequency F_{Res}. The Matlab script performs a circle fit estimating R_0, C_0 and n, a pure number that defines the deviation from the semi-circle in Nyquist plot of the ideal RC circuit. In order to get a better fit, noisy low-frequency data points below an arbitrary frequency (100 Hz-200 Hz) are discarded.

In the dynamic test, on the contrary, the resistance and capacitance of the sample are monitored over time for a given frequency while the conditions change. The output results are similar to the DC curves. However, this kind of measurements is restricted to a range of frequencies that go from 40 Hz to 10 MHz, due to a tool limitation. Basically, the impedance analyzer sweeps the frequencies for each cycle and it collects 126 cycles that needs to be divided in the different conditions. Respectively, one cycle in humid air, fifty-two in dry air, fifty-three under VOCs and twenty in dry air for the recovery.

All the parameters set for the two typologies of experiments are summarized in Figure 3.28 and Table 3.2:

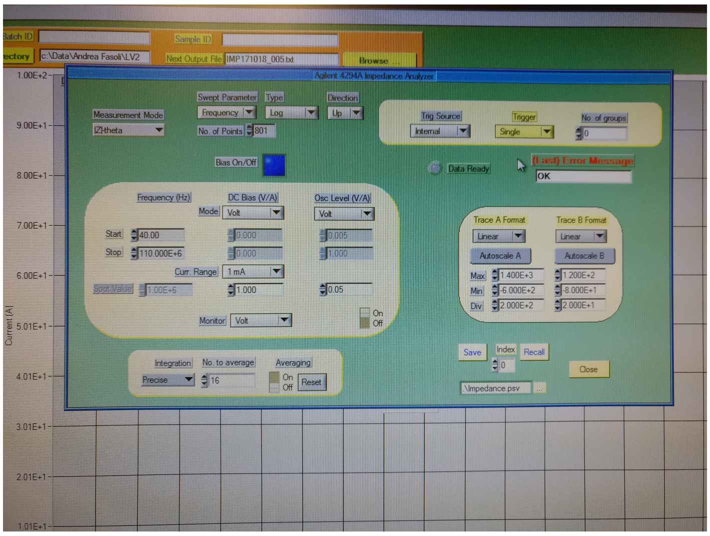
Batch ID
ectory: c:\Data\Andrea Fasoli\LV2
Sample ID
Next Output File: IMP171018_005.txt
Agilent 4294A Impedance Analyzer
Measurement Mode: |Z|-theta
Swept Parameter: Frequency
Type: Log
Direction: Up
No. of Points: 801
Trig Source: Internal
Trigger: Single
No. of groups: 0
Bias On/Off
Data Ready
(Last) Error Message: OK
Frequency (Hz): Start 40.00; Stop 110.000E+6; Spot Value 1.00E+6
DC Bias (V/A): Mode Volt; 0.000; 0.000; Curr. Range 1 mA; 1.000
Osc Level (V/A): Volt; 0.005; 1.000; 0.05
Monitor: Volt
Integration: Precise
No. to average: 16
Averaging
Trace A Format: Linear; Max 1.400E+3; Min -6.000E+2; Div 2.000E+2
Trace B Format: Linear; Max 1.200E+2; Min -8.000E+1; Div 2.000E+1
Index: 0
.\Impedance.psv

FIGURE 3.28: Impedance Analyzer adjustable parameters.

TABLE 3.2: Impedance Analyzer adjustable parameters.

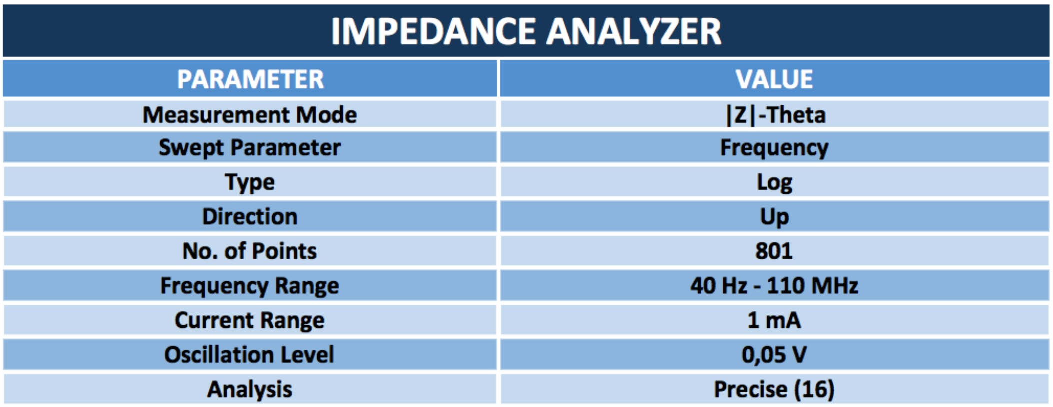
IMPEDANCE ANALYZER	
PARAMETER	**VALUE**
Measurement Mode	|Z|-Theta
Swept Parameter	Frequency
Type	Log
Direction	Up
No. of Points	801
Frequency Range	40 Hz - 110 MHz
Current Range	1 mA
Oscillation Level	0,05 V
Analysis	Precise (16)

Chapter 4

Carbon Black-Polymer Composites

In this chapter of the thesis it is reported a detailed analysis of the experiments carried out on the carbon black-polymer composites, one of the class of the bigger polymer gas sensors category. The aim of the work was to achieve a better understanding of the chemical and physical properties that could affect the sensing performances, trying to correlate the sensing mechanism to the material characteristics. In order to improve sensitivity and selectivity various materials were analyzed through the study of different systematics. In this scenario, this is a quite challenging task because there are many parameters that can be adjusted and tuned with the purpose of creating the best working device employable in the array composing the electronic nose. It is even difficult to report the same results in terms of sensitivity and selectivity of the other commercial sensors compared to the one in-house made. The approach followed to answer some of these still unclear questions was to focus on a single parameter and investigate the electrical response, keeping everything else constant. In light of this, dealing with the materials and the fabrication process of the device, critical variables that can be changed are the choice of the carbon black precursors, the organic thermoplastic insulating matrix, the concentration of the conductive filler and the electrodes distance and geometry. Furthermore, studies of the effect of the thickness, the deposition technique and type of polymerization can be determined. Similarly, in the experimental procedure, acetone and ethanol have been used to test the level of response and selectivity as well as the dependence of the total air flow and different bath temperature in order to reach a wider range of concentrations.

4.1 Research of the Percolation Threshold

Before dealing with the experimental details and the relative results, it is important to clarify the role of the percolation threshold. As it was reported in greater detail, the predominant sensing mechanism of these composites is the swelling of the matrix, where the filler is evenly dispersed. Hence, conducting paths are formed inside the composite where electrons, responsible of the conductivity, can move from a carbon black particle to another generating a current. The hopping of the electrons can occur only if the distance between the filler aggregates is contained. Once the film is exposed in the ambient with the vapor that needs to be tested, it starts to swell because the vapor molecules break the entanglements between the polymeric chains and the free volume increases along with the distance amid the conductive particles. In this way the resistance is incremented due to the fact that electrons can't hop anymore (Fig. 4.1).

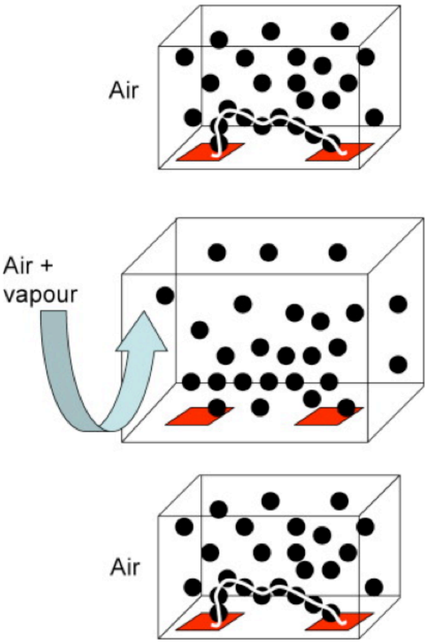

FIGURE 4.1: Sensing mechanism: the swelling of the matrix.
Adapted from: Llobet, 2013.

According to the percolation theory, the behavior of the specific resistance reflects a sigmoid to threshold curve. At the percolation threshold there is a huge drop of the resistance of several orders of magnitude for a small change in the conductive load. If the filler concentration is too high, even when the polymer swells there isn't a relevant change in conductivity; in the same way, if the load of carbon black is too low, the resulting resistance is too high to be measured. In light of what has been said, the percolation threshold is the region where we want to work because extensive variations in resistance are achieved during the swelling due to the right distance amid the particles. For this reason, the determination of the optimal carbon black source for sensor material and its concentration is crucial. For this study the Vulcan XC72 (VXC72) and the Black Pearl 2000 (BP2000), both produced by Cabot Co., were compared in terms of conductivity and sensitivity of sensors, in order to establish the one presenting the sharper percolation threshold (i.e. bigger changes and superior sensitivity). The matrix chosen for this experiment was a block copolymer PS/PDMAEMA with a molar ratio of 2,7 and a PDI = 1,42. The molecular weight of the PS was $5{,}5\,\mathrm{kDa}$, while the PDMAEMA repeating unit was $14{,}7\,\mathrm{kDa}$. The overall average molecular weight was $20{,}2\,\mathrm{kDa}$. The samples were all prepared by flow coating depositing four layers, creating a systematic of different carbon black concentrations ranging from 5 wt% up to 60 wt% with steps of 5 wt%. IBM researchers synthetized eighteen different formulations. In addition to this, within the same formulation, four devices were fabricated for each solution in order to build up a quite good statistic for this study. For the samples using BP2000 the resistances measured were from 280 kΩ (CB/Polymer ratio 20/80) up to 295 Ω (60/40). No resistance was determined for devices with a carbon black concentration lower than 20 wt% because of the limitation of the multimeter up to 50 MΩ. Similarly, for the sample containing VXC72 the resistances were from 3 MΩ (ratio 15/75) up to 500 Ω (60/40). From previous works it is possible to state that the best range is between few kΩ and hundreds of kΩ. The results are reported in Figure 4.2 and they are compared with the Figure 4.3, which shows the percolation for different kinds of carbon black in rubber components according to Cabot (Cabot, 2016).

It appears that devices containing the BP2000 are more conductive respect to the ones with VXC72 with the same amount of filler. In addition the drop seems to be sharper for BP2000 as declared by the manufacturing company. However, because of the very high resistance, it is hard to estimate the baseline of the first part of the graph and conclusions can't be drawn before analyzing the sensitivity. For both types, the percolation region is placed for a carbon black concentration between 15 wt% and 25 wt%. As expected, for both materials the conductivity decreases as the filler load gets smaller. This is true because there are fewer molecules that can build the conductive paths.

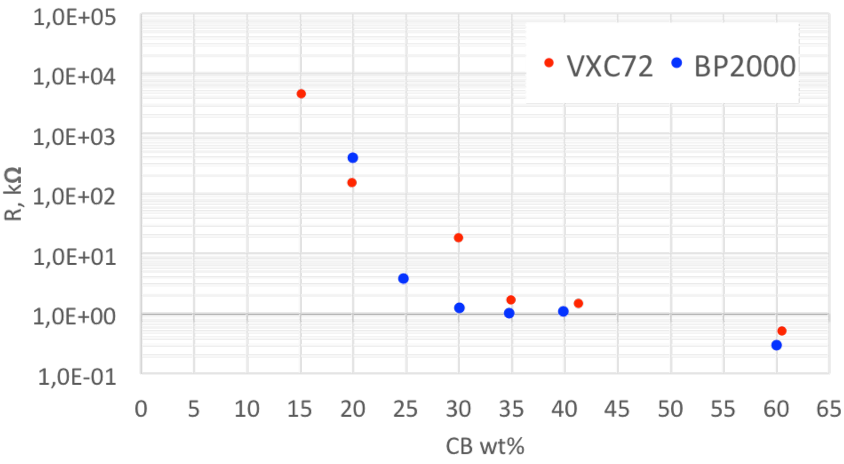

FIGURE 4.2: Experimental percolation curve.
In red samples with VXC72; in blu samples with BP2000.

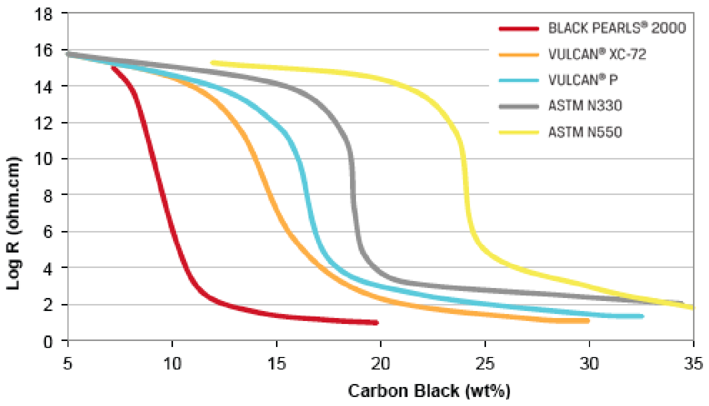

FIGURE 4.3: Theoretical percolation curve. *Adapted from: Cabot, 2016.*

Another study concerning the effect of the thickness was made using a profilometer. It is possible to see different behaviors, as shown in Figure 4.4. All the measurements shown are the average between two different tests in order to increase the statistical significance of the results. In Addition, the roughness was analyzed and it was always in between $18\,\mathrm{nm}$ and $50\,\mathrm{nm}$. While for the BP2000 the thickness increases slightly as a function of carbon black concentration, in the VXC72 samples the opposite behavior is observed. This phenomenon can be explained with the fact that the VXC72 has a lower density, it can be processed easier and it aggregates less than the Black Pearl 2000. As a matter of fact, more molecules that bind together can be translated in thicker layers.

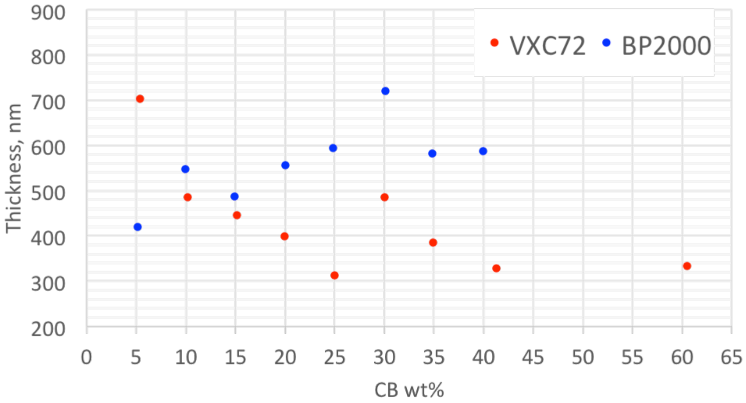

FIGURE 4.4: Thickness as a function of the carbon black load.

4.2 Sensitivity

In this section it will be discussed the trend of the response of the eighteen aforementioned formulations used to build seventy-two sensors. All of them were electrically characterized following the standard protocol explained in section 3.5. The applied voltage was fixed at 100 mV with a constant total flow set to 100 sccm. The experiments were run at room temperature with a flow of 3 sccm of ethanol, corresponding at 1700 ppm. The exposure time was set for 600 seconds as well as the recovery time. These conditions were the same used for all these experiments and they were chosen in this way in order to have the fairest comparison possible. The typical graph obtained is shown in Figure 4.5(a) and 4.5(b), where there is a comparison between the two different precursors at same filler load: 20 wt%.

In this case the sensitivity of the sample on the right is higher and the level of noise of the sensor on the left is greater, even if the starting baselines, and therefore resistances, are different. The VXC72 device presents 6% variation of the original resistance, while the BP2000 sensor only 3,8%. The time response is quite fast: the drop can be observed as soon as the mechanical valve was open and after 600 seconds it looks like the resistance approaches a constant value in a steady-state. Similarly, the baseline is recovered 100% in less than 100 seconds. It can be noticed also that a slight drift of the resistance is present, both at the beginning of the test in the first 100 seconds and at the end of the experiments. This effect is due to the poor stability of these sensors.

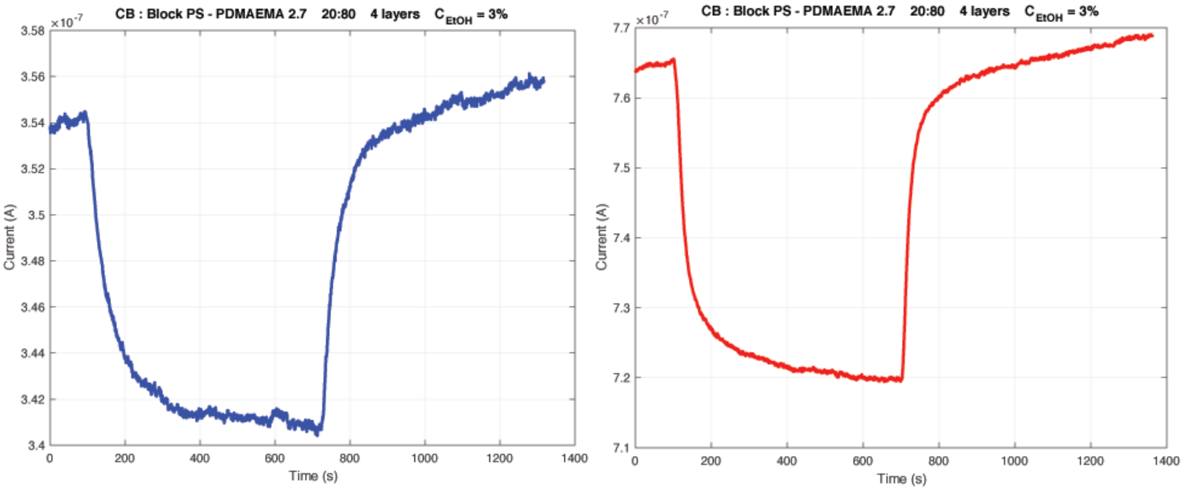

(a) Sensor with 20 wt% BP2000

(b) Sensor with 20 wt% VXC72

FIGURE 4.5: Sensing curves where the output current is plotted as a function of the time.

The overall results are reported in Figure 4.6. By themselves, these data are providing that far from the percolation region, for high amount of carbon black, the sensitivity decreases because there are too many particles and the change of resistance is not significant. On the contrary, as the percolation threshold is approached, the response increases as the magnitude of the change is remarkable. At 5 wt% and 10 wt% the sensitivity is not zero. The starting current is close to zero because the respective resistance is in the range of MΩ. Due to this fact, the signal level is comparable with the noise of the measurement. Concerning the comparison one could say the better response to ethanol is reached for the Vulcan XC72. However, that is a sudden conclusion because, from Figure 4.2, it was said that the materials present different percolation thresholds and we don't know if the two curves are going to intersect themselves again at lower load. In addition, the data point of VXC72 with the ratio 25/75 seems to be out of trend. This might mislead the reader on the sharpness of the curve and its comparison with the one of Black Pearl 2000. An interesting experiment would be the testing of samples 25/75, 20/80 and 15/85 in order to understand the real behavior of devices prepared with VXC72. In this way it would be possible to understand which data point was the wrong one.

In conclusion, according to the theory, the closer the sensor to the percolation threshold, the higher the sensitivity. In light of these results in disagreement with the Cabot statement, the Sensor Group decided to choose the VXC72 as the carbon black precursor because it shows a higher sensitivity at all the filler concentrations and the processability during the carbon black suspension and the flow coating was much easier.

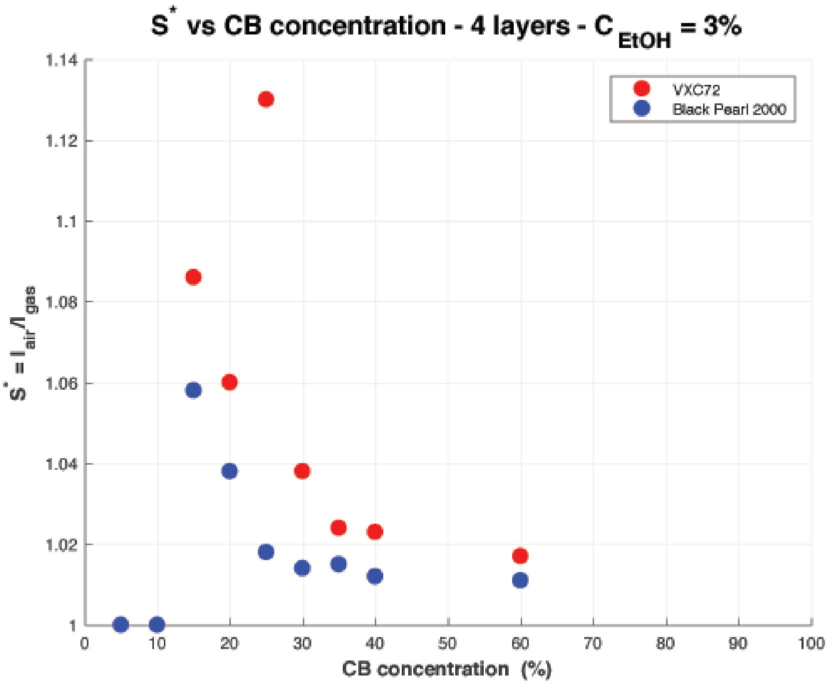

FIGURE 4.6: Sensitivity variation according to different carbon black loads.

4.3 Spacing between Electrodes

A systematic study on the effect of electrodes geometry was carried out, changing the gap between the pads. The distance was increased from $100\,\mu\text{m}$ up to $1000\,\mu\text{m}$, testing $250\,\mu\text{m}$ and $500\,\mu\text{m}$ (Fig. 4.7).

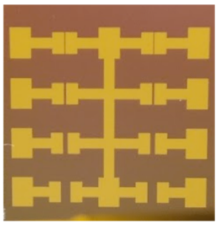

FIGURE 4.7: Systematic study on electrodes geometry.
From top: $100\,\mu\text{m}$; $250\,\mu\text{m}$; $500\,\mu\text{m}$; $1000\,\mu\text{m}$.

This new pattern was possible changing the parameter during the electron beam writing on the wafer preparation process. The matrix chosen for this experiment was a block copolymer PS/PDMAEMA with a molar ratio of 2,7 and a PDI = 1,42. The molecular weight of the PS was 5,5 kDa, while the PDMAEMA repeating unit was 14,7 kDa. The overall average molecular weight was 20,2 kDa. The samples were all prepared by flow coating, where four layers were deposited; the carbon black concentration was fixed at 40 wt%, using both the Vulcan XC72 and the Black Pearl 2000. The targeted analyte was ethanol in a concentration of 1700 ppm. Following always the same standard protocol for the electrical characterization, the response curves obtained are reported in Figure 4.10. As expected, from Figure 4.8, it is possible to notice that the resistances increase in a linear way as a function of the distance in both cases. This is reasonable because the length of the conductive paths is longer and, statistically, there are fewer electrons able to pass across the electrodes, thus the current is lower.

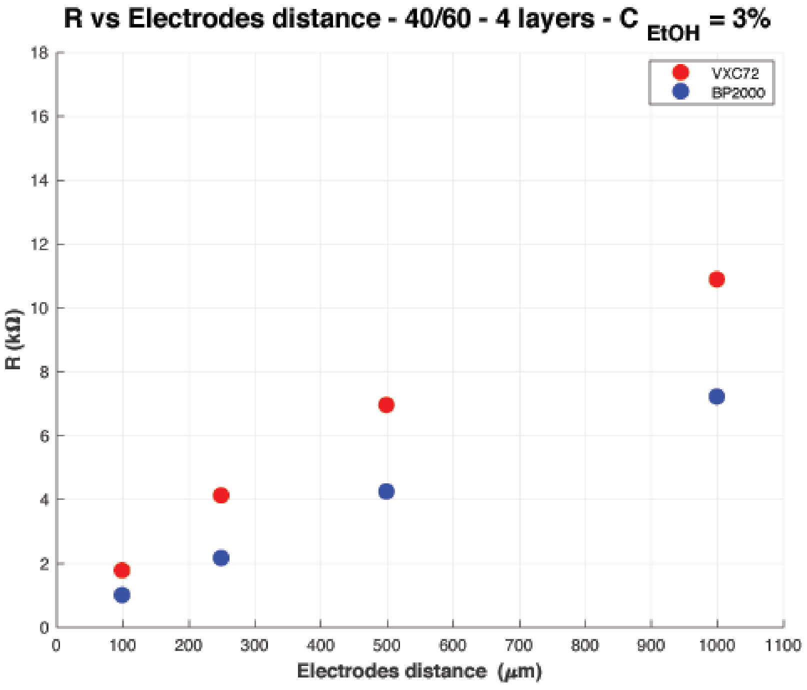

FIGURE 4.8: Resistance as a function of the gap between electrodes.

However, the sensitivity shows a distinctive behavior. In fact, in Figure 4.9, the slope of the curves is constant at zero and, therefore, the two curves are parallel to the x-axis. VXC72 samples have a higher resistance but at the same time they present better sensitivities. In conclusion, from this behavior the following statement can be drawn: different electrodes geometries don't affect sensitivity.

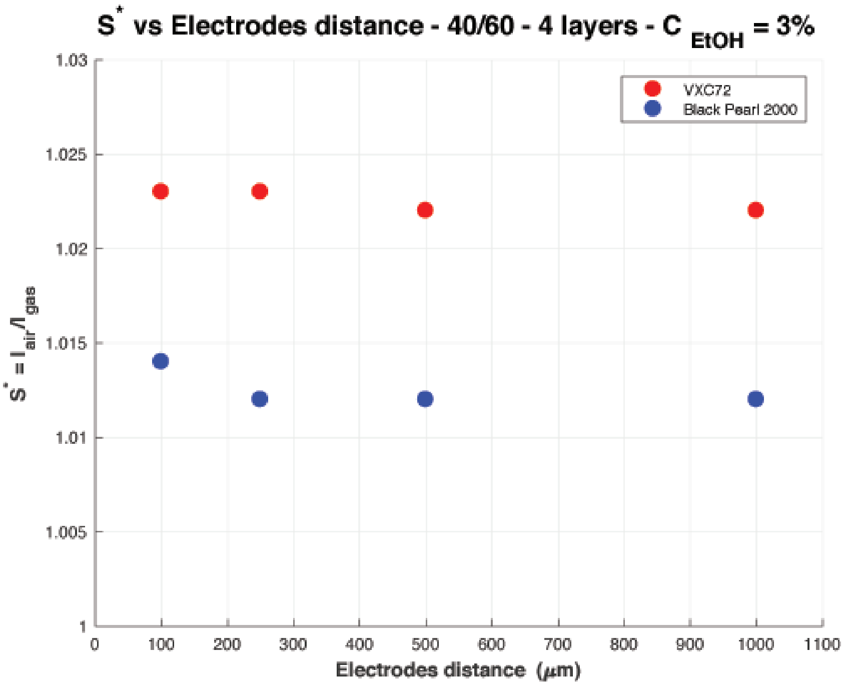

FIGURE 4.9: Sensitivity as a function of the gap between electrodes.

4.4 Lower Detection Limit

This section presents the results of a major study where the aim was the finding of the lower detection limit. It can be defined as the lowest quantity of gas that can be distinguished from the absence of that vapor. This value is strictly related to the sensitivity parameter because the greater is the response of the sensor (i.e. the higher is the sensitivity), the easier will be the possibility of detecting a small fraction of a particular vapor. As for the experiments described above, in this study the matrix chosen was the block copolymer PS/PDMAEMA with a molar ratio of 2,7, a PDI = 1,44 and an overall average molecular weight of $20{,}2\,\mathrm{kDa}$. The devices were all prepared by depositing four layers with the flow coating technique. The carbon black concentration was varied ranging from 5 wt% up to 60 wt% using the Vulcan XC72 only, due to its superior sensitivity and processability.
The thirty-six sensors fabricated were electrically characterized inside the Polymer

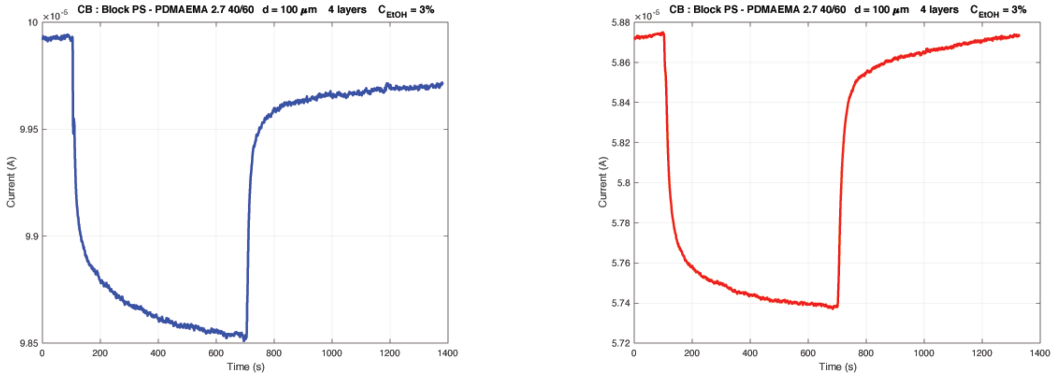

(a) 100 μm gap 40 wt% BP2000 (b) 100 μm gap 40 wt% VXC72

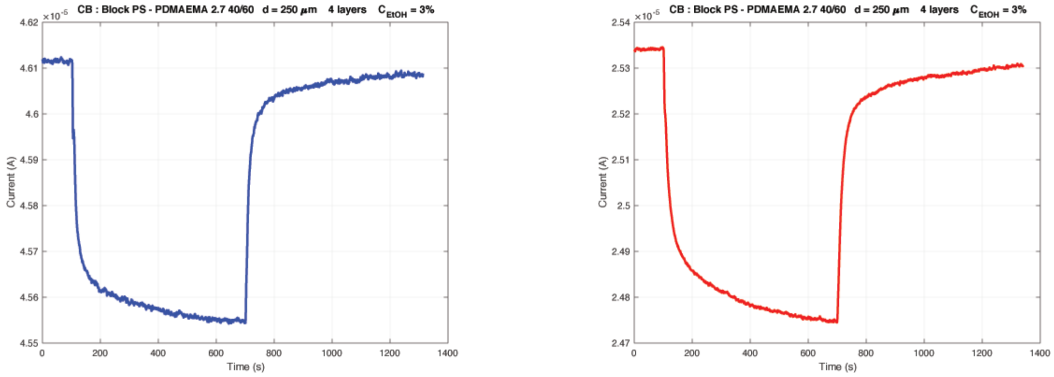

(c) 250 μm gap 40 wt% BP2000 (d) 250 μm gap 40 wt% VXC72

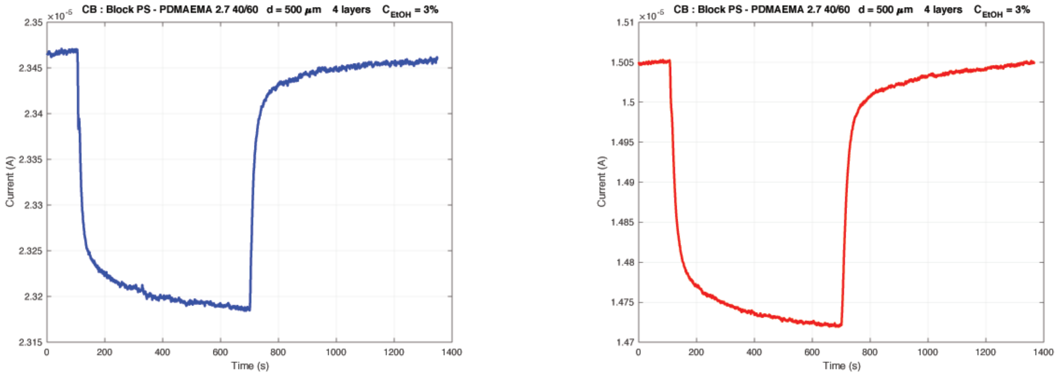

(e) 500 μm gap 40 wt% BP2000 (f) 500 μm gap 40 wt% VXC72

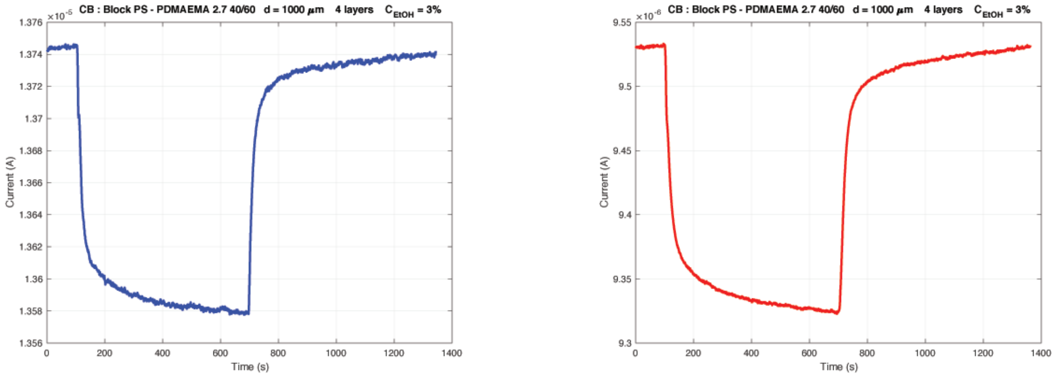

(g) 1000 μm gap 40 wt% BP2000 (h) 1000 μm gap 40 wt% VXC72

FIGURE 4.10: Sensing curves for different electrodes gap.

Chamber following the same procedure. The applied voltage was fixed at $100\,\mathrm{mV}$, the total flow was set at 100 sccm and the only analyte investigated was ethanol. However, this time different baths were prepared inside the Dewar flask. This setup, as it was explained in Chapter 3, allows to exploit a wider range of concentrations. As the temperature goes down, the saturated vapor pressure decreases. Therefore, fewer molecules are in the vapor and the concentrations that can be targeted can reach even few ppm. First of all, the nine different types of sensors were tested with a flow of 3 sccm of ethanol, targeting 1700 ppm at room temperature ($19\,^{\circ}\mathrm{C}$). Secondly, an ice bath was prepared inside the Dewar. In this way the temperature was controlled and settled at $0\,^{\circ}\mathrm{C}$. The mass flow controller of the solvent was set to regulate the flow coming out from the bubbler system, providing 10 sccm, 7 sccm and 3 sccm of ethanol. The targeted concentrations at $0\,^{\circ}\mathrm{C}$ were respectively 1525 ppm, 1067 ppm and 458 ppm. All the results from the seventy-two experiments with the corresponding numerical values are shown in Table 4.1.

TABLE 4.1: Sensitivities of sensors with different carbon black load analyzed for four different EtOH concentrations.

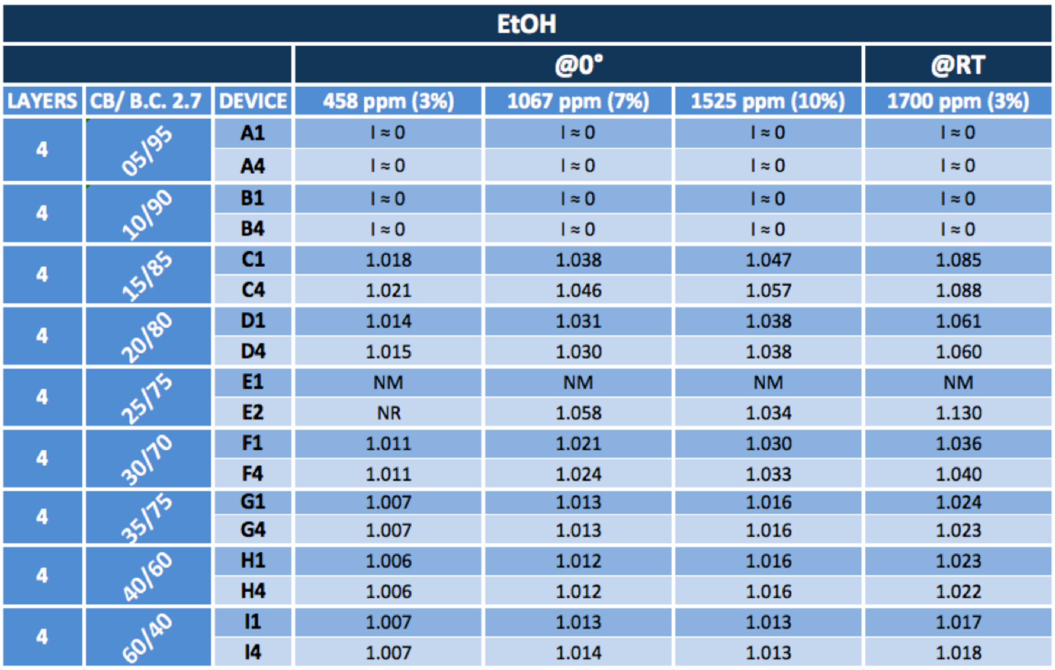

EtOH						
			@0°			@RT
LAYERS	CB/ B.C. 2.7	DEVICE	458 ppm (3%)	1067 ppm (7%)	1525 ppm (10%)	1700 ppm (3%)
4	05/95	A1	I ≈ 0	I ≈ 0	I ≈ 0	I ≈ 0
		A4	I ≈ 0	I ≈ 0	I ≈ 0	I ≈ 0
4	10/90	B1	I ≈ 0	I ≈ 0	I ≈ 0	I ≈ 0
		B4	I ≈ 0	I ≈ 0	I ≈ 0	I ≈ 0
4	15/85	C1	1.018	1.038	1.047	1.085
		C4	1.021	1.046	1.057	1.088
4	20/80	D1	1.014	1.031	1.038	1.061
		D4	1.015	1.030	1.038	1.060
4	25/75	E1	NM	NM	NM	NM
		E2	NR	1.058	1.034	1.130
4	30/70	F1	1.011	1.021	1.030	1.036
		F4	1.011	1.024	1.033	1.040
4	35/75	G1	1.007	1.013	1.016	1.024
		G4	1.007	1.013	1.016	1.023
4	40/60	H1	1.006	1.012	1.016	1.023
		H4	1.006	1.012	1.016	1.022
4	60/40	I1	1.007	1.013	1.013	1.017
		I4	1.007	1.014	1.013	1.018

NM indicates the samples not measured; NR samples with no response; I≈0 samples where the current was below $8\,\mathrm{pA}$ and so the resistance was too high to be measured.

The starting resistance changed over time after the experiments at room temperature. From a SEM analysis the surface of the film was investigated from a side view and top view (Fig. 4.11).

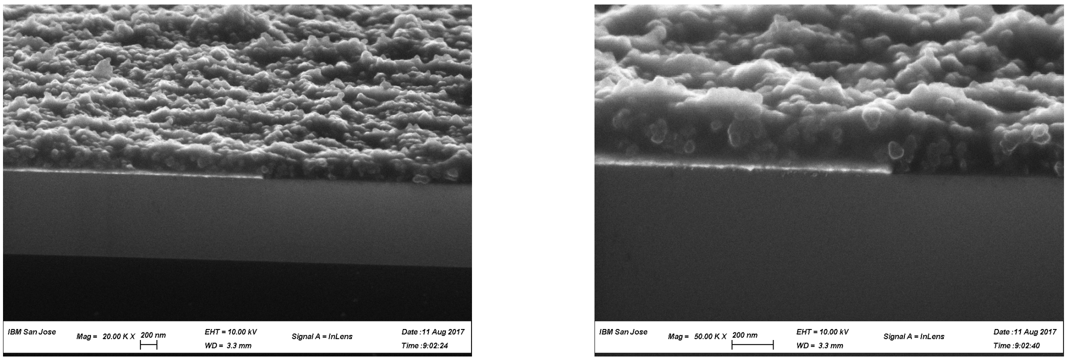

(a) Before exposure, lower magnification.

(b) Before exposure, higher magnification.

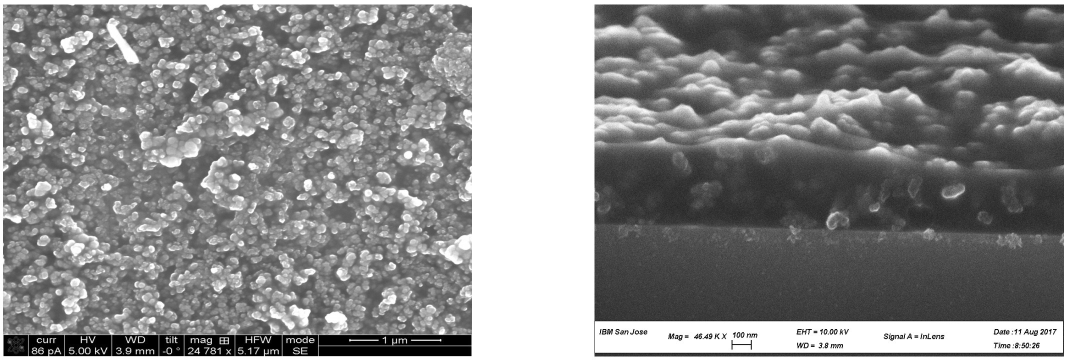

(c) Top view on the polymer chains.

(d) After the exposure.

FIGURE 4.11: SEM pictures for morphological characterization.

The first aspect is that the targeted thickness is very precise compared to the experimental one and it is uniform along the film. The second aspect observed by looking at the SEM pictures of the sensor is the difference of the film before and after exposure to VOCs. It is possible to appreciate the swelling effect looking at the morphology before the characterization and after a prolonged exposition at a very high analyte concentration. In order to avoid poisoning of the samples, the films were baked at 110 °C for three minutes. In this way most of the molecules previously adsorbed can desorb from the polymer chains, restoring the original surface. This can happen because the physical changes are reversible. If the data previously obtained are plotted, the results of this study can be displayed as shown in Figure 4.12.

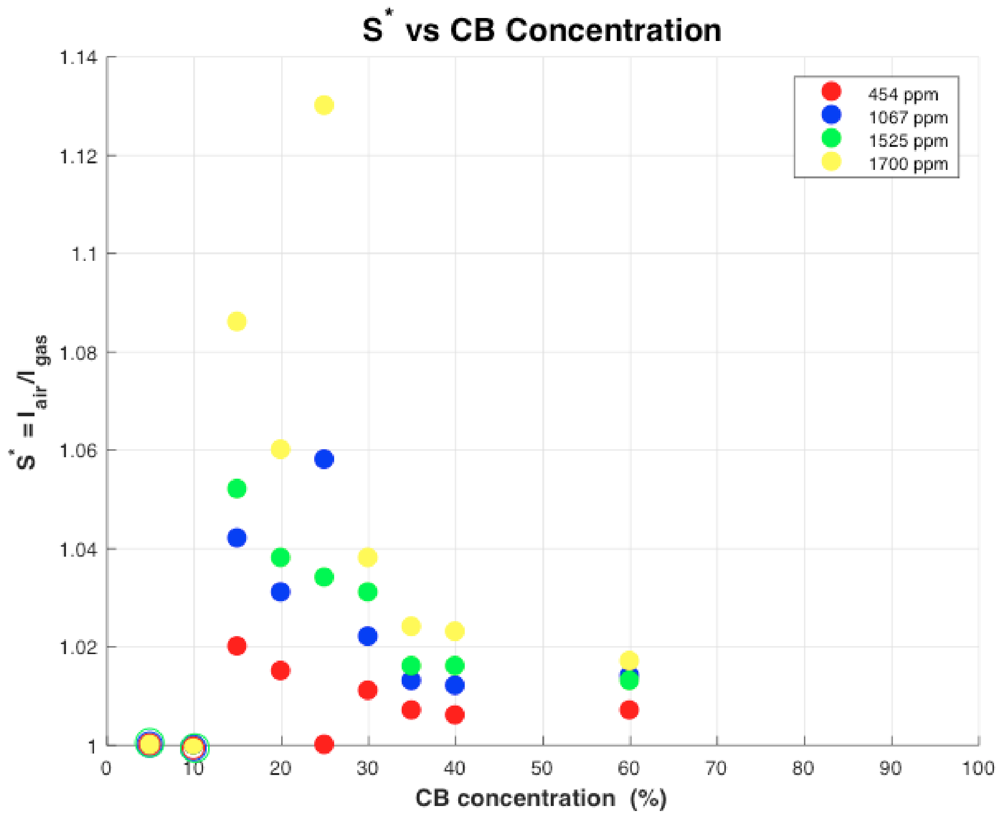

FIGURE 4.12: Sensitivity as a function of carbon black load (VXC72) for four different EtOH concentrations.

Three main observations can be made. The first one is the fact that samples with a small amount of carbon black concentrations (below 15%) show a current that is too low to appreciate a sensing response. Secondly, the sensitivity decreases as the filler load increases because there are too many particles and the percolation region is far away. As expected, the third one demonstrate that the fewer the molecules inside the chamber, the worst the sensitivity. In accord with the theory, this is true because there are less vapor molecules that can adsorb on the surface of the film, contributing in the swelling of the matrix. According to the sensing curves obtained, some sensors presented noisy measurements (Fig. 4.13), but others still showed a good sensing response.

In order to identify the lowest detection limit a single device was chosen and characterized at even lower temperatures: the block copolymer PS/PDMAEMA 2,7 with 35 wt% of Vulcan XC72 as conductive filler. The first set of measurements were still performed at room temperature and at 0 °C because we wanted to be sure of the

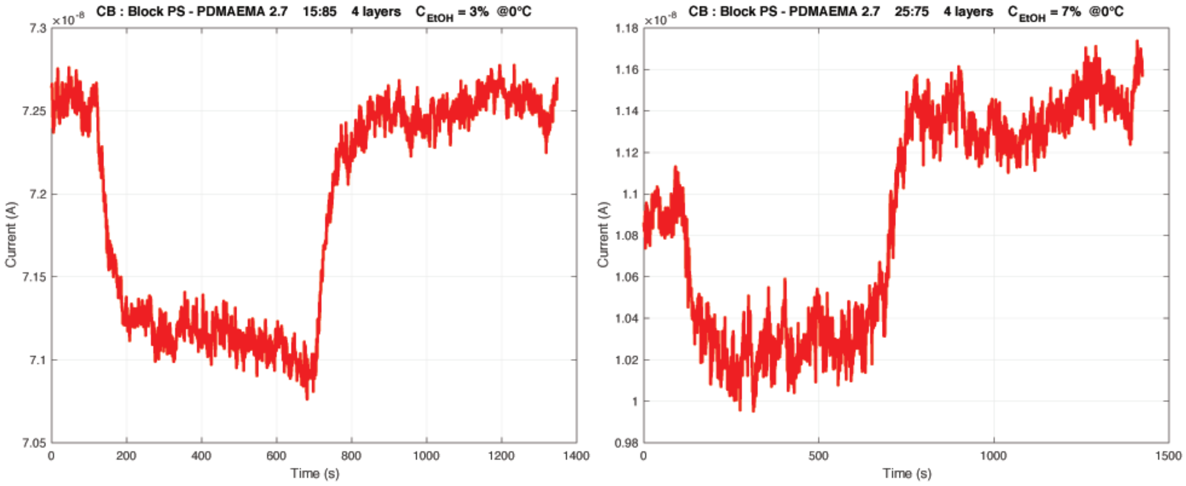

(a) Sensor with 15 wt% VXC72.

(b) Sensor with 25 wt% VXC72.

FIGURE 4.13: Sensing curves performed at 0 °C and 3 sccm of ethanol.

reliability of the system. In more details different overlapping ethanol concentrations were analyzed in the two temperatures configurations in order to verify any possible trend and visualize the match related to the sensitivity. The results are reported in Figure 4.14. The data appear pretty accurate and the discrepancies may be due to different time measurements, reproducibility, errors in the flow/dilution or in the environment.

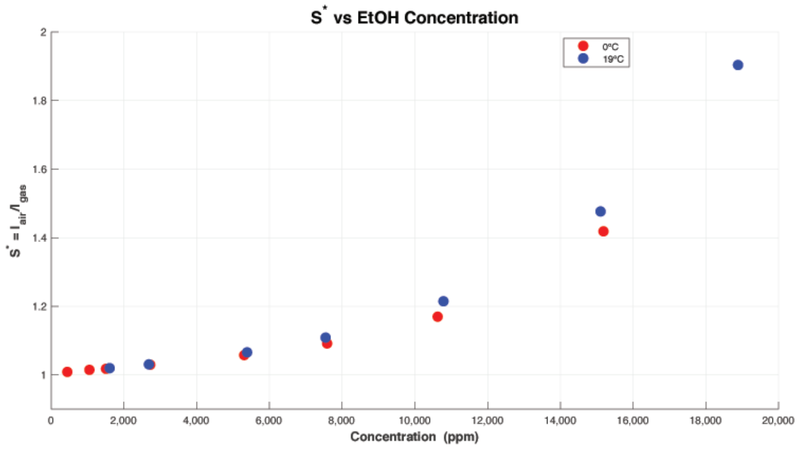

FIGURE 4.14: Overlapping measurements performed at 0 °C and 19 °C in order to test the reliability of the system.

Once the gas delivery system along with the Polymer Chamber were trusted and approved by experimental results, a cooling bath composed of acetonitrile (CH_3CN) and dry ice was poured inside the Dewar flask. It took ten minutes in order to reach the equilibrium and the temperature was fixed at −45 °C. Time to time it was necessary to add more dry ice in order to maintain the desired temperature (Alan, 1972).

Seven measurements were run targeting respectively 8 ppm, 13 ppm, 34 ppm, 65 ppm, 130 ppm, 195 ppm and 260 ppm. These conditions were possible setting respectively 2 sccm, 5 sccm, 13 sccm, 25 sccm, 50 sccm, 75 sccm and 100 sccm of ethanol. The results are reported in Table 4.2 and Figure 4.15.

TABLE 4.2: Sensitivity of VXC72/PS-PDMAEMA 35/65.
Tests performed at different concentrations of EtOH and temperatures.

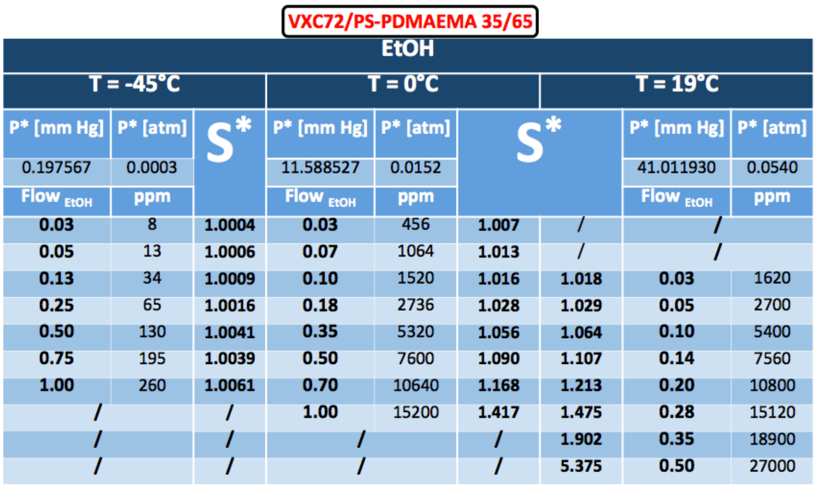

VXC72/PS-PDMAEMA 35/65

EtOH

T = -45°C			T = 0°C				T = 19°C	
P* [mm Hg]	P* [atm]	S*	P* [mm Hg]	P* [atm]	S*		P* [mm Hg]	P* [atm]
0.197567	0.0003		11.588527	0.0152			41.011930	0.0540
Flow $_{EtOH}$	ppm		Flow $_{EtOH}$	ppm			Flow $_{EtOH}$	ppm
0.03	8	**1.0004**	**0.03**	456	**1.007**	/	/	
0.05	13	**1.0006**	**0.07**	1064	**1.013**	/	/	
0.13	34	**1.0009**	**0.10**	1520	**1.016**	**1.018**	**0.03**	1620
0.25	65	**1.0016**	**0.18**	2736	**1.028**	**1.029**	**0.05**	2700
0.50	130	**1.0041**	**0.35**	5320	**1.056**	**1.064**	**0.10**	5400
0.75	195	**1.0039**	**0.50**	7600	**1.090**	**1.107**	**0.14**	7560
1.00	260	**1.0061**	**0.70**	10640	**1.168**	**1.213**	**0.20**	10800
/		/	**1.00**	15200	**1.417**	**1.475**	**0.28**	15120
/		/	/		/	**1.902**	**0.35**	18900
/		/	/		/	**5.375**	**0.50**	27000

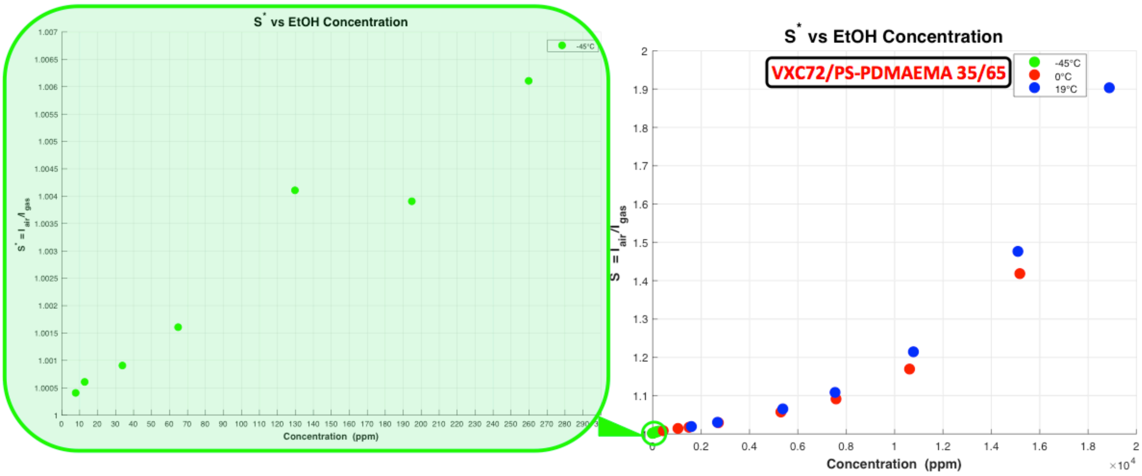

FIGURE 4.15: Sensitivity of the device VXC72/PS-PDMAEMA 35/65 tested at −45 °C in order to identify the lower detection limit.

This is a remarkable discovery. One of the weakness concerning the polymeric chemiresistive sensors is the not so good sensitivity at very low fractions of vapor but, now, it is possible to state that they can be employed for applications where there is the need of detect tens of ppm of a particular gas. Even if the sensing response is low, less than 1% of variation respect to the starting resistance, still it is seen a change in the curves. Almost all the time the film recovered completely at the original baseline in few seconds. Measurements at $-45\,^{\circ}\mathrm{C}$ are noisier than the others and when the concentration is less than 16 ppm the level of noise is comparable with the change of the output signal. In the other tests it is possible to observe a quite big spike. This behavior is still unclear and might be due to the gas delivery system when the temperature changes immediately from $-45\,^{\circ}\mathrm{C}$ to $19\,^{\circ}\mathrm{C}$. After all, this achievement can't be accomplished by human panels and it shows the importance on the development of electronic noses. For the purpose of providing complete information, in the following three pages all the sensing measurements related to the sample with 35 wt% of carbon black are reported in Figures 4.16, 4.17 and 4.18 showing the results at room temperature (Red graphs), $0\,^{\circ}\mathrm{C}$ (Blu graphs) and $-45\,^{\circ}\mathrm{C}$ (Green graphs) respectively.

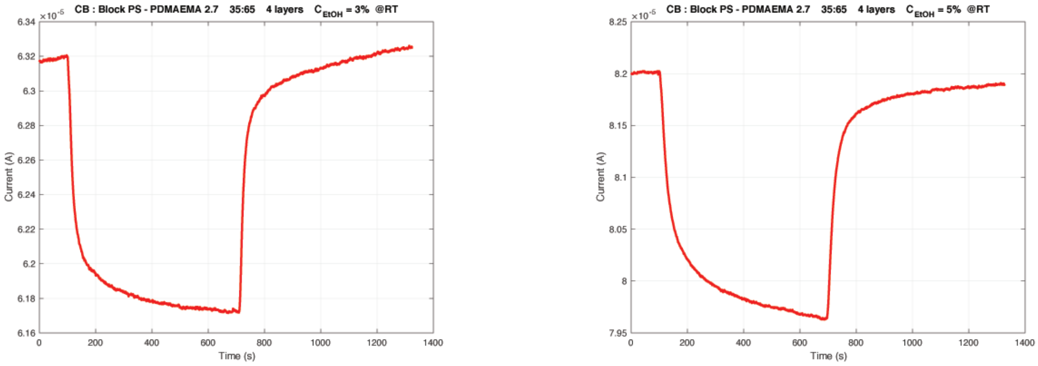

(a) 1620 ppm of EtOH.

(b) 2700 ppm of EtOH.

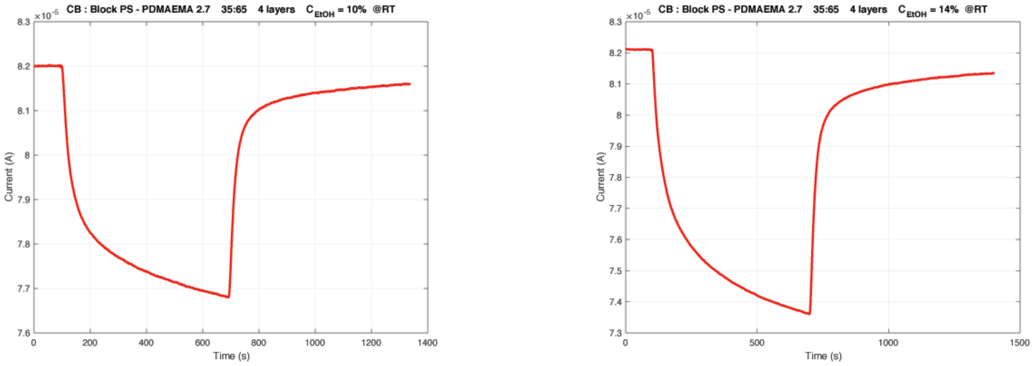

(c) 5400 ppm of EtOH.

(d) 7560 ppm of EtOH.

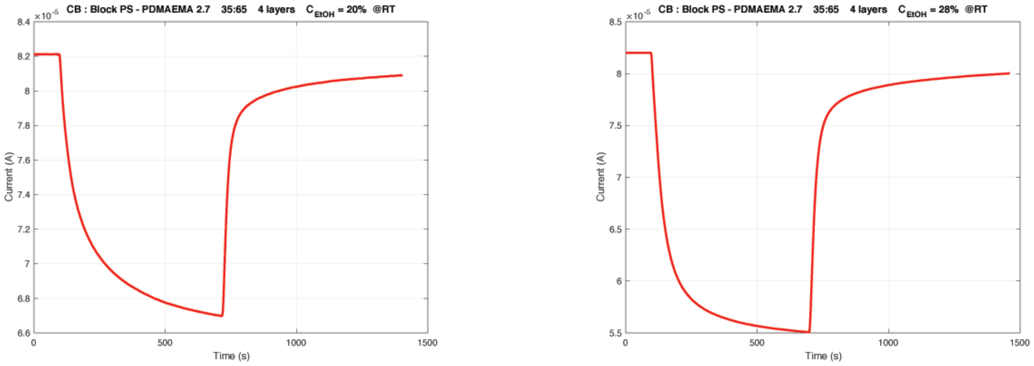

(e) 10.800 ppm of EtOH.

(f) 15.120 ppm of EtOH.

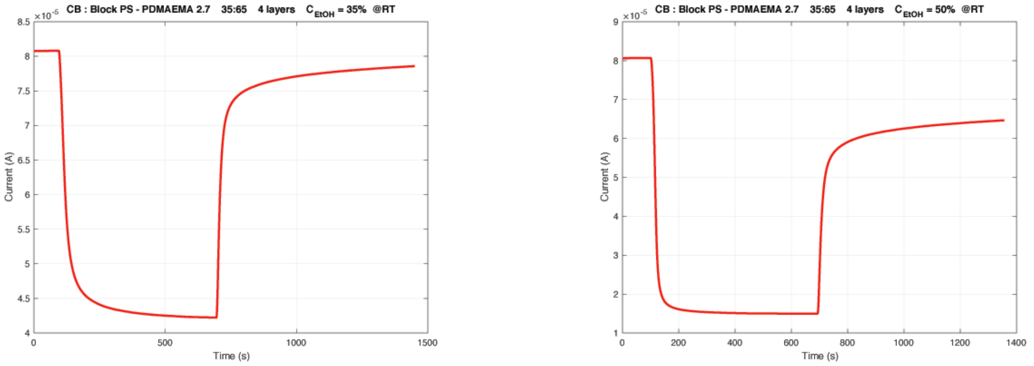

(g) 18.900 ppm of EtOH.

(h) 27.000 ppm of EtOH.

FIGURE 4.16: Sensing measurements tested at 19 °C for various EtOH concentrations on sensor VXC72/PS-PDMAEMA 35/65.

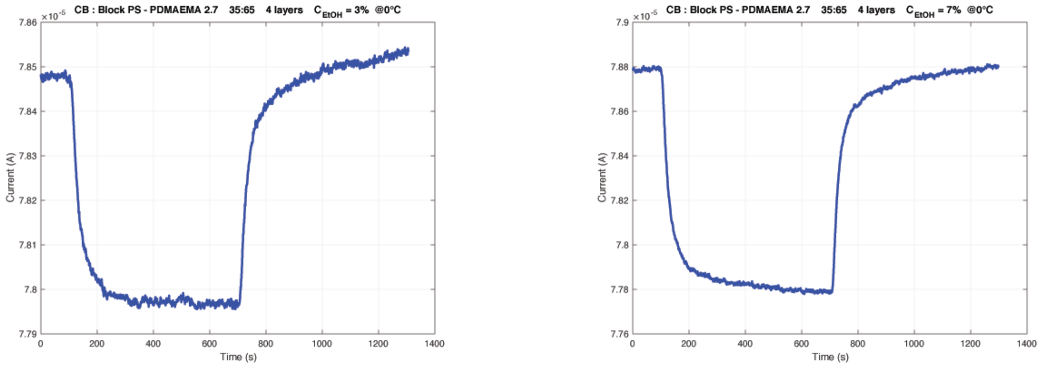

(a) 456 ppm of EtOH. (b) 1064 ppm of EtOH.

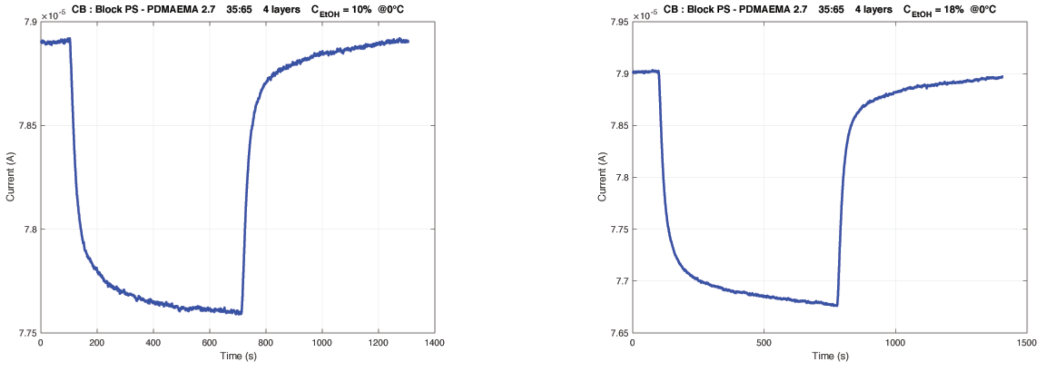

(c) 1520 ppm of EtOH. (d) 2736 ppm of EtOH.

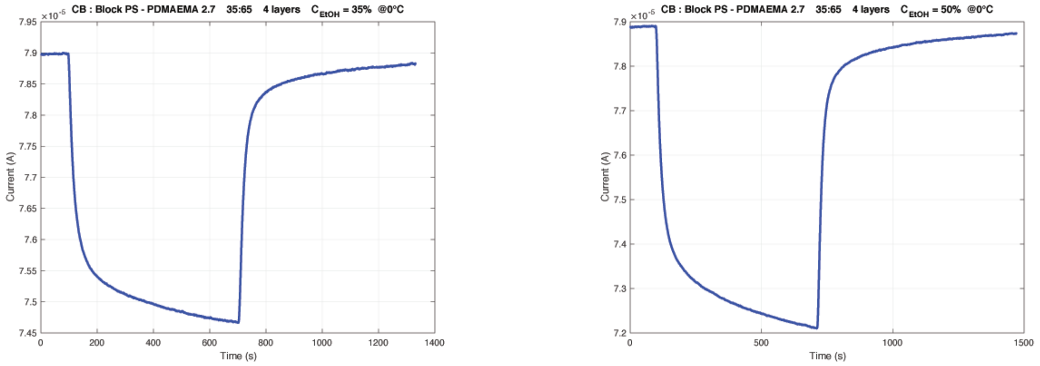

(e) 5320 ppm of EtOH. (f) 7600 ppm of EtOH.

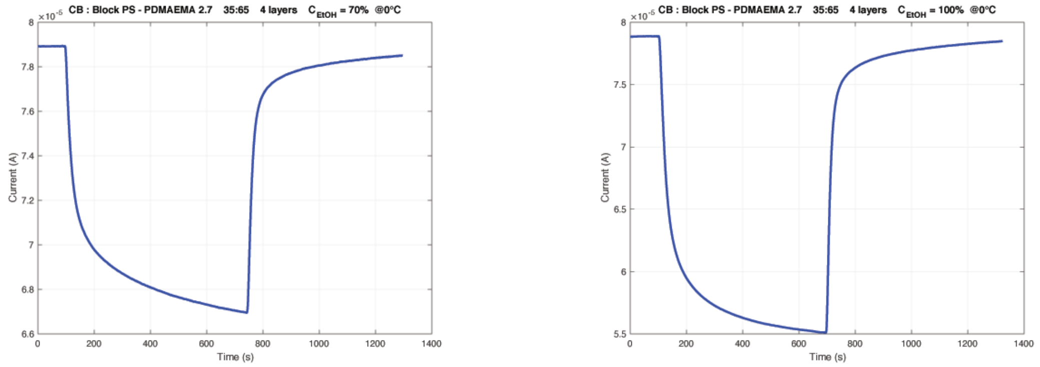

(g) 10.640 ppm of EtOH. (h) 15.200 ppm of EtOH.

FIGURE 4.17: Sensing measurements tested at 0 °C for various EtOH concentrations on sensor VXC72/PS-PDMAEMA 35/65.

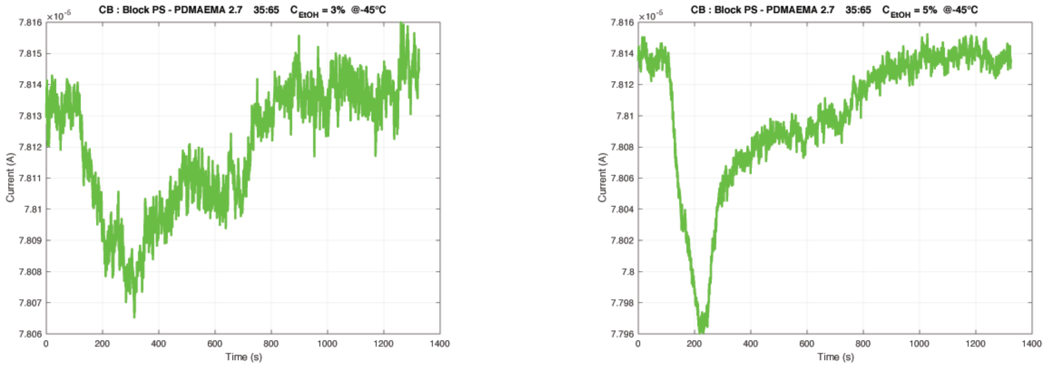

(a) 8 ppm of EtOH.

(b) 13 ppm of EtOH.

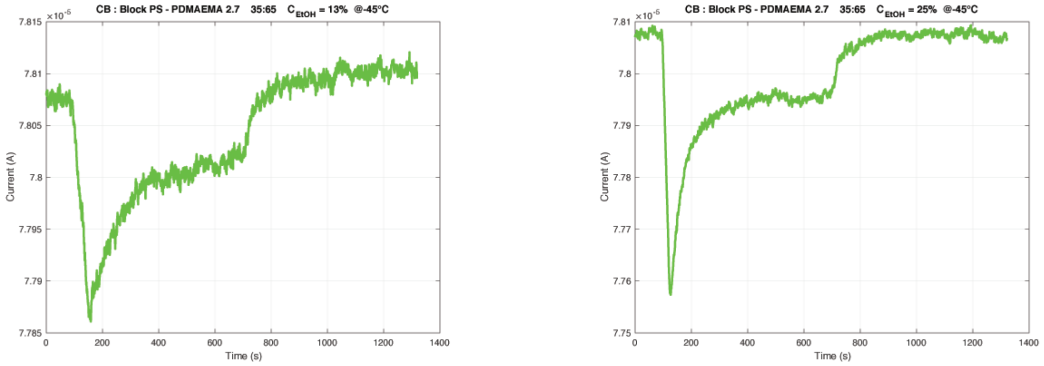

(c) 34 ppm of EtOH.

(d) 65 ppm of EtOH.

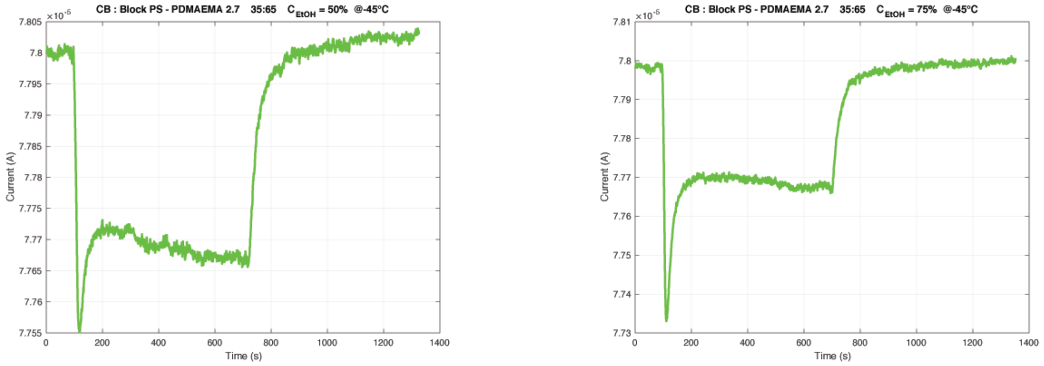

(e) 130 ppm of EtOH.

(f) 195 ppm of EtOH.

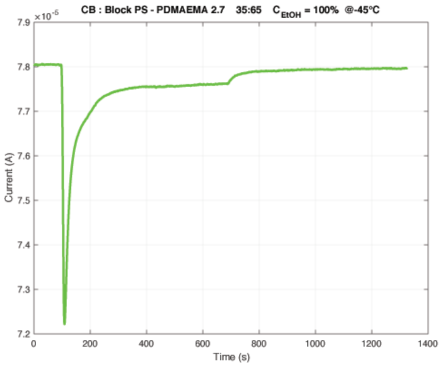

(g) 260 ppm of EtOH.

FIGURE 4.18: Sensing measurements tested at −45 °C for various EtOH concentrations on sensor VXC72/PS-PDMAEMA 35/65.

4.5 Role of PS as a Universal Stabilizer

Another important study carried out at the facility of IBM Research Center was the investigation of the role of polystyrene (PS) in gas sensors. This thermoplastic polymer is the most utilized in the frame of chemiresistors according to the literature. As a matter of fact, it is also the IBM starting material used for the preparation of the devices. It is always present when synthetizing copolymers or blends, where only the other repeating unit was varied. The reason of this decision seems to be related to the fact that the styrene units play a key role in the dispersion of the carbon black particles inside the polymer, stabilizing the mixed solution. This statement can be verified looking at the microscopy pictures in 4.19. PMMA has a very poor affinity with the conductive filler and, when mixing the polymer with the carbon black, heavy precipitations can be observed. On the contrary, when PS is added and the mixed solution is re-sonicated the precipitations disappear. In the figures a blend of PMMA with a molecular weight of 120 kDa is mixed with PS with a molecular weight of 35 kDa in different ratios. It appears that increasing the PS concentration the dispersion is better and less big aggregates are formed. An even better result is noticed in 4.19(d), where a block copolymer PMMA-b-PS was synthetized in 1:1 ratio. In conclusion it seems PS really helps the stabilization of the mixed solution.

(a) PMMA 120 kDa + PS 35 kDa ratio 15:1.

(b) PMMA 120 kDa + PS 35 kDa ratio 10:1.

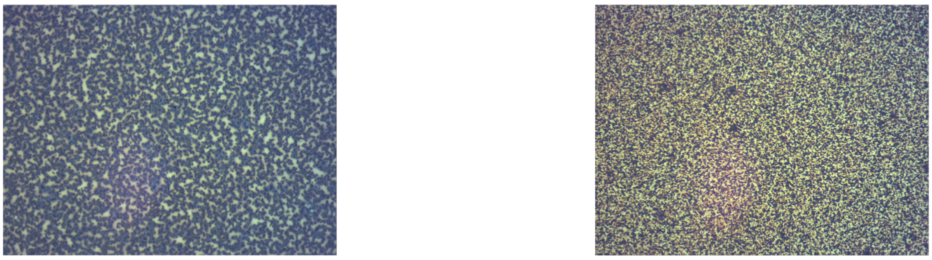

(c) PMMA 120 kDa + PS 35 kDa ratio 5:1.

(d) PMMA-b-PS 100 kDa-150 kDa ratio 1:1.

FIGURE 4.19: Effect of PS as an universal stabilizer in carbon black-polymer solution.

4.6 Selectivity Towards Different Gases

In this last section the main focus is on the selectivity of the carbon black-polymer sensors. In general these kinds of sensors are only partially specific. In fact, just one sensor is not able to provide us a lot of information simultaneously. It could detect a particular gas and, analyzing the magnitude of the response, it could give the concentration. However, if there are more vapors in the environment, it could not classify the category of the analytes. The sensor might respond in different ways at different gases and a high sensitivity towards a specific analyte might be confused with a large signal of another vapor with less affinity but present in larger quantities. For all these reasons the electronic nose was born in order to overcome these issues and an array of sensors is employed to collect multiple data from different devices creating a unique fingerprint. In this way it is possible to know the typology of the gas and its concentration simultaneously.
Having said that, still a lot of research is made in order to develop new materials that could show distinctive selectivity. Luckily, one of the points of strength of polymers is the wide availability of different repeating units. In this way combining them in block copolymers, random copolymers or blends with different ratios and different molecular weight permit to control and tune their properties in order to show different affinities towards different analytes. Moreover this feature can be improved by functionalizing the surface.

At IBM Research Center different strategies were tried, changing the functional groups of the monomer used in combination with PS, always present as explained in section 4.5. The samples were tested in DC inside the Polymer Chamber following the same protocol. The applied voltage was fixed at $100\,\mathrm{mV}$, the total flow was set at 100 sccm and two different solvents were tested: acetone and ethanol. The latter is an alcohol containing polar groups in its structure, while acetone is a carbonyl compound containing two CH groups that are non polar and a carbonyl group that is slightly polar compared to the alcoholic group. The results are shown in Figure 4.20, where three different polymeric devices are compared. According to the different graphs, it is possible to say that the chemiresistors fabricated using PS or PS/PMAA have a better affinity towards acetone rather then ethanol. On the contrary the block copolymer PS/PDMAEMA shows a better behavior towards ethanol.

Dealing with selectivity it is very important to study the solubility and affinity between the matrix and the analyte in order to understand the possible physical and chemical interactions that can occur. Ethanol is more polar than acetone because the carbon that the oxygen is bonded to in ethanol is sp^3 hybridized where as the one in acetone is sp^2 hybridized. Since the sp^2 carbon is more polar than the sp^3 carbon, acetone has a lower dielectric constant and it is less polar then ethanol.
Likewise PS and PMAA don't have high polarity because of their functional groups. The adsorption of ethanol molecule is harder than acetone ones.
Differently, PDMAEMA has oxygen and amino groups, which can bind with the OH group of ethanol through hydrogen bonds. Because of these interactions, more molecules can be adsorbed resulting in a bigger swelling and thus sensing response. As a general rule it can be said: "*Similia similibus solvuntur*".

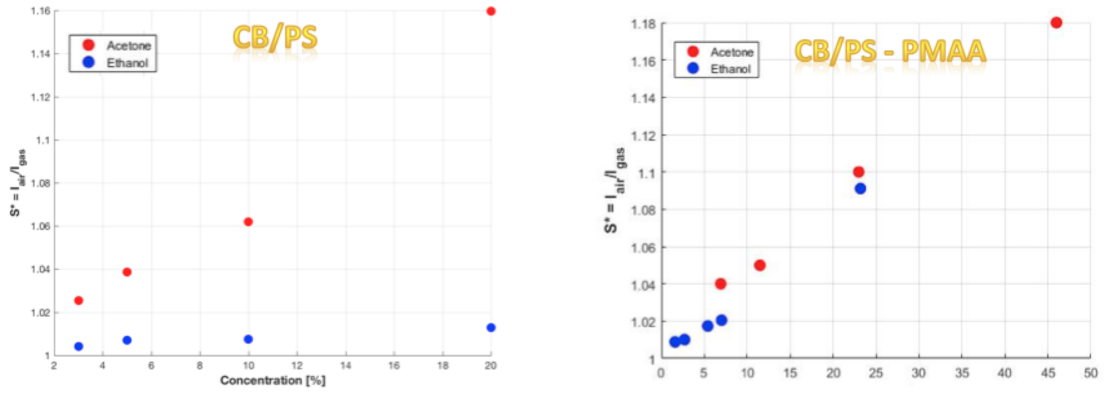

(a) CB/PS sensor.

(b) CB/PS-PMAA sensor.

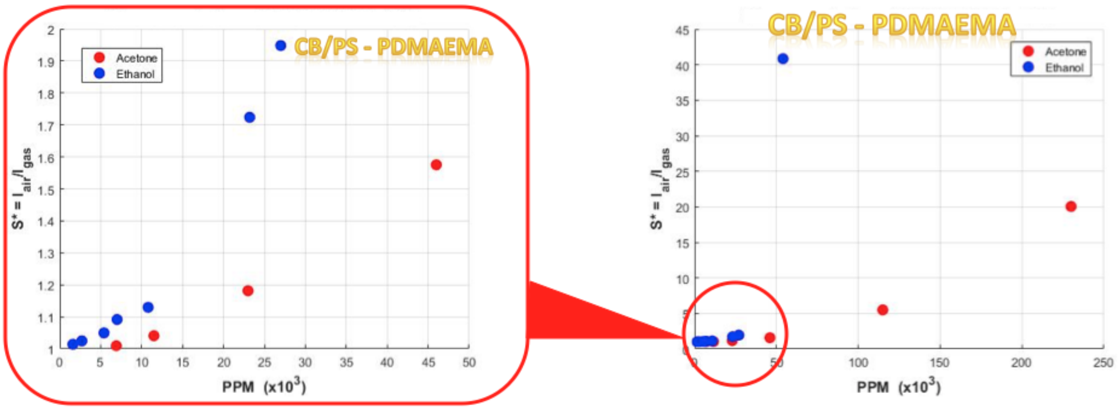

(c) CB/PS-PDMAEMA sensor.

FIGURE 4.20: Selectivity towards different gases on carbon black-polymer composites.

Chapter 5

In Situ Photopolymerized Composites

In this chapter of the thesis it is reported the results of a detailed study on the in situ photopolymerized composites, both the polypyrrole-based and the ones containing the MWCNTs as conductive filler. The aim of the experiments is to try understanding the sensing mechanism that is way more complex and still unclear in some parts than just the swelling of the matrix. The innovations of these sensors are the polymers used for the insulating matrix and their synthesis process. In fact, thermosetting resins are photopolymerized through UV light together with the conductive material starting from oligomers and creating cross-linked interpenetrated networks. In literature many reports on PPy-based electronic devices can be found, but nothing using the UV photopolymerization technique, that brings with it numerous advantageous and something new to add in this field. Therefore, synthesis parameters as the photoinitiator amount and material properties as the glass transition temperatures (T_g) are trying to be correlated with the sensing response in general. Only in the future it will be possible to work on different variables of the films in order to improve sensitivity, selectivity and stability. In light of this, the two categories of sensors have been tested in DC with the Polymer Chamber and later in AC by means of the impedance analyzer, comparing the results collected.

5.1 Polypyrrole-based Sensors

All the twenty-four different kinds of films were prepared in the Polymer Laboratory at Politecnico di Torino, as explained in section 3.2. At IBM Research Center, instead, the electrical characterization was performed on sensors based only on twelve different formulations, divided in two batches (Tab. 5.1).

TABLE 5.1: Photocurable formulations preprared to fabricate PPy-based sensors.

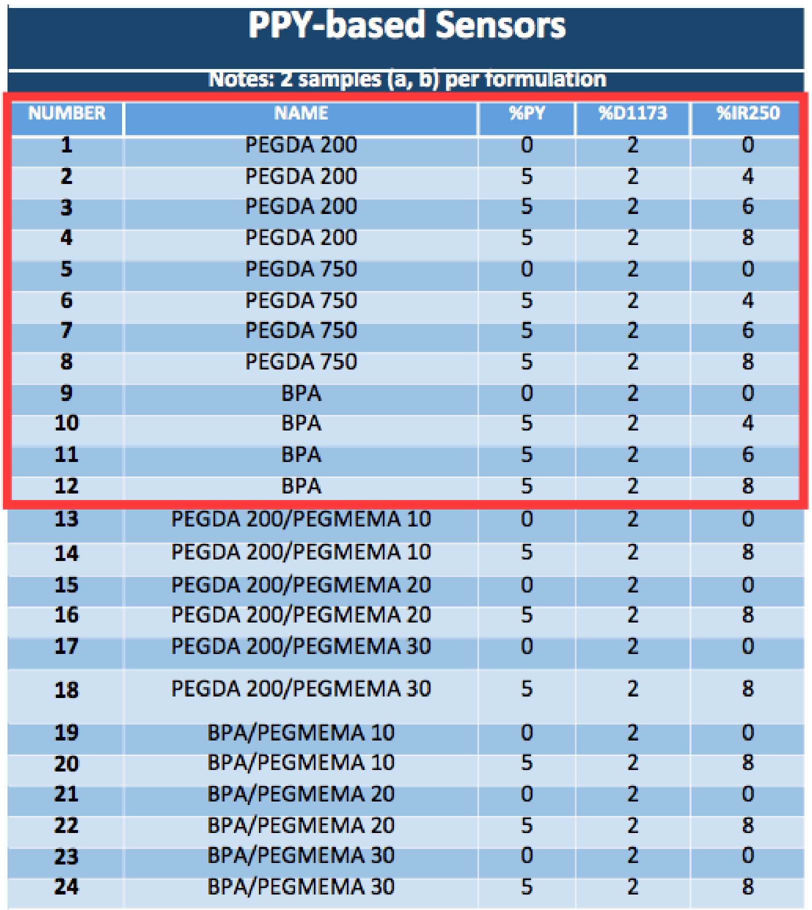

PPY-based Sensors

Notes: 2 samples (a, b) per formulation

NUMBER	NAME	%PY	%D1173	%IR250
1	PEGDA 200	0	2	0
2	PEGDA 200	5	2	4
3	PEGDA 200	5	2	6
4	PEGDA 200	5	2	8
5	PEGDA 750	0	2	0
6	PEGDA 750	5	2	4
7	PEGDA 750	5	2	6
8	PEGDA 750	5	2	8
9	BPA	0	2	0
10	BPA	5	2	4
11	BPA	5	2	6
12	BPA	5	2	8
13	PEGDA 200/PEGMEMA 10	0	2	0
14	PEGDA 200/PEGMEMA 10	5	2	8
15	PEGDA 200/PEGMEMA 20	0	2	0
16	PEGDA 200/PEGMEMA 20	5	2	8
17	PEGDA 200/PEGMEMA 30	0	2	0
18	PEGDA 200/PEGMEMA 30	5	2	8
19	BPA/PEGMEMA 10	0	2	0
20	BPA/PEGMEMA 10	5	2	8
21	BPA/PEGMEMA 20	0	2	0
22	BPA/PEGMEMA 20	5	2	8
23	BPA/PEGMEMA 30	0	2	0
24	BPA/PEGMEMA 30	5	2	8

The devices characterized were made with PEGDA 200, PEGDA 750, BPA and a 5 wt% fixed amount of pyrrole. On the contrary, the cationic photoinitiator, Irgacure 250, was varied from 4 wt% up to 8 wt%.

The viscoelastic properties of the cross-linked films were investigated by means of dynamic mechanical thermal analysis (DMTA), that was performed using a Triton DMTA apparatus equipped with tension-film clamp assembly and operating in multi-frequency strain mode. All samples were measured using an electronic caliper. Every PPy film was held in tension mode at a designed preload force equal to $0{,}001\,\mathrm{N}$ while sinusoidal stress was applied. The temperature range was set from $-100\,^{\circ}\mathrm{C}$ up to $150\,^{\circ}\mathrm{C}$. The heating rate was fixed at $3\,^{\circ}\mathrm{C}$ per minute. Both the loss and storage modulus were collected over the range of temperature and from their ratio $tan(\delta)$ was evaluated. The glass transition temperature for every film was estimated as the temperature at which the $tan(\delta)$ reaches its maximum. The results are shown in Table 5.2.

TABLE 5.2: Glass transition temperatures of cross-linked materials.

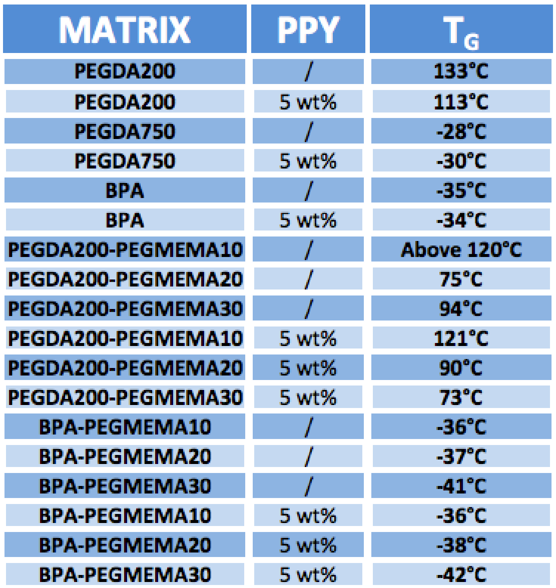

MATRIX	PPY	T_G
PEGDA200	/	133°C
PEGDA200	5 wt%	113°C
PEGDA750	/	-28°C
PEGDA750	5 wt%	-30°C
BPA	/	-35°C
BPA	5 wt%	-34°C
PEGDA200-PEGMEMA10	/	Above 120°C
PEGDA200-PEGMEMA20	/	75°C
PEGDA200-PEGMEMA30	/	94°C
PEGDA200-PEGMEMA10	5 wt%	121°C
PEGDA200-PEGMEMA20	5 wt%	90°C
PEGDA200-PEGMEMA30	5 wt%	73°C
BPA-PEGMEMA10	/	-36°C
BPA-PEGMEMA20	/	-37°C
BPA-PEGMEMA30	/	-41°C
BPA-PEGMEMA10	5 wt%	-36°C
BPA-PEGMEMA20	5 wt%	-38°C
BPA-PEGMEMA30	5 wt%	-42°C

The glass transition temperature is very low for most the samples excepet the ones containing PEGDA 200. These results match the request of high flexibility of the sensing materials because they are in their rubbery state. With the addition of the pyrrole, the final conversion decreases because its polymerization is in competition with the one of the matrix. This effect can be seen in a decrease in the T_g.

Concerning the electrical characterization, the first step was the measurements of the resistance in laboratory air using the multimeter. However, the majority of the films had a resistance above $50\,\mathrm{M\Omega}$ that couldn't be measured with the tool. Only the sample made with the higher cationic photoinitiator amount and PEGDA 200 showed a resistance of $23\,\mathrm{M\Omega}$. Equivalent samples from the material point of view had also a resistance higher than $50\,\mathrm{M\Omega}$. These results show a very poor reproducibility of the same formulation, fabricating devices with different properties.

Dealing with the DC measurements, all the tests were performed applying $100\,\mathrm{mV}$, using a total constant flow fixed at 100 sccm, flushing 50 sccm of acetone as analyte. The targeted concentration was 115.000 ppm. According to the results, the expected curve as shown in Figure 5.1, came out only a few times.

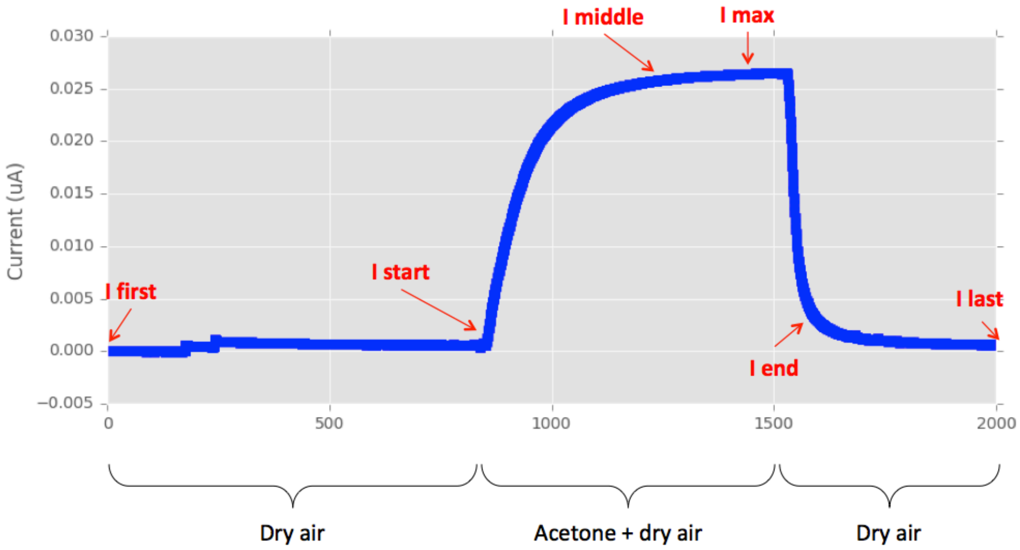

FIGURE 5.1: Real time DC measurement of sample PEGDA 200 with Irgacure 250 fixed at 8 wt%.

It appears that due to the capacitance of the films, the samples keep charging in direct current and it wasn't possible to reach a baseline. The drift occurred in all the devices without any gas present in the chamber. Also the stability was very poor. Without applying any voltage, the resistance could change of one order of magnitude if the samples were measured into two different consecutive days.

In light of the results just obtained in DC, the chemiresistors were modeled as a RC circuit where the device is composed of a resistance R_0 in parallel with a capacitance C_0. In order to be able to monitor the behavior of R_0 and C_0, the impedance analyzer was used. In this way, applying a sinusoidal current, the sample should charge and discharge at the same time, stabilizing the baseline. However, several weeks were spent in order to understand the working principle of the impedance analyzer and many issues were faced due to the setup. As it was well explained in section 3.6, the cables used to connect the impedance analyzer to the detecting chamber had a huge influence on the measurements.

First, we evaluated the series and parallel parasitic contributions (R_s, L_s, and C_p); the parallel capacitance C_p was significant but the value obtained was unphysical, likely due to the use of an oversimplified model. It was decided not to remove this contribution from our calculations and thus the total capacitance C_{Tot}, herein obtained was strongly affected by parasitic effects. The actual sample capacitance C_0

was estimated to be $\approx 2\,\mathrm{pF}$, while R_0 was not affected by C_p.
Most samples showed response to highly concentrated acetone vapors, with typical sensitivity ≈ 2; the capacitance also varied but the relative change was not known due to lack of an accurate estimate of the parasitic capacitance.
The chemiresistors were tested performing dynamic and the static analysis. Some of the most relevant results of the dynamic tests are shown in Figure 5.2.

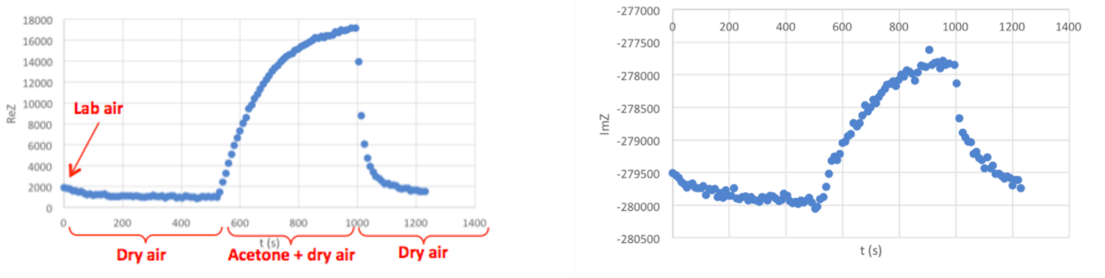

(a) $Re(Z)$ as a function of time.

(b) $Im(Z)$ as a function of time.

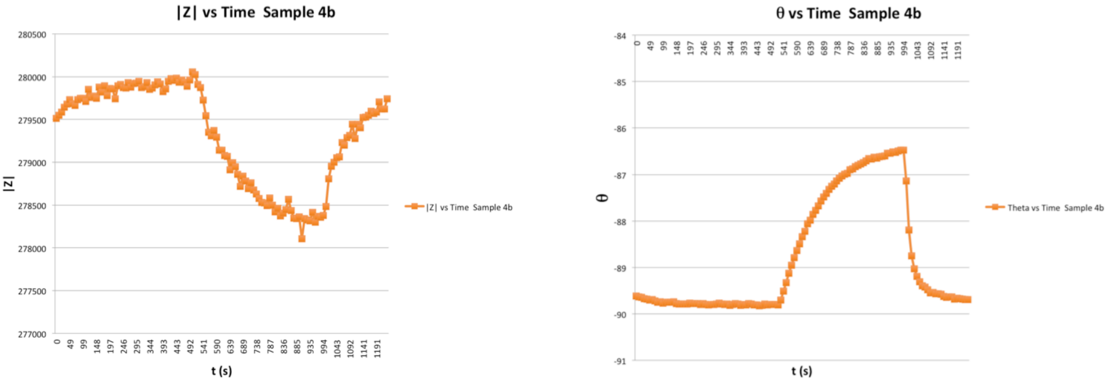

(c) $|Z|$ as a function of time.

(d) θ as a function of time.

FIGURE 5.2: Dynamic test on sample 4b at $5077{,}56\,\mathrm{Hz}$ (PEGDA 200 with 8 wt% of Irgacure 250).

It is possible to monitor in real time the $Re(Z)$, $Im(Z)$, $|Z|$ and θ for a range of frequencies going from $40\,\mathrm{Hz}$ up to $10\,\mathrm{MHz}$. From these data the graphs R_0 and C_0 were plotted (Fig. 5.3). It is easy to notice that the sensors do respond but there is an effect of the frequency. The initial baseline is shifted as a function of the frequency and this can't be true. This shift might be due to the subtraction of the parasitic components.

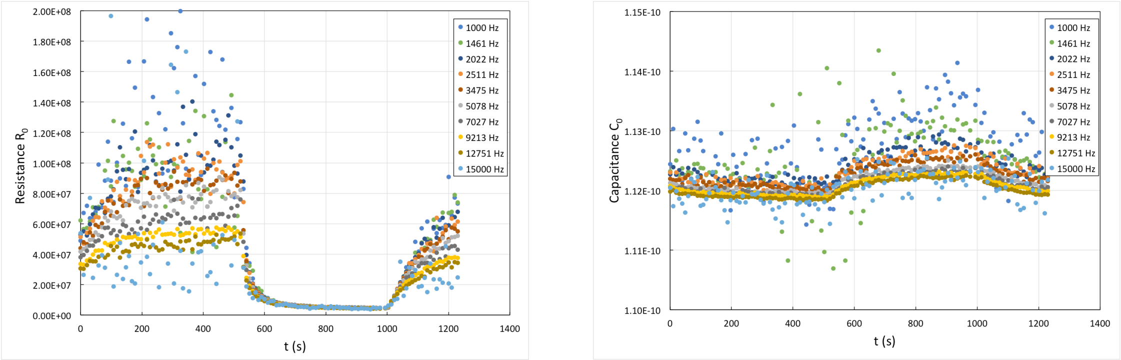

(a) R_0 as a function of time.

(b) C_0 as a function of time.

FIGURE 5.3: R_0 and C_0 of sample 4b (PEGDA 200 with 8 wt% of Irgacure 250) tested at different frequencies with 50 sscm of acetone.

The issue related to the geometry of the cables was solved connecting a different polymer chamber directly to the impedance analyzer by means of two short copper leads. In this new configuration, the sample capacitance C_0 was estimated to be $\approx 4\,\mathrm{pF}$; this result had a physical meaning and it was more consistent with the value obtained connecting directly the sample to the tool without cables ($\approx 2\,\mathrm{pF}$). Samples from the second batch (higher cationic photoinitiator percentage) have been tested with acetone as analyte at different concentrations with the new setup and the results were compared with the DC measurements. Strong correlations were found between AC and DC measurements: whenever the samples showed low DC current, AC test showed high noise. Both AC and DC results suggest that samples that do not respond have very high resistances ($\gg 10\,\mathrm{M\Omega}$), beyond the capabilities of what the instrumentation can reliably measure. Even in this configuration no greater improvements were made in terms of reliability and accuracy of the results. Within the twelve formulations tested, we could not identify clear trends in resistance nor sensitivity; however each sample showed a consistent resistance trend: resistance increases from humid to dry air and decreases upon exposure to acetone (Fig. 5.4).

At the same time, the only sample who displayed a relative low resistance was tested multiple times and the starting resistance was always different moving from $25\,\mathrm{M\Omega}$ up to $5\,\mathrm{M\Omega}$. In the static tests, where three snapshots were taken in the different environments, the behaviors were contradictory and not repeatable.

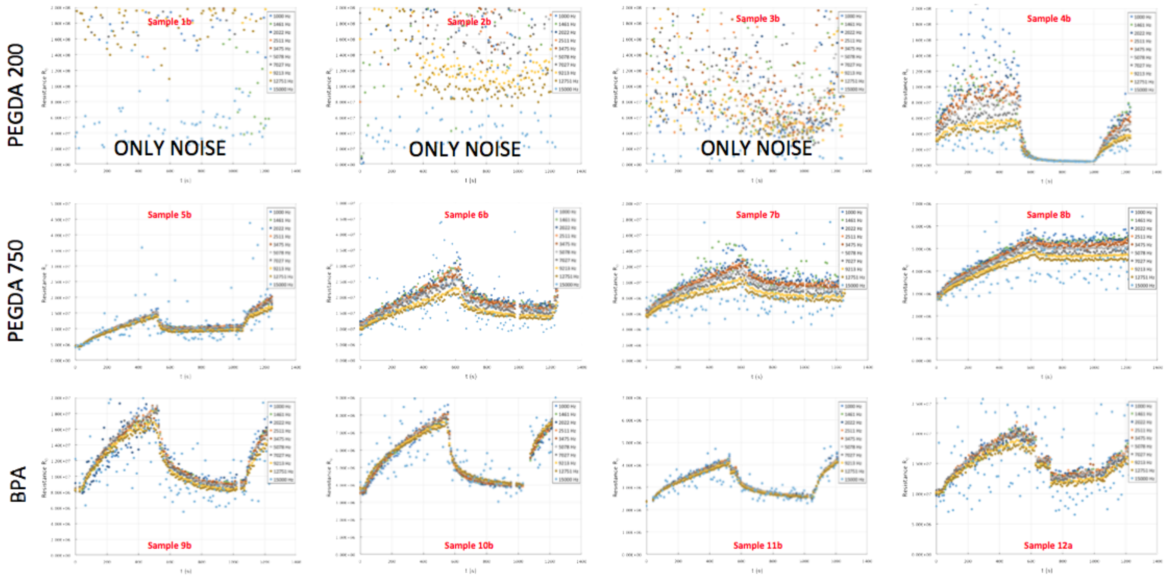

(a) Real time response of R_0 for the PPy-based sensors.

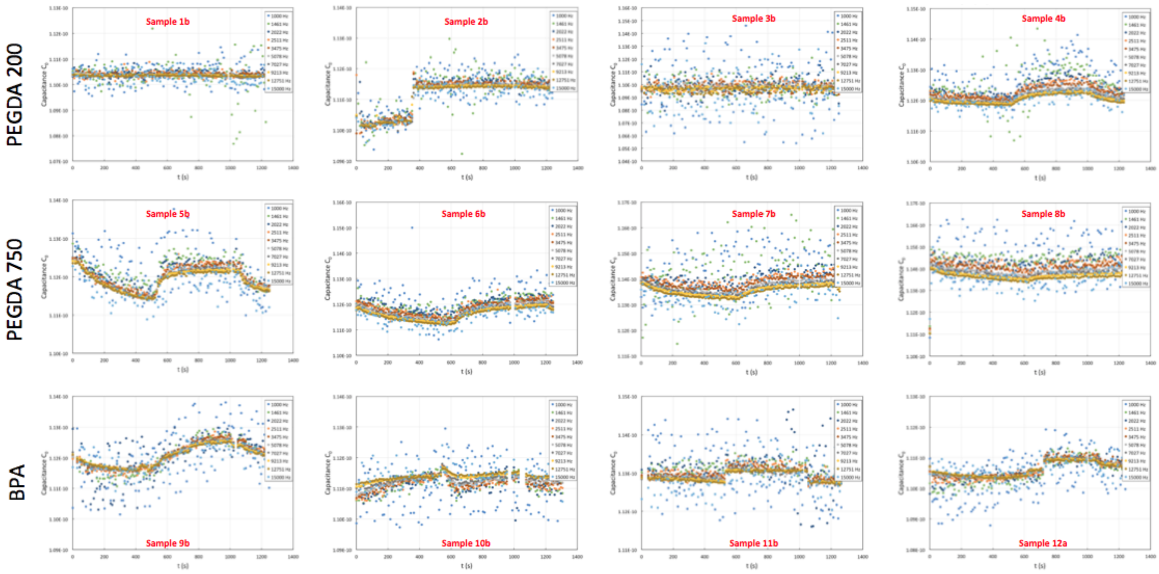

(b) Real time response of C_0 for the PPy-based sensors.

FIGURE 5.4: Full list of real time measurements on PPy-based sensors.

In conclusion the polypyrrole-based sensors have a lot of troubles. There is no reproducibility of the results, the response is different even analyzing the same sample in the same condition and the stability is very poor. The drift of the resistance with no gas tells us that these polymeric devices are strongly affected by humidity. It is possible that the reason why the films are not responding consistently may be due to their very high resistance. It would be very interesting running some analysis on samples where the active sensing part is in larger quantity. Increasing the amount of doped polypyrrole will reduce the resistance and might stabilize the samples. In this way, also the main requirements that every sensor should have could be improved.

5.2 MWCNT-based Sensors

The other type of in situ photopolymerized sensors are the MWCNT-based.
PEGDA 575 was the insulating polymer used and it acts as the matrix. The conductivity is acquired through the dispersion of MWCNTs, nanosized materials with a diameter of tenths nanometers used as the conductive filler. These kinds of sensors combine the swelling of the polymer based on the percolation theory with a charge transfer mechanism due to the interactions between the analyte and the surface of both the matrix and the particles. Due to the high surface area, the MWCNT composites can reach the percolation threshold at lower values than the carbon black composites and, in this case, 0,3 wt% was used.

The following study is all based on the characterization of one single sample. From the profilometry analysis, the thickness was estimated to be around $650\,\mu\mathrm{m}$ with a roughness of $64\,\mathrm{nm}$. The starting resistance was measured with the multimeter and it was evaluated to be $2{,}13\,\mathrm{k\Omega}$. These resistances in the range of the $\mathrm{k\Omega}$ appear to be more reliable and efficient respect to the PPy-based sensors, where the resistance was more than three orders of magnitude higher.
After developing a better knowledge of the impedance analyzer, the first measurements were carried out in AC. This time it wasn't run a dynamic test but the approach used was the static analysis over the whole spectrum ranging from $40\,\mathrm{Hz}$ up to $110\,\mathrm{MHz}$.
From the preliminary tests it was observed a constant drift of the current that didn't stabilize. It kept increasing over time and thus the electrical resistance went down. For this reason, the nanocomposite film was exposed to a flux of dry air overnight for more than twelve hours every day before starting the measurements. This arrangement seems to work but sensibility towards water vapor must be improved to widen the range of practical applications.
In the morning the first snapshot was taken as reference in dry air. The second one was captured after having exposed the film for 600 seconds in an environment with different concentrations of ethanol and acetone. In order to evaluate the recovery of

the film, dry air was flushed for other 600 seconds and the test run again. The data were then processed with a Matlab script and the output results can be interpreted from the Nyquist plots. Even if it is not a real time analysis, from the low frequencies data points it is possible to extract the real part of the impedance and thus, the resistance of the film with the relative change after the exposure (Fig. 5.5).

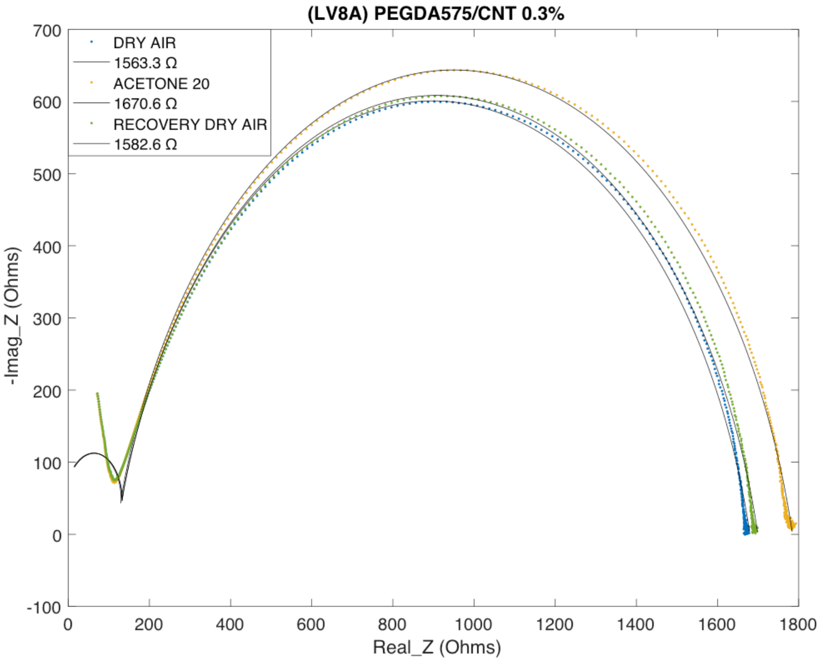

FIGURE 5.5: Static analysis of MWCNT-based sensor with relative Nyquist plot.

In the order, the film moves from the blue line to the yellow one and comes back to the green line. The recovery is not completed at 100% but it is very close to that value. In addition, from the graph it is possible to observe the beginning of a second arc. This could be due to the fact that the sample is composed of two distinctive phases that can be identified: the filler and the matrix. The frequency of resonance, calculated as the frequency of the maximum of the curve, does not show a significant shift.

All the precise numbers extracted from the single experiments are collected in Table 5.3. As expected, the resistance increases when the film gets in contact with the target analyte and it recovers to the original value almost every time. A similar behavior can be found for the capacitance, even if the absolute value is still unknown.

TABLE 5.3: AC results on MWCNT sample.

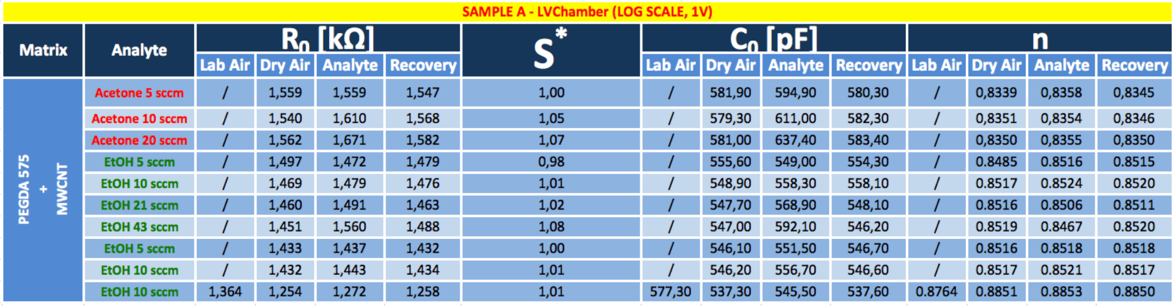

SAMPLE A - LVChamber (LOG SCALE, 1V)

Matrix	Analyte	R_0 [kΩ]				S^*	C_0 [pF]				n			
		Lab Air	Dry Air	Analyte	Recovery		Lab Air	Dry Air	Analyte	Recovery	Lab Air	Dry Air	Analyte	Recovery
PEGDA 575 + MWCNT	Acetone 5 sccm	/	1,559	1,559	1,547	1,00	/	581,90	594,90	580,30	/	0,8339	0,8358	0,8345
	Acetone 10 sccm	/	1,540	1,610	1,568	1,05	/	579,30	611,00	582,30	/	0,8351	0,8354	0,8346
	Acetone 20 sccm	/	1,562	1,671	1,582	1,07	/	581,00	637,40	583,40	/	0,8350	0,8355	0,8350
	EtOH 5 sccm	/	1,497	1,472	1,479	0,98	/	555,60	549,00	554,30	/	0.8485	0.8516	0.8515
	EtOH 10 sccm	/	1,469	1,479	1,476	1,01	/	548,90	558,30	558,10	/	0.8517	0.8524	0.8520
	EtOH 21 sccm	/	1,460	1,491	1,463	1,02	/	547,70	568,90	548,10	/	0.8516	0.8506	0.8511
	EtOH 43 sccm	/	1,451	1,560	1,488	1,08	/	547,00	592,10	546,20	/	0.8519	0.8467	0.8520
	EtOH 5 sccm	/	1,433	1,437	1,432	1,00	/	546,10	551,50	546,70	/	0.8516	0.8518	0.8518
	EtOH 10 sccm	/	1,432	1,443	1,434	1,01	/	546,20	556,70	546,60	/	0.8517	0.8521	0.8517
	EtOH 10 sccm	1,364	1,254	1,272	1,258	1,01	577,30	537,30	545,50	537,60	0.8764	0.8851	0.8853	0.8850

This previous AC analysis can be compared with the DC measurements carried out on the sample in term of electrical response. The sample was baked on a hot plate in lab air at $70\,^{\circ}\mathrm{C}$ for five minutes in order to eliminate water molecules or other contaminant from previous tests. Secondly, the device was housed inside the Polymer Chamber for two entire days flushing dry air. In this way a baseline could be reached. The standard sensing protocol employed was always the same. The applied voltage was fixed at $100\,\mathrm{mV}$, the total flow was set at 100 sccm and the temperature was constant at $19\,^{\circ}\mathrm{C}$. The focus of the analysis was on selectivity. For this reason five analytes with different chemical and physical properties were investigated: one ketone, two alcohols, an aromatic compound and the water vapor.

More than sixty-seven tests were run in order to monitor the sensitivity over a wide range of concentrations. Different gas fluxes were used because the analytes have different vapor pressures, precisely water<toluene<isopropanol<ethanol<acetone. For this reason, the fluxes were carefully chosen in order to make comparisons between vapors in term of part per million (Tab. 5.4).

In Figure 5.6, the sensing curves of all the five various analytes related to a concentrations range from 10.000 ppm up to 23.000 ppm are reported. The initial current for each experiment is constant between $58{,}2\,\mu\mathrm{A}$ and $61{,}1\,\mu\mathrm{A}$. This points out that when the sample is stabilized inside the chamber with a flux of dry air, the drift is minimized.

In general, the drop is sharper when testing toluene and isopropanol as well as the recovery time. It takes fewer seconds to reach the baseline again. On the contrary, acetone, water and ethanol curves present drops with a smaller slope and the time needed to recovery the film is longer. In the ethanol curve it doesn't even recover properly. It needs to be said that also the relative change for the five plots is different and apparently the acetone one shows the higher signal-to-noise ratio.

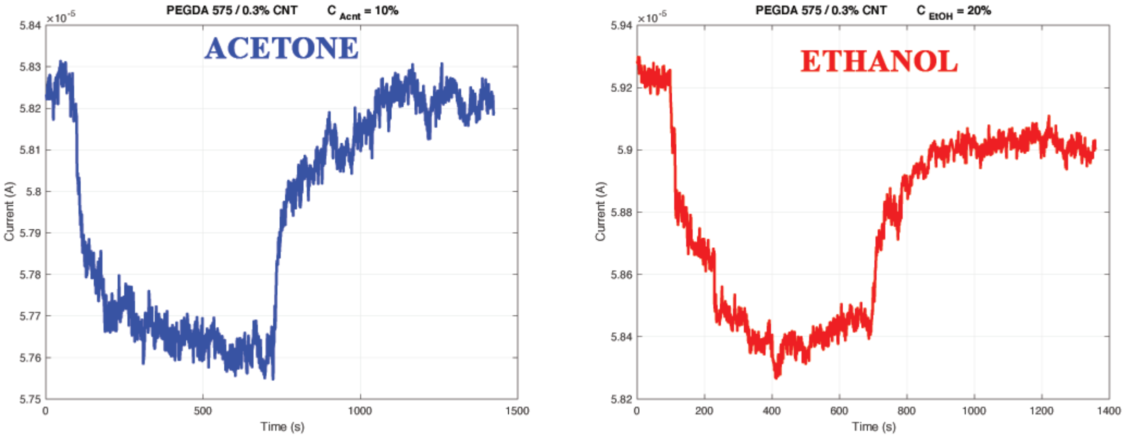

(a) 23.221 ppm of acetone.

(b) 10.793 ppm of ethanol.

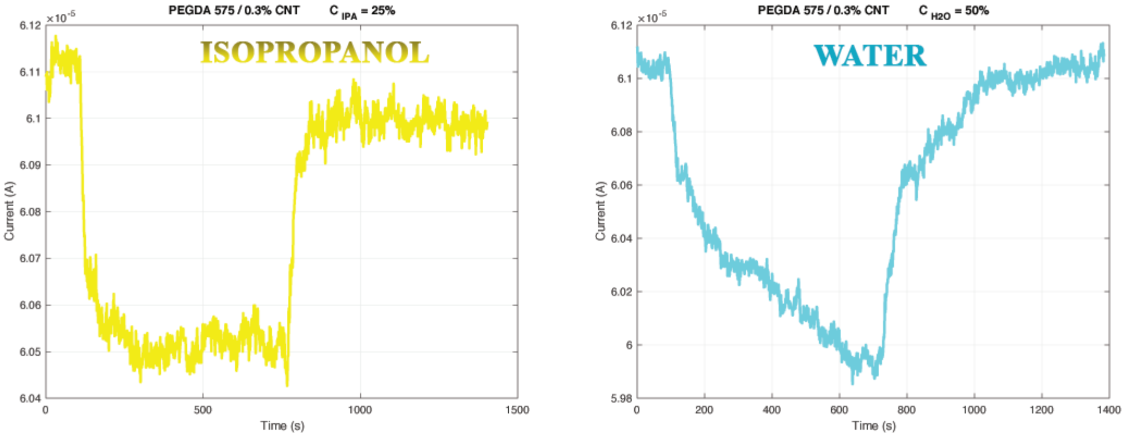

(c) 9.876 ppm of isopropanol.

(d) 10.801 ppm of water.

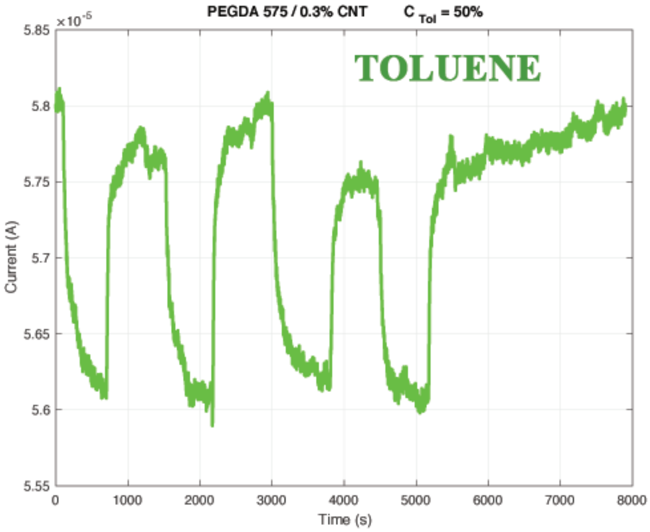

(e) 13.599 ppm of toluene.

FIGURE 5.6: Sensing respone of MWCNT-based sensor to five different analyte.

A study on the stability of the film was carried out, where the sample was exposed to multiple repetitive cycles of toluene at the same concentration over three hours (Fig. 5.6(e)). Although the recovery is not always 100%, the four cycles still have the same variation in current and thus in resistance. From the last cycle it can be seen that the recovery will eventually reach the original baseline but it just takes longer time.
This is a encouraging result because it shows that the sensor can be employed multiple times without losing its sensing properties and so the replacements are little and the costs are reduced.

The final results can be plotted together on the same graph, where it is shown the sensitivity as a function of the analytes concentration (Fig. 5.7).

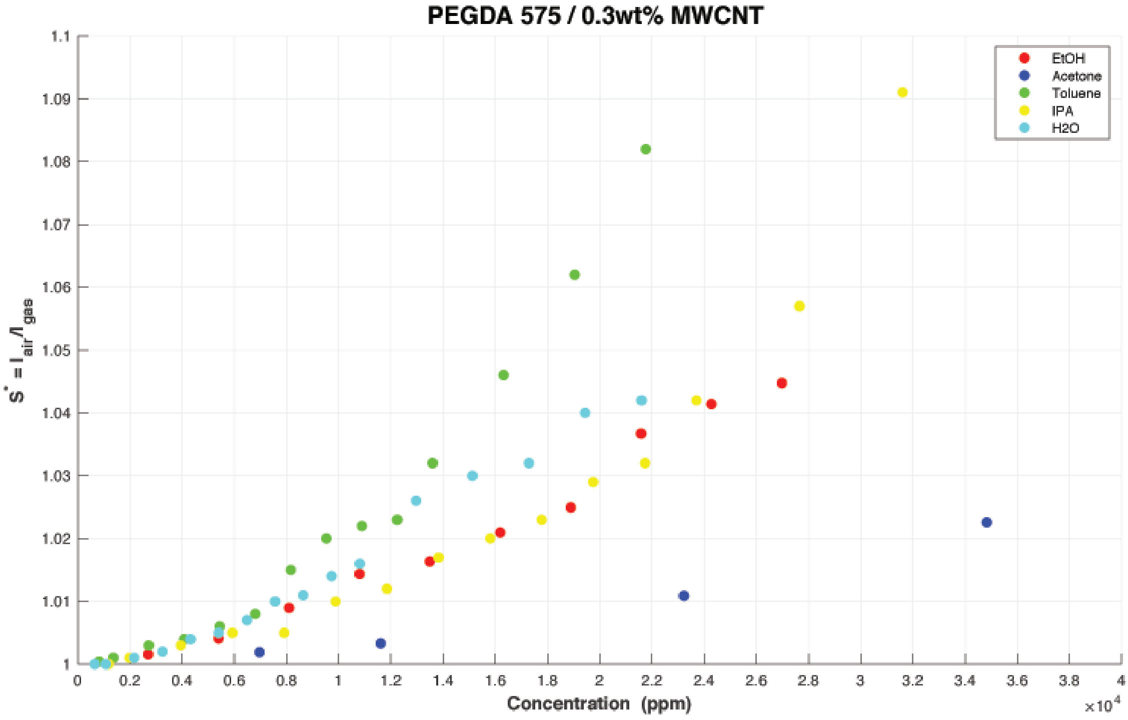

FIGURE 5.7: Selectivity study on MWCNT-based sensor tested on five differnt analytes.

It appears that the electrical response increases in different ways as the analytes concentration increases. The affinity towards acetone is the smallest. In fact, the ketone has very little polarity, while the matrix presents some polar groups along the chains. Ethanol and propanol, instead, show a similar response. This is reasonable because they both belong to the same class. The sensitivity, along with the one of the water, is much higher respect to the acetone one. Due to the presence of OH groups, it is possible to bind easily with the oxygen of the surface and allow a bigger swell. However, the best response is towards toluene, that doesn't have any polar group and it is strongly non-polar. This fact might be explained with interactions that occur between the analyte and the surface of the nanotubes.

In conclusion, it is possible to state that a particular selectivity is observed, where the sample specifically responds in different ways. However, it is early to draw any conclusion because it would be better to test more samples rather than just a single one in order to have a better statistic.

MWCNT-based sensors promise good results but more measurements are required where also other properties, such as the MWCNTs and photoinitiator amount, need to be investigated in order to improve the performance. In the future, it would be of interest to study the morphology of the film by means of a transmission electron microscope (TEM). In this way it would be possible to see how the carbon nanotubes are dispersed, the alignment and their orientation. From the scanning electron microscopy it wasn't possible to capture relevant images because the characterization was really hard due to the fact that the load of MWCNTs was very low and the insulating surface's sample charged dramatically. For this reason it was a hard task focusing the images and be able to localize the tubes. However, it seems that the carbon nanotubes are randomly dispersed, creating small bundles.

TABLE 5.4: DC results on MWCNT sample.

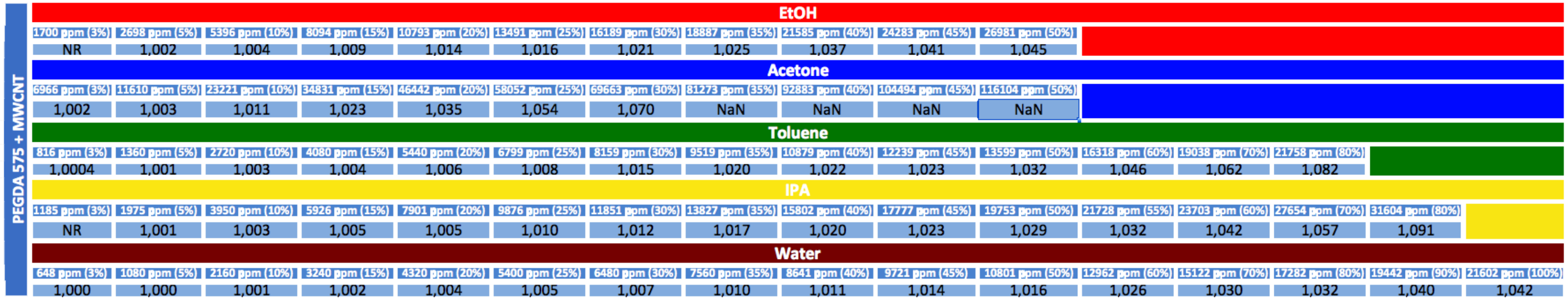

PEGDA 575 + MWCNT	**EtOH**															
	1700 ppm (3%)	2698 ppm (5%)	5396 ppm (10%)	8094 ppm (15%)	10793 ppm (20%)	13491 ppm (25%)	16189 ppm (30%)	18887 ppm (35%)	21585 ppm (40%)	24283 ppm (45%)	26981 ppm (50%)					
	NR	1,002	1,004	1,009	1,014	1,016	1,021	1,025	1,037	1,041	1,045					
	Acetone															
	6966 ppm (3%)	11610 ppm (5%)	23221 ppm (10%)	34831 ppm (15%)	46442 ppm (20%)	58052 ppm (25%)	69663 ppm (30%)	81273 ppm (35%)	92883 ppm (40%)	104494 ppm (45%)	116104 ppm (50%)					
	1,002	1,003	1,011	1,023	1,035	1,054	1,070	NaN	NaN	NaN	NaN					
	Toluene															
	816 ppm (3%)	1360 ppm (5%)	2720 ppm (10%)	4080 ppm (15%)	5440 ppm (20%)	6799 ppm (25%)	8159 ppm (30%)	9519 ppm (35%)	10879 ppm (40%)	12239 ppm (45%)	13599 ppm (50%)	16318 ppm (60%)	19038 ppm (70%)	21758 ppm (80%)		
	1,0004	1,001	1,003	1,004	1,006	1,008	1,015	1,020	1,022	1,023	1,032	1,046	1,062	1,082		
	IPA															
	1185 ppm (3%)	1975 ppm (5%)	3950 ppm (10%)	5926 ppm (15%)	7901 ppm (20%)	9876 ppm (25%)	11851 ppm (30%)	13827 ppm (35%)	15802 ppm (40%)	17777 ppm (45%)	19753 ppm (50%)	21728 ppm (55%)	23703 ppm (60%)	27654 ppm (70%)	31604 ppm (80%)	
	NR	1,001	1,003	1,005	1,005	1,010	1,012	1,017	1,020	1,023	1,029	1,032	1,042	1,057	1,091	
	Water															
	648 ppm (3%)	1080 ppm (5%)	2160 ppm (10%)	3240 ppm (15%)	4320 ppm (20%)	5400 ppm (25%)	6480 ppm (30%)	7560 ppm (35%)	8641 ppm (40%)	9721 ppm (45%)	10801 ppm (50%)	12962 ppm (60%)	15122 ppm (70%)	17282 ppm (80%)	19442 ppm (90%)	21602 ppm (100%)
	1,000	1,000	1,001	1,002	1,004	1,005	1,007	1,010	1,011	1,014	1,016	1,026	1,030	1,032	1,040	1,042

Chapter 6

Conclusions

This is the conclusive chapter of the dissertation where the key aspects of this work are trying to be drawn out.
During these 10 months spent between the laboratories of Politecnico di Torino and the facility of IBM Almaden, the development, fabrication and electrical characterization of polymeric vapor sensors have been deeply investigated. In particular, in the frame of the gas sensor project the literature has been reviewed and the majority of the efforts have been put into the investigation of the working principles and the interactions between the gas and the sensing material, establishing relationships amid chemical and physical properties compared to the electrical response and performances.
The main studies have been conducted on two important classes of polymeric chemiresistors: the carbon black-polymer composites and the in-situ photopolymerized composites.

Concerning the first category, the aim was to improve the three main requirements that are set for any kind of sensor: sensitivity, selectivity and stability. In order to do this, different series of sensors were fabricated by flow coating, synthetizing block copolymers (PS-co-PDMAEMA) by ATRP and mixing the solution with a carbon black suspension (filler load from 5 wt% up to 60 wt%). The approach used was to focus on one single parameter and investigate how this could affect the electrical response carried out by means of a DC Polymer Chamber connected to a gas delivery system, keeping everything else constant. Some good results were achieved. For both the carbon black tested (Vulcan XC72 and Black Pearl 2000) the percolation threshold seems to be between 15 wt% and 25 wt%. The Black Pearl 2000 is more conductive and the drop of the percolation curve is sharper, however the Vulcan XC72 presents a better sensitivity towards ethanol at any given filler concentrations respect to the Black Pearl 2000 and the processability during the carbon black suspension and the flow coating was much easier. According to the theory, the closer the sensor to the percolation threshold, the higher the sensitivity. Furthermore, the fewer the molecules inside the detecting chamber, the worst the sensitivity, because there are less vapor molecules that can adsorb on the surface of the film, contributing in the swelling of the matrix. The targeted resistance should be in the range of $\mathrm{k\Omega}$ because it was observed as the right one in term of efficiency. Studying the effect of the electrodes geometry, it is possible to notice that this parameter does affect the conductivity but not the sensitivity. The resistances increase in a linear way as a function of the gap between the electrodes, while sensitivity remains constant. A remarkable discovery was the identification of the lower detection limit. It is possible to state that these sensors can be employed for applications where there is the need to detect tens of ppm of a particular gas. In addition, it was proven the role of polystyrene (PS) as a universal stabilizer because in different ratios with another repeating unit it helps the dispersion of the carbon black suspension in the polymer solution. Dealing with selectivity, polymeric sensors are only partially specific. This is one of the main limitations but, working on the functional groups of the main chains, it is possible to have different behaviors towards different analytes, especially distinguishing between polar and non-polar solvents.

Regarding the other category, the main goal was to understand the complex sensing mechanism of these devices, way more complex than the first one. The novelty and strategy used for those chemiresistors was to perform a simultaneous UV-curing of an acrylic insulating thermosetting network and a conductive polymer, polypyrrole (PPy), starting from their precursors. Conductive sensors were also fabricated by dispersion of MWCNTs as the conductive filler. Thanks to this single-step process of UV photopolymerization it is possible to create cross-linked interpenetrated networks starting from a liquid photocurable formulation. Apparently, the results achieved for the polypyrrole-based sensors are not completely positive but they are not conclusive by themselves, in the sense that it is not possible to draw any strict conclusion. Many issues have been faced both regarding the samples and the experimental setup of the impedance analyzer, used to electrically characterize the devices in AC modeled as RC circuits. These samples show no reproducibility, the response is different even analyzing the same device in the same condition and the stability is very poor. The drift of the resistance with no gas is a hint that these polymeric devices are strongly affected by humidity. The reason why the films are not responding consistently might be due to the very high resistance (above $50\,\mathrm{M\Omega}$). In a future work, it would be very interesting to run some analysis on samples where the active sensing part is present in larger quantity. Increasing the amount of doped polypyrrole will reduce the resistance and might stabilize the samples. In this way also the main requirements that every sensor should have could be improved. Analyzing the MWCNT-based sensor, the results obtained in DC are pretty consistent with the AC measurements. This new material looks very promising because a particular selectivity was observed, where the sample specifically responded to five different analytes in different ways. However, it is early to draw any conclusion because it would be better to test more samples rather than just a single one in order to have a better statistic. In the future, it would be nice to investigate how other properties affect the sensing response and study the morphology of the film by means of a transmission electron microscopy (TEM). In this way it would be possible to see how the carbon nanotubes are dispersed, their alignment and orientation.

In conclusion, it is possible to say that the work done during this internship has brought some good results, even though a lot of research remains to be done. The polymeric sensors are very promising because they can be tuned and tailored. Changes in the films structure can influence and control the reactions between gases and the sensing material. Morphology, composition, solubility and other physical properties are strictly linked to the sensing performances. In the future, it will be possible to create an array of polymeric sensors in order to build an electronic nose, which is able to detect particular gases at low concentrations, giving a fingerprint response that can be univocally identified by a pattern recognition engine.

Bibliography

Alan, M.P. (1972). “Cooling Bath Compositions”. In: *Education*, pp. 0–3.

Albert, K.J. et al. (2000). “Cross-Reactive Chemical Sensor Arrays”. In: *Chem. Rev.* 100.7, pp. 2595–2626.

Alves, A.C. et al. (2018). “Project-Based Learning and its Effects on Freshmen Social Skills in an Engineering Program”. In: *Hum. Cap. Competences Proj. Manag.* Vol. 3.

Amrani, M.E.H., K.C. Persaud, and P.A. Payne (1995). “High-frequency measurements of conducting polymers: Development of a new technique for sensing volatile chemicals”. In: *Meas. Sci. Technol.* 6, pp. 1500–1507.

Arshak, K. et al. (2004). “A review of gas sensors employed in electronic nose applications”. In: *Sens. Rev.* 24.2, pp. 181–198.

Azzarelli, J.M. et al. (2014). “Wireless gas detection with a smartphone via rf communication”. In: *Proc. Natl. Acad. Sci.* 111.51, pp. 18162–18166.

Badhulika, S., N.V. Myung, and A. Mulchandani (2014). “Conducting polymer coated single-walled carbon nanotube gas sensors for the detection of volatile organic compounds”. In: *Talanta* 123, pp. 109–114.

Bai, Hua and Gaoquan Shi (2007). *Gas sensors based on conducting polymers*.

Cabot, Co (2016). “Black Pearl 2000 and Vulcan XC72 carbon black”. In: *Cabot*, pp. 2000–2001.

Castro, M. et al. (2009). “Carbon nanotubes/poly(ϵ-caprolactone) composite vapour sensors”. In: *Carbon N. Y.* 47.8, pp. 1930–1942.

Chen, Z. and C. Lu (2005). “Humidity Sensors: A Review of Materials and Mechanisms”. In: *Sens. Lett.* 3.4, pp. 274–295.

Chiu, S.W. and K.T. Tang (2013). *Towards a chemiresistive sensor-integrated electronic nose: A review*.

Cho, J.H. et al. (2005). “Sensing behaviors of polypyrrole sensor under humidity condition”. In: *Sensors Actuators, B Chem.* Vol. 108. 1-2 SPEC. ISS. Pp. 389–392.

Concina, I., M. Falasconi, and V. Sberveglieri (2012). “Electronic Noses as Flexible Tools to Assess Food Quality and Safety: Should We Trust Them?” In: *IEEE Sens. J.* 12, pp. 3232–3237.

Davis, R.L. et al. (2014). “Creating controlled thickness gradients in polymer thin films via flowcoating”. In: *Langmuir* 30.19, pp. 5637–5644.

Di Natale, C. et al. (2001). “The evaluation of quality of post-harvest oranges and apples by means of an electronic nose”. In: *Sensors Actuators, B Chem.* 78.1-3, pp. 26–31.

Di Natale, C. et al. (2003). “Lung cancer identification by the analysis of breath by means of an array of non-selective gas sensors”. In: *Biosens. Bioelectron.* 18.10, pp. 1209–1218.

Fan, Q. et al. (2011). “Vapor sensing properties of thermoplastic polyurethane multifilament covered with carbon nanotube networks”. In: *Sensors Actuators, B Chem.* 156.1, pp. 63–70.

Fine, George F. et al. (2010). “Metal oxide semi-conductor gas sensors in environmental monitoring”. In: *Sensors* 10.6, pp. 5469–5502.

Gao, T. et al. (2006). “Chemiresistors for array-based vapor sensing using composites of carbon black with low volatility organic molecules”. In: *Chem. Mater.* 18.22, pp. 5193–5202.

Gardner, J.W. (1988). “Electronic Nose”. In: *Eighth Int. Congr. Eur. Chemorecept. Res. Organ.* Coventry, p. 9.

Gardner, J.W. and P.N. Bartlett (1999). *Electronic Noses Principles and Applications*. Oxford Science Publications, p. 264.

Gardner, J.W. et al. (1990). “The Design Of An Artificial Olfactory System”. In: *Chemosens. Inf. Process.* H39, pp. 131–173.

Goschnick, J. and M. Harms (2002). “Landmine Detection with an Electronic Nose Mounted on an Airship”. In: *Detect. Explos. Landmines*, pp. 83–91.

Hao, Q., V. Kulikov, and V.M. Mirsky (2003). “Investigation of contact and bulk resistance of conducting polymers by simultaneous two- and four-point technique”. In: *Sensors Actuators, B Chem.* 94.3, pp. 352–357.

Hunter, G.W. et al. (1998). “Chemical Gas Sensors for Aeronautic and Space Applications 2”. In:

Janata, J. and M. Josowicz (2003). “Conducting polymers in electronic chemical sensors”. In: *Nat. Mater.* 2.1, pp. 19–24.

Jia, L. and B. Shi (2011). "A new equation between surface tensions and solubility parameters without molar volume parameters simultaneously fitting polymers and solvents". In: *J. Macromol. Sci. Part B Phys.* 50.6, pp. 1042–1046.

Khlebarov, Z.P., A.I. Stoyanova, and D.I. Topalova (1992). "Surface acoustic wave gas sensors". In: *Sensors Actuators B. Chem.* 8.1, pp. 33–40.

Kopecká, J. et al. (2016). "Polypyrrole nanotubes and their carbonized analogs: Synthesis, characterization, gas sensing properties". In: *Sensors (Switzerland)* 16.11.

Leidinger, M. et al. (2014). "Selective detection of hazardous VOCs for indoor air quality applications using a virtual gas sensor array". In: *J. Sensors Sens. Syst.* 3.2, p. 253.

Llobet, Eduard (2013). "Gas sensors using carbon nanomaterials: A review". In: *Sensors Actuators, B Chem.* 179, pp. 32–45.

Lonergan, M.C. et al. (1996). "Array-based vapor sensing using chemically sensitive, polymer\ncomposite resistors". In: *Chem. Mater.* 8.9, pp. 2298–2312.

Mabrook, M.F., C. Pearson, and M.C. Petty (2006). "Inkjet-printed polypyrrole thin films for vapour sensing". In: *Sensors Actuators, B Chem.* 115.1, pp. 547–551.

Miasik, J.J., A. Hooper, and B.C. Tofield (1986). "Conducting polymer gas sensors". In: *J. Chem. Soc. Faraday Trans. 1 Phys. Chem. Condens. Phases* 82.4, pp. 1117–1126.

MicroChemicals (2017). *HDMS*.

Muñoz, B.C., G. Steinthal, and S. Sunshine (1999). "Conductive polymer-carbon black composites-based sensor arrays for use in an electronic nose". In: *Sens. Rev.* 19.4, pp. 300–305.

Munstedt, H. and Z. Stary (2016). "Is electrical percolation in carbon-filled polymers reflected by rheological properties?" In: *Polymer (Guildf).* 98, pp. 51–60.

Musio, F. and M.C. Ferrara (1997). "Low frequency a. c. response of polypyrrole". In: *Sensors Actuators B* 41.1-3, pp. 97–103.

Nagle, T.H., S.S. Schiffman, and R. Gutierrez-Osuna (1998). "The How and Why of Electronic Noses". In: *IEEE Spectr.* 35.9, pp. 22–34.

Partridge, A.C., M.L. Jansen, and W.M. Arnold (2000). "Conducting polymer-based sensors". In: *Mater. Sci. Eng. C* 12.1, pp. 37–42.

Pearce, Tim C. et al. (2004). "Book Review: Handbook of Machine Olfaction." In: *Adv. Mater.* 16.12, pp. 1028–1029.

Persaud, K.C. (2005). *Polymers for chemical sensing*.

Philip, B. et al. (2003). "Carbon nanotube/PMMA composite thin films for gas-sensing applications". In: *Smart Mater. Struct.* 12.6, pp. 935–939. ISSN: 09641726.

Potyrailo, R.A. (2016). *Multivariable Sensors for Ubiquitous Monitoring of Gases in the Era of Internet of Things and Industrial Internet*.

Priola, A. et al. (1993). “Properties of polymeric films obtained from u . v . cured poly(ethylene glycol) diacrylates”. In: *Polymer (Guildf).* 34.17, pp. 3653–3657.

Razza, N. et al. (2017). “UV-Printable and Flexible Humidity Sensors Based on Conducting/Insulating Semi-Interpenetrated Polymer Networks”. In: *Macromol. Mater. Eng.* 302.10, pp. 1–7.

Röck, F., N. Barsan, and U. Weimar (2008). *Electronic nose: Current status and future trends*.

Rong, J. et al. (2003). “Carbon black / polystyrene composites as candidates for gas sensing materials”. In: *Carbon N. Y.* 41, pp. 2353–2360.

Ruangchuay, L., A. Sirivat, and J. Schwank (2004a). “Electrical conductivity response of polypyrrole to acetone vapor: Effect of dopant anions and interaction mechanisms”. In: *Synth. Met.* 140.1, pp. 15–21.

– (2004b). “Selective conductivity response of polypyrrole-based sensor on flammable chemicals”. In: *React. Funct. Polym.* 61.1, pp. 11–22.

Savage, N.O. (2009). “Gas sensing composites of metal oxides with vapor-deposited polypyrrole”. In: *Sensors Actuators, B Chem.* 143, pp. 6–11.

Schaller, E. et al. (2000). “Use of preconcentration techniques applied to a MS-based "Electronic Nose"”. In: *Analusis* 28, pp. 743–749.

Sisk, B.C. and N.S. Lewis (2006). “Vapor sensing using polymer/carbon black composites in the percolative conduction regime”. In: *Langmuir* 22.18, pp. 7928–7935.

Stafford, Christopher M. et al. (2006). “Generating thickness gradients of thin polymer films via flow coating”. In: *Rev. Sci. Instrum.* 77.2, pp. 1–7.

Wilson, A.D. (2012). “Review of Electronic-nose Technologies and Algorithms to Detect Hazardous Chemicals in the Environment”. In: *Procedia Technol.* 1, pp. 453–463.

Yeow, J.T.W. and Y. Wang (2009). *A review of carbon nanotubes-based gas sensors*.

Zhang, L. et al. (2012). “Classification of multiple indoor air contaminants by an electronic nose and a hybrid support vector machine”. In: *Sensors Actuators, B Chem.* 174, pp. 114–125.